

**FUNCTIONAL AND STRUCTURAL  
CHARACTERIZATION OF THE  
RECOMBINANTLY EXPRESSED  
GLUTAMATE RECEPTOR-B ION CHANNEL**

DISSERTATION  
ZUR ERLANGUNG DES DOKTORGRADES DER  
NATURWISSENSCHAFTEN

Vorgelegt beim Fachbereich  
Chemische und Pharmazeutische Wissenschaften (FB 14)  
der Johann Wolfgang Goethe – Universität  
in Frankfurt am Main

von  
Günther Kümmerle  
aus Reutlingen

Frankfurt am Main  
im Februar 2002  
(DF1)

Vom Fachbereich Chemische und Pharmazeutische Wissenschaften (FB 14)  
der Johann Wolfgang Goethe - Universität als Dissertation angenommen

Dekan : Prof. Dr. Walter E. Müller

Gutachter : Prof. Dr. Dieter Steinhilber (Universität Frankfurt),  
Prof. Dr. Kenneth C. Holmes (Max Planck Institut für Medizinische Forschung,  
Heidelberg)

Datum der Disputation : 27. Juni 2002

## ACKNOWLEDGMENTS

First I would like to thank all the non-scientific employees of the Max Planck Institute for the support during my Ph.D. project. I wish everyone who worked with me during the past three years the best for the future.

Prof. Steinhilber (University of Frankfurt) I thank for the friendly supervision of this project and its evaluation. Prof. Kenneth Holmes (Max Planck Institute for Medical Research, Department of Biophysics) I thank for the supervision of this project, his encouragement and for making available the electron microscopy facilities.

Dr. Dean Madden I thank for the chance to work on the glutamate receptor in his group and for all scientific discussions. He was an excellent teacher and I soon appreciated his analytical mind. In Dean's laboratory I learnt a lot about biochemistry and experienced that it can take enormous efforts to establish new projects in the field of membrane proteins.

My predecessor Dr. Markus Safferling I thank for all the practical teaching during the time when Doris Bader and I started with this project. This "collaboration" was productive and very motivating for all three of us. Doris was a very reliable coworker during this project. I will miss her assistance.

Our collaborators at the University of Helsinki who generated recombinant viruses and the stable insect cell lines are acknowledged. Bettina Schupp and Dr. G. Köhr from the department of Neurobiology were very helpful and carried out the patch-clamp experiments. Dr. P. Osten I thank for his advise with the cross-linking experiments.

The head of the electron microscopy group Dr. R. Schröder and his coworkers Dr. I. Angert, Endre Majorovits and Oliver Vossen I thank for technical advise. I enjoyed our discussions about image processing. Dr. W. Jahn I would like to thank for the collaborative effort to detect glutamate receptor ion channels by cryo-electron microscopy during the first year of this project.

Dr. Willem Tichelaar and Helga Clasen I thank for the introduction into the operation of an electron microscope. Willem's advise during image processing was important and his experience with different image formats was very helpful.

Dr. Eckhard Hofmann I want to thank for the computer relevant support. All the other colleagues in our „Nachwuchsgruppe“, namely Uschi Reygers, Dr. Laure Delarbre and Dr. Stefan Reinelt I thank for their friendship, their support and the good atmosphere.

My colleagues Endre Majorovits, Hartmut Niemann, Boris Klockow, Volker Mack and Thilo Borchardt were very open-minded towards my project and I appreciated the (scientific) discussions, their friendship and the fun we had together.

Finally, I would like to thank Anke. Her love and the support of my family were (and will continue to be) very important.

The financial support by the Max Planck society is gratefully acknowledged.

## LIST OF ABBREVIATIONS

ABB	AMPA-binding buffer
AcMNPV	<i>Autographa californica</i> multi nuclear polyhedrosis virus
AMPA	$\alpha$ -amino-3-hydroxy-5-methyl-4-isoxazole propionic acid
APS	ammoniumperoxodisulfate
AR	angular reconstitution
ATG	aurothioglucose
BCA	bicinchoninic acid
CC	cross correlation
CLP	common line projection theorem
CMC	critical micellar concentration
CV	column volume
CTF	contrast transfer function
dd-H <sub>2</sub> O	double distilled water
DDM	dodecyl- $\beta$ -D-maltosid
DMSO	dimethylsulfoxid
DTSSP	3,3'-dithio bis(sulfosuccinimidylpropionate)
DTT	1,4-dithio-DL-threitol
ECL	enhanced chemiluminescence
EDTA	ethylendiammintetraacetate
EM	electron microscopy
<i>E. coli</i>	<i>Escherichia coli</i>
Glu	L-Glutamate
GluR / GluRs	glutamate receptor / glutamate receptors
iGluR	ionotropic glutamate receptor
HFCO	high-frequency cut-off
IMAC	immobilized metal-chelate affinity chromatography
K <sub>D</sub>	dissociation constant
kD	kilo dalton
kV	kilo volt
LFCO	low-frequency cut-off
LTP	long-term potentiation

mGluR	metabotropic glutamate receptors
MOI	multiplicity of infection
MRA	multi-reference alignment
MSA	multivariate statistical analysis
MW	molecular weight
MWCO	molecular weight cut off
nAChR	nicotinic acetylcholine receptor
NMDA	N-Methyl-D-aspartate
NMR	nuclear magnetic resonance
o.N.	over night
PAGE	polyacrylamide gel electrophoresis
PBS	phosphate buffered saline
PC	phosphatidylcholine
PEG	polyethylen glycol
PFU	plaque forming units
PMSF	phenylmethyl sulfinyl fluoride
RCT	random conical tilt technique
RPM	rounds per minute
RT	room temperature
SDS	sodium dodecyl sulfate
Sf	<i>Spodoptera frugiperda</i> (insect cells)
SNR	signal to noise ratio
S1S2	soluble ligand binding-domain of GluR
TBS	tris buffered saline
TCA	trichloroacetic acid
TEM	transmission electron microscopy
TEMED	<i>N,N,N,N</i> -tetramethylethylen diamine
TMV	tobacco mosaic virus
Tris	Tris(hydroxymethyl)amminomethan
TX-100	Triton X-100
2D	two-dimensional
3D	three-dimensional
WT	wild type

## SUMMARY

Glutamate receptors (GluRs) are ligand-gated cation-selective ion channels, which play a key role in the fast excitatory synaptic signalling. Especially in the *hippocampus*, a brain region underneath the cortex that is important for learning and memory, the density of glutamate receptors is high. Being ligand-gated ion channels GluRs convert extracellular binding of the ligand glutamate into ion flux into the postsynaptic nerve cell. So far there is no direct structural information, which could prove that full-length glutamate receptors have either a tetrameric or a pentameric subunit stoichiometry. This open question was addressed in this project.

For this purpose recombinant homomeric GluR-B ion channels of the AMPA subtype were isolated from cultivated insect cells, which constitutively express the foreign GluR gene. This newly established expression system has been used in this project for the first time. The purified membrane protein was characterized biochemically. For structural analysis of single receptor molecules electron microscopy and image processing techniques were applied.

We could show that the purified GluR-B protein has a high specific activity for ligand binding. During cross-linking experiments the detection of a four-band-pattern confirmed the suggested tetrameric architecture of the glutamate receptor. To evaluate the integrity of the isolated GluR-B oligomer images of negatively stained single protein molecules were used for a 3-D reconstruction. The refined 3D model has the dimensions  $180 \text{ \AA} \times 140 \text{ \AA} \times 120 \text{ \AA}$  and shows a central channel. This would suggest that the recombinantly expressed and isolated GluR-B subunits were assembled into oligomeric protein complexes. Since subunit boundaries are not resolved the likely tetrameric architecture of the GluR ion channel is not obvious in this model. However, it is notable that the model's two-fold symmetry is consistent with the suggested tetrameric receptor structure formed by dimers of dimers.

In addition the potential of baculovirus mediated GluR-B protein for 2D crystallization was evaluated by the crystallization approach of G. Scarborough. However, these experiments did not yield any GluR-B crystals.

**(Eine ausführliche deutsche Zusammenfassung ist in Kapitel 6 zu finden.)**

<b>1.</b>	<b>INTRODUCTION</b>	<b>1</b>
1.1.	BACKGROUND AND MOTIVATION	1
1.2.	NEURONAL SIGNAL TRANSMISSION	3
1.3.	GLUTAMATE RECEPTORS	4
1.3.1.	CLASSIFICATION OF GLUTAMATE RECEPTORS AND THEIR ROLE IN NEURONAL SIGNAL TRANSMISSION	4
1.3.2.	MOLECULAR BIOLOGY AND MEMBRANE TOPOLOGY OF GLUTAMATE RECEPTORS	6
1.3.3.	SUBUNIT ASSEMBLY AND SUBUNIT STOICHIOMETRY OF GLUTAMATE RECEPTORS	8
1.3.4.	STRUCTURAL ANALYSIS OF GLUTAMATE RECEPTORS	9
1.4.	STATUS OF RESEARCH IN 1998/1999	11
1.5.	GOAL AND STRUCTURE OF THIS PROJECT	12
	REFERENCES OF CHAPTER 1	13
<b>2.</b>	<b>STRUCTURAL BIOLOGY BY ELECTRON MICROSCOPY</b>	<b>17</b>
2.1.	ELECTRON MICROSCOPY	17
2.1.1.	POTENTIAL OF ELECTRON MICROSCOPY	17
2.1.2.	ELECTRON MICROSCOPY – TECHNICAL PRINCIPLES	19
2.1.3.	ELECTRON MICROSCOPY – IMAGE FORMATION	21
2.2.	3D RECONSTRUCTION BY ANGULAR RECONSTITUTION	24
	REFERENCES OF CHAPTER 2	27
<b>3.</b>	<b>MATERIALS AND METHODS</b>	<b>29</b>
3.1.	PRIMARY STRUCTURE OF GLUR-B	29
3.2.	EXPRESSION OF GLUR-B IN INSECT CELLS	30
3.2.1.	CULTIVATION OF INSECT CELLS	30
3.2.2.	FREEZING OF INSECT CELLS	31
3.2.3.	THAWING OF INSECT CELLS	31
3.2.4.	VIRUS AMPLIFICATION	31
3.2.5.	VIRUS TITRATION	31
3.2.6.	TRYPAN BLUE DETECTION	33

<b>3.3.</b>	<b>SOLUBILIZATION AND PURIFICATION OF GLUR-B</b>	<b>34</b>
3.3.1.	HARVEST AND SOLUBILIZATION OF GLUR-B	34
3.3.2.	IMMOBILIZED METAL-CHELATE AFFINITY CHROMATOGRAPHY	34
3.3.3.	IMMUNOAFFINITY CHROMATOGRAPHY	35
<b>3.4.</b>	<b>GENERAL METHODS</b>	<b>36</b>
3.4.1.	SDS-PAGE	36
3.4.2.	SILVER STAINING	36
3.4.3.	WESTERN-BLOT ANALYSIS	37
3.4.4.	AMIDO-BLACK ASSAY	37
3.4.5.	GLUR-B CONCENTRATION IN CENTRIFUGAL CONCENTRATORS	38
3.4.6.	DETERGENT EXCHANGE	38
3.4.7.	DDM-MONITORING	39
3.4.8.	TWO-DIMENSIONAL CYRSTALLIZATION EXPERIMENTS	39
<b>3.5.</b>	<b>BIOCHEMICAL PROTEIN CHARACTERIZATION</b>	<b>41</b>
3.5.1.	FILTER-BINDING OF THE RADIOLIGAND [ <sup>3</sup> H]-AMPA	41
3.5.2.	ELECTROPHYSIOLOGICAL ANALYSIS	41
<b>3.6.</b>	<b>INDIRECT ANALYSIS OF THE OLIGOMERIC PROTEIN STRUCTURE BY CROSS-LINKING</b>	<b>42</b>
<b>3.7.</b>	<b>DIRECT ANALYSIS OF THE OLIGOMERIC PROTEIN STRUCTURE BY ELECTRON MICROSCOPY</b>	<b>44</b>
3.7.1.	NEGATIVE STAINING	44
3.7.2.	CRYO-ELECTRON MICROSCOPY	44
3.7.3.	CRYO-NEGATIVE STAINING	44
3.7.4.	ELECTRON MICROSCOPY	45
	REFERENCES OF CHAPTER 3	46
<hr/>		
<b>4.</b>	<b>RESULTS</b>	<b>47</b>
<b>4.1.</b>	<b>GLUR EXPRESSION IN STABLE INSECT CELLS</b>	<b>47</b>
4.1.1.	ELECTROPHYSIOLOGICAL ANALYSIS OF GLUR-D AND GLUR-B	47
4.1.2.	OPTIMIZATION OF IMAC PURIFICATION	48
4.1.3.	GLUR-B PROTEIN AT HIGHER PROTEIN CONCENTRATIONS	51

<b>4.2.</b>	<b>BIOCHEMICAL CHARACTERIZATION OF GLUR-B</b>	<b>53</b>
4.2.1.	RADIOLIGAND-BINDING	53
<b>4.3.</b>	<b>INDIRECT ANALYSIS OF THE OLIGOMERIC PROTEIN STRUCTURE BY CROSS-LINKING</b>	<b>55</b>
4.3.1.	CROSS-LINKING OF PURIFIED GLUR-B HOMOMERS	55
4.3.2.	CROSS-LINKING OF TOTAL RAT BRAIN LYSATE	56
<b>4.4.</b>	<b>DIRECT ANALYSIS OF THE OLIGOMERIC PROTEIN STRUCTURE BY ELECTRON MICROSCOPY</b>	<b>58</b>
4.4.1.	CRYO-ELECTRON MICROSCOPY	58
4.4.2.	CRYO-NEGATIVE STAINING	59
4.4.3.	NEGATIVE STAINING	61
4.4.3.1.	GLUR-B NEGATIVELY STAINED IN AUROTHIOGLUCOSE	61
4.4.3.2.	IMAGE PROCESSING OF GLUR-B STAINED IN AUROTHIOGLUCOSE	62
4.4.3.3.	GLUR-B NEGATIVELY STAINED IN URANYLACETATE	64
4.4.3.4.	SINGLE PARTICLE ANALYSIS AND 3D RECONSTRUCTION OF GLUR-B	65
	REFERENCES OF CHAPTER 4	77
<hr/>		
<b>5.</b>	<b>DISCUSSION AND OUTLOOK</b>	<b>78</b>
<b>5.1.</b>	<b>DISCUSSION OF BIOCHEMICAL RESULTS</b>	<b>78</b>
<b>5.2.</b>	<b>DISCUSSION OF ELECTRON MICROSCOPY RESULTS</b>	<b>82</b>
<b>5.3.</b>	<b>OUTLOOK</b>	<b>88</b>
	REFERENCES OF CHAPTER 5	89
<hr/>		
<b>6.</b>	<b>ZUSAMMENFASSUNG</b>	<b>91</b>
<b>6.1.</b>	<b>DIE BEDEUTUNG VON GLUTAMATREZEPTOREN – STAND DER STRUKTURANALYSE ZUM BEGINN DIESER ARBEIT</b>	<b>91</b>
<b>6.2.</b>	<b>FUNKTIONELLE UND STRUKTURELLE CHARAKTERISIERUNG DES GLUR-B IONENKANALS</b>	<b>94</b>
	REFERENZEN VON KAPITEL 6	99
<hr/>		

<b>APPENDIX</b>	<b>100</b>
<b>A.1. RECOMBINANT EXPRESSION OF EUKARYOTIC MEMBRANE PROTEINS</b>	<b>100</b>
<b>A.2. RECOMBINANT EXPRESSION OF GLUR-B IN INSECT CELLS</b>	<b>101</b>
A.2.1. BACULOVIRUS MEDIATED EXPRESSION OF GLUR-B	101
A.2.2. EXPRESSION OF GLUR-B IN STABLE INSECT CELLS	104
<b>A.3. TWO-DIMENSIONAL PROTEIN CRYSTALLIZATION</b>	<b>105</b>
A.3.1. TWO-DIMENSIONAL CRYSTALLIZATION OF A H <sup>+</sup> -ATPase	105
A.3.2. TWO-DIMENSIONAL CRYSTALLIZATION OF A BACULOVIRUS- MEDIATED GLUR-B PROTEIN	106
<b>REFERENCES OF THE APPENDIX</b>	<b>109</b>

## **PUBLICATION:**

FIRST IMAGES OF A GLUTAMATE RECEPTOR ION CHANNEL: OLIGOMERIC  
STATE AND MOLECULAR DIMENSION OF GLUR-B HOMOMERS

# 1. INTRODUCTION

## 1.1. BACKGROUND AND MOTIVATION

The 1990's were declared "The Decade of the Brain". This initiative stimulated different disciplines to focus their techniques on open questions in the field of neuroscience. In the introduction of a special issue of *Neuron* two leading experts, Thomas Jessell and Eric Kandel (Jessell and Kandel, 1998), recently summarized the essential experiments of neuroscience in six decades and asked: "Where is neuroscience heading in the decades ahead?". The authors think that the field will focus increasingly on developmental and cognitive neuroscience, on brain systems and mental processes. They point out that a detailed understanding of the biology of mind and brain might be reflected in the development of more effective treatments for neurological disorders. For the pharmacological treatment of such disorders structural analysis of ion channels and receptor proteins involved in synaptic transmission could play a key role and give new insights how these proteins work. The crystal structures of the soluble ligand-binding domain of a glutamate receptor (GluR) (Armstrong et al., 1998) and of a soluble acetylcholine binding protein (Brejc et al., 2001) are already accessible for rational design of psycho-active drugs. However, both structures reveal only partial information for the fundamental understanding of two membrane proteins, which are insoluble at full-length in the absence of detergent. Due to the membrane spanning part crystallization of membrane proteins, like ion channels, is far from being routine work. For soluble proteins thousands of high-resolution structures have been determined by X-ray crystallography or NMR spectroscopy. Compared to this only few membrane protein structures have been determined. The natural abundance or prokaryotic expression of these membrane proteins was one important prerequisite for their successful crystallization. A list of membrane proteins of known structures is maintained and continuously updated by the department of Prof. H. Michel at the Max Planck Institute for Biophysics in Frankfurt, Germany. It is accessible under: <http://www.mpibp-frankfurt.mpg.de/michel/public/memprotstruct.html>.

To obtain structural information about membrane proteins with low abundance in natural tissues several tools for recombinant expression were developed (Grisshammer and Tate, 1995), (Tate and Blakely, 1994). One of the most recent developments in the field of recombinant expression of eukaryotic proteins are insect cells constitutively expressing foreign genes (Pfeifer et al., 1998). In the project described here insect cells constitutively expressing a full-length ionotropic glutamate receptor (iGluR) were used. Beside the expression system a further point is mostly critical: membrane proteins require the presence of

detergent or lipid molecules, which saturate the hydrophobic residues in the transmembrane domain and thus prevent protein aggregation. Disorder caused by detergent molecules or missing lipid molecules and the inherent flexibility of transmembrane  $\alpha$ -helices relative to each other can make crystallization of membrane proteins very difficult.

The breakthrough in structural analysis of membrane proteins at atomic resolution was marked by the structure of the photosynthetic reaction center of *Rhodospseudomonas viridis* in 1985 (Deisenhofer et al., 1985). The increased effort during the last 15 years to get structural data of membrane proteins stimulated the structural analysis of ion channels. In 1993 Nigel Unwin, a pioneer in the field, summarized the status of structural analysis on ligand-gated ion channels: "We do not know what any of the neurotransmitter-gated channels look like at atomic resolution, but a rudimentary picture, at least, is emerging from studies on the acetylcholine receptor with the electron microscope." (Unwin, 1993). At that time the model of the nicotinic acetylcholine receptor (nAChR) from *Torpedo* had a resolution of 9 Å. This receptor is strongly expressed and densely packed in the membranes of the *Torpedo* fish. After isolation, acetylcholine receptors form tubular structures, which can be analyzed by cryo-electron microscopy. Improvement of electron-microscopy techniques and image processing over the years yielded a structure of the acetylcholine receptor with a resolution of 4.6 Å (Unwin, 1995). So far this is the most detailed electron microscopic structure of a ligand-gated ion channel. In the meantime however, a prokaryotic potassium channel became the flagship of ion channel research. The atomic structure at a resolution of 3.2 Å explained the ion selectivity of this channel (Doyle et al., 1998) and most recently even the chemistry of ion hydration and ion coordination in a K<sup>+</sup> channel-Fab complex were detected at a resolution of 2.0 Å (Zhou et al., 2001). These X-ray experiments revealed structural and functional insights into an ion channel in unparalleled detail.

When membrane proteins do not crystallize despite optimization of the detergent at least low-resolution information of the protein structure is accessible by a combination of electron microscopy and image processing called "single particle analysis". The same applies for proteins that can be isolated at low yields only. Analysis of ca. 6000 negatively stained molecules recently revealed the tetrameric structure of voltage-gated potassium channel *Shaker* from *Drosophila* at a resolution of 25 Å (Sokolova et al., 2001).

In this project single particle analysis and biochemical techniques were used to evaluate the potential of insect cells constitutively expressing a recombinant full-length glutamate receptor. Glutamate receptors (GluRs) are ligand gated cation-selective ion channels, which play an important role in excitatory synaptic transmission. Embedded in the postsynaptic membrane structures of nerve cells ligand-gated ion channel receptors control membrane permeability for ions and convert extracellular binding of the ligand glutamate into ion influx into the postsynaptic cell. Structural information of the full-length protein could help to understand fundamental processes like channel activation and desensitization. Before the biology and the structure of GluRs are discussed in more detail the general aspects of neuronal signalling will be explained in the following paragraph.

## **1.2. NEURONAL SIGNAL TRANSMISSION**

The human brain consists of ca.  $10^{11}$  nerve cells, which can be classified into ca. 1000 different cell types (Kandel et al., 1996). Because of this diversity and the fact that each neuron makes ca. 10 000 specific contacts with various target cells the complexity of the brain exceeds all other organs. Neuronal cells -regardless of their shape, size, location and function- consist of four compartments: the cell body, dendrites, the axon and the nerve terminal. All four play a distinct role in signalling. The dendrites and the cell body can be regarded as input components of the neuron, whereas the presynaptic terminal is the output component of the cell. The axon is the long-range signalling component of the cell in such a model. Cell-to-cell communication between neurons or between muscle cells and neurons occurs at specific sites called synapses. According to the nature of signal transmission electrical and chemical synapses are distinguished. Signal transmission by electrical means is faster and consists of direct current flows between neurons through low-resistance connections provided by “gap junctions”. In chemical signal transmission the presynaptic action potential induces the release of neurotransmitters from the presynaptic nerve terminal. The small transmitter molecules diffuse across the synaptic cleft and bind to their specific postsynaptic receptors, which become permeable for ions. Thereby the chemical information is retransformed into an electrical signal on the postsynaptic target site. Together with other receptors and ion channels some types of glutamate receptors like the metabotropic glutamate receptors are important for the modulation of chemical synapses. A model of a glutamatergic synapse is discussed in the next paragraph.

### 1.3. GLUTAMATE RECEPTORS

#### 1.3.1. CLASSIFICATION OF GLUTAMATE RECEPTORS AND THEIR ROLE IN NEURONAL SIGNAL TRANSMISSION

The amino acid L-glutamate (Glu) is the predominant excitatory neuro-transmitter in the mammalian brain. Three synthetic agonists were found to activate ionotropic glutamate receptors (iGluRs) selectively. These agonists are  $\alpha$ -amino-3-hydroxy-5-methyl-4-isoxazole propionic acid (AMPA), kainate and N-methyl-D-aspartate (NMDA). According to their pharmacological profiles for these three agonists iGluRs were classified into three families comprising AMPA receptors, kainate receptors and NMDA receptors (Seeburg, 1993), (Hollmann and Heinemann, 1994), (Dingledine et al., 1999). The first two are referred to as non-NMDA receptor-channels. Activation and desensitization kinetics of non-NMDA receptors are faster than those of NMDA receptors. Non-NMDA receptor channels have high permeability for  $\text{Na}^+$ - and  $\text{K}^+$ -ions but a low permeability for  $\text{Ca}^{2+}$ -ions. In excitatory synapses AMPA- and NMDA receptors are mostly co-localized. Both are activated by glutamate. At a typical resting potential of about -70 mV NMDA receptors are blocked by  $\text{Mg}^{2+}$ -ions (Mayer et al., 1984). This block is removed when the postsynaptic membrane is depolarized because of activation of AMPA receptors and other ligand- or voltage-gated ion channels. After depolarization and ligand-binding NMDA channels are activated and become permeable to  $\text{Na}^+ / \text{K}^+$  and  $\text{Ca}^{2+}$ -ions.

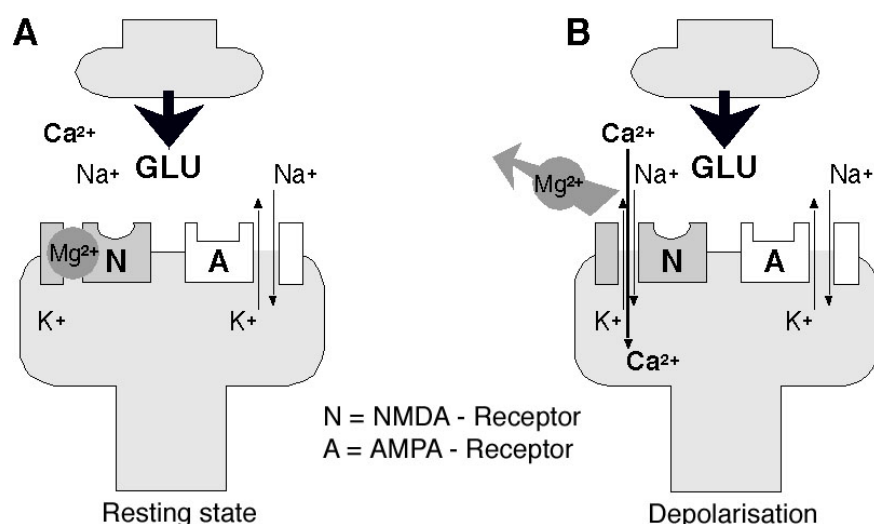


**Figure 1.3.1.A:** Model of a glutamatergic synapse showing colocalized NMDA- and AMPA-receptors in the postsynaptic membrane A) resting state and B) depolarized state. In A) the NMDA receptor is blocked by  $\text{Mg}^{2+}$ -ions. The presynaptically released neuro-transmitter glutamate activates AMPA receptors. Thereby the postsynaptic membrane is depolarized and the  $\text{Mg}^{2+}$ -block is removed. Induced by glutamate-binding NMDA ion channels become permeable to  $\text{Na}^+ / \text{K}^+$ -ions.

The postsynaptic influx of  $\text{Ca}^{2+}$  ions activates  $\text{Ca}^{2+}$ -dependent second messenger signalling cascades. This process is thought to be fundamental for synaptic modulation (Bliss and Collingridge, 1993). In this context it is important to mention metabotropic glutamate receptors (mGluR), which constitute a separate type of glutamate receptor. Compared to ionotropic glutamate receptors, mGluRs do not form intrinsic ion channels and beside the large extracellular glutamate-binding domain there is no structural relation between the ionotropic glutamate receptors and mGluRs. Coupled via seven transmembrane domains to G-proteins and intracellular second messenger systems, the mGluRs initiate much slower responses and thus modulate synaptic transmission (Nakanishi, 1990).

Since glutamatergic synapses are extremely important for plasticity they are in the center of interest when long-lasting changes of the synaptic plasticity like long-term potentiation are studied. The stimulation of presynaptic nerve terminals by brief high frequency pulses of action potentials was found to produce an increase in the strength of synaptic connections between the pyramidal cells in the CA3 region and the CA1 region in the hippocampus where the density of glutamate receptors is high (Andersen et al., 1977), (Bliss and Lomo, 1973). This facilitation in the synaptic efficacy is called “long-term potentiation” (LTP). LTP is being investigated intensively since it is thought to play an important role in learning and memory (Asztely and Gustaffson, 1996). The  $\text{Ca}^{2+}$  activated second-messenger cascades in the postsynaptic nerve cell are thought to be the metabolic basis for the development of LTP. However, so far there is no commonly accepted explanation for the postulated relation between LTP and explicit learning. In the “Morris Water Maze” test it was found that in  $\text{GluR-A}^{-/-}$  knockout mice spatial learning was not affected even though the knockout showed no LTP (Zamanillo et al., 1999). At present it seems that the molecular basis for learning and memory is more complex.

Recently the first prokaryotic glutamate receptor channel (GluR0) has been identified in a cyanobacterium by database comparison (Chen et al., 1999). Earlier iGluR homologues have been cloned from invertebrates (Schuster et al., 1991) and plants (Lam et al., 1998) where they are thought to be involved in light-signal transduction. All these findings indicate that the GluR family is evolutionarily old. The molecular biology of eukaryotic GluRs and the structural nature of this class of ion channels will be discussed in the next paragraph.

### 1.3.2. MOLECULAR BIOLOGY AND MEMBRANE TOPOLOGY OF GLUTAMATE RECEPTORS

The three classes of ionotropic glutamate receptors are encoded by six gene families and show considerable subunit diversity. AMPA receptor subunits, encoded by one gene family, are named GluR-A to GluR-D (or alternatively GluR1 to GluR4). Kainate receptors are named KA1 and KA2 (or alternatively GluR5 and GluR6) and are encoded by two gene families. Three gene families encode the class of NMDA receptors (NR), which consists of NR1, NR2A to NR2D plus NR3A and NR3B. Mammalian GluR subunits vary in length from ca. 900 to 1500 amino acids. Subunits of the same subfamily and subunits of different subfamilies show sequence homology (Hollmann and Heinemann, 1994). AMPA receptors contain 4 to 6 *N*-glycosylation sites. A glycosylated GluR-B subunit has a molecular mass of ca. 104 kD.

There are two post-transcriptional alterations that increase the functional diversity of glutamate receptors: alternative splicing and RNA editing. When a gene is alternatively spliced this means that different proteins can be made from this gene. All AMPA receptor subunits occur in at least two alternatively spliced versions, which are called flip and flop (Monyer et al., 1991). The difference is a 35 amino acid long segment just before M4, which is alternatively coded by one of two adjacent exons (exon 14 and exon 15) (Sommer et al., 1990). While flip variants predominate before birth the flop variants are in low abundance till eight days after birth. Flip and flop tune the responses of the receptors to ligand-binding by changing their desensitization kinetics; while flop variants desensitize quickly and profoundly, flip variants of most subunits show delayed desensitization (Mosbacher et al., 1994). The second post-transcriptional alteration, which is RNA editing determines the nature of the GluR-B subunit as a regulator for the calcium permeability. RNA editing is an enzymatic action by which the nucleotide sequence of the RNA is changed after transcription. Thus the nucleotide sequence of the gene is not identical with the nucleotide sequence of the transcript. The mRNA sequence of the GluR-B subunit is altered in such a way that the RNA codon for glutamine (CAG) is converted to the codon for an arginine (CGG) (Sommer et al., 1991), i.e. although the genomic DNA codes for a glutamine (Q) the residue in the protein is an arginine (R). Located in the M2 channel lining pore-loop the arginine stops the passage of  $\text{Ca}^{2+}$  ions.

The diversity of GluRs becomes even bigger when different subunits are assembled to form functional channels. Recombinant expression of an individual type of subunit in non-neuronal cells leads to the formation of functional homomeric channels (Wenthold et al., 1996), (Wenthold et al., 1992). However, coexpression of two or more subunits of the same subtype result in the formation of heteromeric channels (Verdoorn et al., 1991), (Boulter et al., 1990), (Hollmann et al., 1989). The question how many subunits compose a functional channel is discussed in the next paragraph.

When the different ionotropic glutamate receptors were cloned it was thought that each subunit had four membrane-crossing segments like those in the acetylcholine receptor family. Glycosylation experiments identified extracellular sites between transmembrane domains M3-M4 and revealed an extracellular amino terminal domain, which suggested a three transmembrane domain topology for the GluR subunit (Hollmann et al., 1994). Since both ends of the putative M2 transmembrane domain were found to be on the cytoplasmic side it was concluded that the M2 segment forms a re-entrant membrane loop (Kuner et al., 1996).

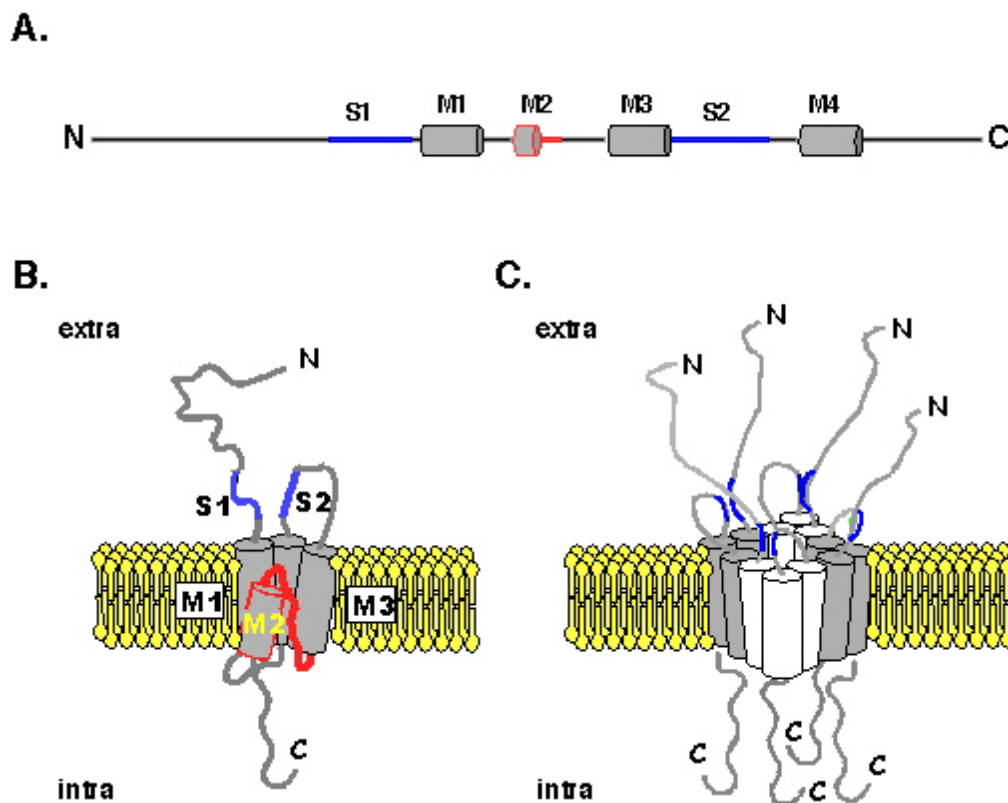


Figure 1.3.2.A: A) Structural elements of a GluR subunit in a linear drawing starting with the amino terminus (N) ending with the carboxy terminus (C). B) Transmembrane topology of a single GluR subunit in a schematic representation according to (Paas, 1998). S1 and S2 form the ligand-binding domain. C) Model of a putative tetrameric AMPA-receptor complex.

The transmembrane topology as shown in Figure 1.3.2.A. is thought to be the same for all GluR subtypes. It is now commonly accepted and excludes glutamate receptors from the acetylcholine receptor family, which shows four transmembrane domains.

### **1.3.3. SUBUNIT ASSEMBLY AND SUBUNIT STOICHIOMETRY OF GLUTAMATE RECEPTORS**

In the past the subunit stoichiometry of GluR caused controversial debates. There are investigations, which support a tetrameric structure (Laube et al., 1997), (Mano and Teichberg, 1998), (Rosenmund et al., 1998), (Ayalon and Stern-Bach, 2001), (Safferling et al., 2001) and there are publications, which proposed a pentameric architecture (Ferrer-Montiel and Montal, 1996), (Hawkins et al., 1999), (Premkumar and Auerbach, 1997). Native receptors are thought to be heteromultimers of at least two different subunits. The assembly of GluR subunits is subtype-restricted. This means that AMPA-receptors consist of a combinatorial assembly of the four different subunits (GluR-A, GluR-B, GluR-C and GluR-D) and cannot incorporate subunits of the NMDA or kainate subtype. The electrophysiological findings were confirmed by co-immunoprecipitation experiments with detergent-solubilized receptors, which showed that all AMPA subunits co-assemble into heterooligomers (Wenthold et al., 1996). The rules that govern the selectivity of the further assembly process are even more specific. Using chimeric receptors and truncation fragments of subunits it was shown by co-immunoprecipitation experiments that the specificity of assembly is determined by N-terminal subunit regions (Leuschner and Hoch, 1999). Another group used four different subunit chimeras to show by co-immunoprecipitation and patch-clamp experiments that beside the N-terminal domain, the membrane sector (Stern-Bach et al., 1994) and the C-terminal part of S2 are critical determinants in the formation of functional GluR oligomers (Ayalon and Stern-Bach, 2001). These results suggest that the N-terminal domain only mediates the initial subunit association into dimers. Subunit-dimerization is a plausible initial assembly step and the importance of the C-terminal part of S2 for receptor assembly (Ayalon and Stern-Bach, 2001) are consistent with X-ray analysis of the soluble ligand-binding domain of GluR-B, which revealed that the subunits crystallized as dimers (Armstrong et al., 1998). These findings and the observation that the activation of non-NMDA receptors is a multi-step process that involves the binding of four molecules of agonist (Rosenmund et al., 1998) are consistent with a tetrameric structure. In conclusion it can be said that the most recent publications suggest a tetrameric structure for GluR molecules and helped indeed to make the subunit stoichiometry issue less controversial.

The characterization of the prokaryotic glutamate receptor GluR0 is additional evidence for a putative tetrameric GluR subunit stoichiometry. On the basis of amino-acid sequence and functional relationships between GluR0 and eukaryotic GluRs the Gouaux group proposed that GluR0 or an as yet undiscovered GluR0 homologue is the precursor to eukaryotic GluRs (Chen et al., 1999). This concept is supported by the sequence identity between GluR0 and K<sup>+</sup>-channels between the first and second transmembrane segment and the electrophysiology of both channels; GluR0 was shown to be a glutamate-gated potassium selective channel. Since eukaryotic GluRs show sequence homology to the tetrameric potassium channel (Chen et al., 1999), (Wo and Oswald, 1995) it is conceivable indeed that GluR0 is the missing link between tetrameric potassium channels (Doyle et al., 1998) and glutamate receptors. Furthermore, the crystal structures of the ligand-binding core of GluR0 in complex with glutamate and serine (Mayer et al., 2001) confirmed the homology between the bacterial periplasmatic binding protein and ligand-binding domain of GluR-B.

Although all these hints strongly suggest that the eukaryotic glutamate receptor ion channel has a tetrameric architecture only biochemical and structural analysis of the full-length protein can reveal the subunit stoichiometry and end the debate. For the development of new drugs the rich structural information of the ligand-binding domain is at the moment more important than a detailed understanding of the correlation between ligand-binding and channel gating. The present status of structural analysis of the GluR ligand-binding domain will be summarized in the next paragraph.

#### **1.3.4. STRUCTURAL ANALYSIS OF GLUTAMATE RECEPTORS**

No full length GluR ion channel has been crystallized yet. Crystallization of the soluble ligand-binding domain (S1S2) came into reach, after a recombinantly expressed construct was shown to have pharmacological properties similar to those of the wild-type membrane-bound receptor (Kuusinen et al., 1995). This construct consists of the two lobes S1 and S2 of the extracellular ligand-binding domain of GluR-D coupled by a 13-residue linker. Generation of similar but shortened GluR-B constructs (Chen et al., 1998), their expression in *E. coli*, refolding and the co-crystallization with kainate resulted in the first crystal structure of a GluR ligand-binding domain (Armstrong et al., 1998). Thereby it was found that S1 and S2 are arranged in the shape of a kidney. The S1S2 structure in complex with kainate suggested that ligand-binding induces a flytrap-like closure of the cleft between the two lobes (Armstrong et al., 1998). Since the structure is strikingly similar to the structure of the *E. coli*

glutamine-binding protein (Sun et al., 1998) it confirmed sequence homologies of the GluR ligand-binding domain with bacterial periplasmic binding proteins (Nakanishi et al., 1990). All seven residues that make direct interactions with kainate in the GluR-B S1S2 complex are identical or conservatively substituted among the members of GluR subfamilies.

Subsequent crystallization of S1S2 in the presence of the antagonist DNQX and the agonists kainate (partial agonist), glutamate and AMPA showed that the extent of domain separation is decreasing in the order apo > DNQX > kainate > glutamate  $\cong$  AMPA (Armstrong and Gouaux, 2000). This order matches with the extent of activation. On the basis of these structures it was proposed that cleft-closure of the ligand-binding domain activates (opens) the glutamate receptor ion channel. Since channel opening is not a binary process, which involves the two states open and closed, the gating process may involve a number of different conformational states in the transmembrane domain. The mechanism of a possible allosteric coupling (Monod et al., 1965), (Perutz, 1989), (Changeux and Edelstein, 1998) between the degree of cleft closure in the ligand-binding domain and the channel gate of GluRs are discussed in a recent review (Madden, 2002), which integrates the structural insights into GluR function with new functional and biochemical data.

#### 1.4. STATUS OF RESEARCH IN 1998/1999

During the first 10 months isolation of GluR-B protein expressed in the baculovirus expression-system was part of this Ph.D. project. By that time the baculovirus-mediated expression and purification of GluR-B at the mg scale had been established (Safferling, 1999). Centrifugation of the purified GluR-B protein in glycerol density gradients showed that the protein was in a uniform oligomeric state. Its ligand-binding activity was confirmed by radioligand-binding. The molecular mass of the complex was calibrated relative to soluble proteins, yielding a value of 495 kD consistent with a tetramer (Safferling et al., 2001). Reconstitution experiments of purified GluR-B channels into liposomes were not successful (Safferling, 1999). To get an initial low-resolution structure, negatively stained GluR-B samples were visualized by electron microscopy (EM). For image processing with the IMAGIC software package W. Tichelaar, a research associate in our group, selected more than 10 000 GluR-B molecules, which were negatively stained in uranyl acetate. The final 3D reconstruction of this approach is shown in Figure 1.4.A. The projected dimensions of the model correspond to a molecule with a long dimension of 17 nm and a perpendicular cross section of  $11 \times 14$  nm. It does not show a distinct symmetry reflecting the subunit stoichiometry of the GluR-B complex. The particle is indented or hollow, i.e., it contains internal solvent accessible volumes seen as stain-filled structures. The model does not display a distinct channel but shows several cavities, which may contribute to the ion-conducting pathway.

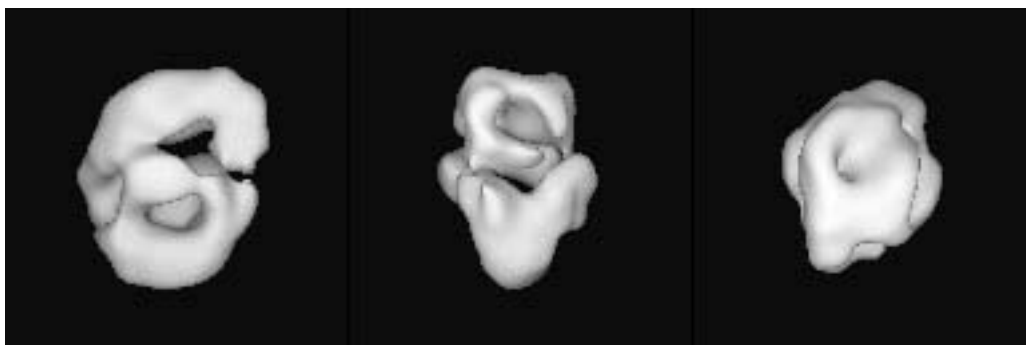


**Figure 1.4.A: First reconstruction of 10000 GluR-B protein molecules. Three projections of the model with the dimension 17 nm  $\times$  14 nm  $\times$  11 nm are shown. (Courtesy of Dr. W. Tichelaar)**

To rule out possible negative effects of negative staining on protein preservation we started to do cryo-electron microscopy experiments with GluR-B protein.

## 1.5. GOAL AND STRUCTURE OF THIS PROJECT

The goal of this project was to evaluate the potential of a stable cell line for the expression of GluRs and to reveal the subunit stoichiometry of a full length AMPA receptor homomer consisting of GluR-B subunits. The ligand-binding activity of the isolated receptor protein, which was available in sub-milligram amounts, was assessed by radio-ligand binding. For structural analysis of single protein molecules by EM and subsequent image processing techniques it can be said in general that the optical homogeneity of the protein sample is an important prerequisite for success. In initial negative stain experiments with uranyl acetate homogeneity of GluR-B oligomers was rather poor. To rule out harmful effects of partial staining and protein flattening in negatively stained specimen, cryo-electron microscopy and the cryo-negative stain approach were applied. The tobacco mosaic virus (TMV) was used as a reference to establish cryo-electron microscopy in our research group. For reasons, which will be discussed it was not possible to detect GluR-B molecules by cryo-electron microscopy and by the cryo-negative stain approach. When the detection of vitrified of GluR-B molecules did not succeed, efforts were directed towards an improved negative stain approach: Aurothioglucose, which is applicable at a more physiological pH-range was recommended as an alternative to uranyl acetate by other membrane protein researchers (B. Böttcher, personal communication). To support the formation of thicker stain layers only grids with freshly floated carbon films were used (M. Radermacher, personal communication). To evaluate the preservation of GluR-B by ATG stain 3400 protein particles stained in aurothioglucose were selected for image processing despite the poor contrast enhancement. However, it turned out that a reliable classification of these particles was not achievable. During the search for an alternative stain the “standard stain” uranyl acetate was constantly used to evaluate concentration and protein quality of GluR-B preparations. Some of these uranyl acetate controls with freshly floated carbon films produced micrographs of GluR-B, which looked promising in terms of protein preservation and contrast enhancement.

To get a first *ab initio* envelope of the ion channel protein ca. 500 GluR-B molecules were selected from areas where stain layers had a maximum thickness. The variation of parameters during band-pass filtering revealed the influence of low-frequency information on particle classification and 3D image reconstruction of GluR-B particles.

**REFERENCES OF CHAPTER 1**

- Andersen, P., Sundberg, S. H., Sveen, O., and Wigstrom, H. (1977). Specific long-lasting potentiation of synaptic transmission in hippocampal slices. *Nature* 266, 736-737.
- Armstrong, N., and Gouaux, E. (2000). Mechanisms for activation and antagonism of an AMPA-sensitive glutamate receptor: crystal structures of the GluR2 ligand binding core. *Neuron* 28, 165-181.
- Armstrong, N., Sun, Y., Chen, G.-Q., and Gouaux, E. (1998). Structure of a glutamate-receptor ligand binding core in complex with kainate. *Nature* 395, 913-917.
- Asztely, F., and Gustaffson, B. (1996). Ionotropic glutamate receptors. Their possible role in the expression of hippocampal synaptic plasticity. *Molecular Neurobiology* 12, 1-11.
- Ayalon, G., and Stern-Bach, Y. (2001). Functional assembly of AMPA and kainate receptors is mediated by several discrete protein-protein interactions. *Neuron* 31, 103-113.
- Bliss, T. V., and Collingridge, G. L. (1993). A synaptic model of memory: long-term potentiation in the hippocampus. *Nature* 361, 31-39.
- Bliss, T. V. P., and Lomo, T. (1973). Long-lasting potentiation of synaptic transmission in the dentate area of the anaesthetized rabbit following stimulation of the perforant path. *Journal of Physiology* 232, 331-356.
- Boulter, J., Hollmann, M., O'Shea-Greenfield, A., Hartley, M., Deneris, E., Maron, C., and Heinemann, S. (1990). Molecular cloning and functional expression of glutamate receptor subunit genes. *Science* 249, 1033-1037.
- Brejč, K., van Dijk, W. J., Klaassen, R. V., Schuurmans, M., van der Oost, J., Smit, A. B., and Sixma, T. K. (2001). Crystal structure of an ACh-binding protein reveals the ligand-binding domain of nicotinic receptors. *Nature* 411, 269-276.
- Changeux, J.-P., and Edelstein, S. J. (1998). Allosteric receptors after 30 years. *Neuron* 21, 959-980.
- Chen, G.-Q., Cui, C., Mayer, M. L., and Gouaux, E. (1999). Functional characterization of a potassium-selective prokaryotic glutamate receptor. *Nature* 402, 817-821.
- Chen, G.-Q., Sun, Y., Rongsheng, J., and Gouaux, E. (1998). Probing the ligand binding domain of the GluR2 receptor by proteolysis and deletion mutagenesis defines domain boundaries and yields a crystallizable construct. *Protein Science* 7, 1-8.
- Deisenhofer, J., Epp, O., Huber, R., and Michel, H. (1985). Structure of the protein subunits in the photosynthetic reaction center of rhodospseudomonas-viridis at 3 Å resolution. *Nature* 318, 618-624.
- Dingledine, R., Borges, K., Bowie, D., and Traynelis, S. F. (1999). The glutamate receptor ion channels. *Pharmacological Reviews* 51, 7-61.
- Doyle, D. A., Cabral, J. M., Pfuetzner, R. A., Kuo, A., Gulbis, J. M., Cohen, B. T., and Chait, R. (1998). The structure of the potassium channel: molecular basis of K<sup>+</sup>-conduction and selectivity. *Science* 280, 69-77.
- Ferrer-Montiel, A. V., and Montal, M. (1996). Pentameric subunit stoichiometry of a neuronal glutamate receptor. *Proceedings of the National Academy of Science USA* 93, 2747-2744.
- Grisshammer, R., and Tate, C. G. (1995). Overexpression of integral membrane proteins for structural studies. *Quarterly Review of Biophysics* 28, 315-422.

- Hawkins, L. M., Chazot, P. L., and Stephenson, F. A. (1999). *Journal of Biological Chemistry* 274, 27211-27218.
- Hollmann, M., and Heinemann, S. (1994). Cloned glutamate receptors. *Annu Rev Neurosci* 17, 31-108.
- Hollmann, M., Maron, C., and Heinemann, S. (1994). N-glycosylation site tagging suggests a three-transmembrane domain topology for the glutamate receptor GluR1. *Neuron* 13, 1331-1343.
- Hollmann, M., O'Shea-Greenfield, A., Rogers, A., and Heinemann, S. (1989). Cloning by functional expression of a member of the glutamate receptor family. *Nature* 342, 643-648.
- Jessell, T., and Kandel, E. (1998). Introduction: One decade of *Neuron*, six decades of neuroscience. *Neuron* 20, 367-369.
- Kandel, E., Schwartz, J. H., and Jessell, T. (1996). *Neurowissenschaften* (Heidelberg, Spektrum Akademischer Verlag).
- Kuner, T., Wollmuth, L. P., Karlin, A., Seeburg, P. H., and Sakmann, B. (1996). Structure of the NMDA receptor channel M2 segment inferred from accessibility of substituted cysteines. *Neuron* 17, 343-352.
- Kuusinen, A., Arvola, M., and Keinänen, K. (1995). Molecular dissection of the agonist binding site of an AMPA receptor. *The EMBO Journal* 14, 6327-6332.
- Lam, H., Chiu, J., Hsieh, M., Meisel, L., Oliveira, I., Shin, M., and Coruzzi, G. (1998). Glutamate-receptor genes in plants. *Nature* 396, 125-126.
- Laube, B., Hirai, H., Sturgess, M., Betz, H., and Kuhse, J. (1997). *Neuron* 18, 493-503.
- Leuschner, W. D., and Hoch, W. (1999). Subtype-specific assembly of  $\alpha$ -amino-3-hydroxy-5-methyl-4-isoxazole propionic acid receptor subunits is mediated by their N-terminal domain. *The Journal of Biological Chemistry* 274, 16907-16916.
- Madden, D. R. (2002). The structure and function of glutamate receptor ion channels. *Nature Rev Neuroscience* 3, 91-101.
- Mano, I., and Teichberg, V. I. (1998). *Neuroreport* 9, 327-331.
- Mayer, M. L., Olson, R., and Gouaux, E. (2001). Mechanisms for ligand binding to GluR0 ion channels: crystal structures of the glutamate and serine complexes and a closed apo State. *Journal of Molecular Biology* 311, 815-836.
- Mayer, M. L., Westbrook, G. L., and Guthrie, P. B. (1984). Voltage-dependent block by  $Mg^{2+}$  of NMDA responses in spinal cord neurons. *Nature* 309, 261-263.
- Monod, J., Wyman, J., and Changeux, J.-P. (1965). On the nature of allosteric transitions: a plausible model. *Journal of Biological Chemistry* 12, 88-118.
- Monyer, H., Seeburg, P. H., and Wisden, W. (1991). Glutamate-operated channels: developmentally early and mature forms arise by alternative splicing. *Neuron* 6, 779-810.
- Mosbacher, J., Schoepfer, R., Monyer, H., Burnashev, N., Seeburg, P. H., and Ruppersberg, J. P. (1994). A molecular determinant for submillisecond desensitization in glutamate receptors. *Science* 266, 1059-1061.

- Nakanishi, N., Schneider, N. A., and Axel, R. (1990). A family of glutamate receptor genes: evidence for the formation of heteromultimeric receptors with distinct channel properties. *Neuron* 5, 569-581.
- Nakanishi, S. (1990). Molecular diversity of glutamate receptors and implication for brain function. *Science* 258, 597-630.
- Paas, Y. (1998). The macro- and microarchitectures of the ligand-binding domain of glutamate receptors. *Trends in Neurosciences* 21, 117-125.
- Perutz, M. F. (1989). Mechanisms of cooperativity and allosteric regulation in proteins. *Quarterly Review of Biophysics* 22, 139-236.
- Pfeifer, T. A., Hegedus, D. D., Grigliatti, T. A., and Theilmann, D. A. (1998). Baculovirus immediate-early promoter-mediated expression of the Zeocin<sup>TM</sup> resistance gene for use as a dominant selectable marker in Dipteran and Lepidopteran insect cell lines. *Gene* 188, 183-193.
- Premkumar, L. S., and Auerbach, A. (1997). Stoichiometry of recombinant NMDA receptor channels inferred from single-channel current patterns. *Journal of General Physiology* 110, 485-502.
- Rosenmund, C., Stern-Bach, Y., and Stevens, C. F. (1998). The tetrameric structure of a glutamate receptor channel. *Science* 280, 1596-1599.
- Safferling, M. (1999). Expression und Charakterisierung von Neurotransmitterrezeptoren am Beispiel des nikotinischen alpha7-Acetylcholinrezeptors und des ionotropen Glutamatrezeptors GluRB. Dissertation, Universität Kaiserslautern.
- Safferling, M., Tichelaar, W., Kümmerle, G., Jouppila, A., Kuusinen, A., Kainänen, K., and Madden, D. R. (2001). First images of a glutamate receptor ion channel: oligomeric state and molecular dimensions of GluRB homomer. *Biochemistry* 40, 13948-13953.
- Schuster, C. M., Ultsch, A., Schloss, P., Cox, J. A., Schmitt, B., and Betz, H. (1991). Molecular cloning of an invertebrate glutamate receptor subunit expressed in *Drosophila* muscle. *Science* 254, 112-114.
- Seeburg, P. H. (1993). The molecular biology of mammalian glutamate receptor channels. *Trends in Pharmacological Sciences* 16, 359-365.
- Sokolova, O., Kolmakova-Partensky, L., and Grigorieff, N. (2001). Three-dimensional structure of a voltage-gated potassium channel at 2.5 nm resolution. *Structure* 9, 215-220.
- Sommer, B., Keinänen, K., Verdoorn, T. A., Wisden, W., Burnashev, N., Herb, A., Köhler, M., Takagi, T., Sakmann, B., and Seeburg, P. H. (1990). Flip and flop: a cell-specific functional switch in glutamate-operated channels of the CNS. *Science* 249, 1580-1585.
- Sommer, B., Kohler, M., Sprengel, R., and Seeburg, P. H. (1991). RNA editing in brain controls a determinant of Ion flow in glutamate-gated channels. *Cell* 67, 11-19.
- Stern-Bach, Y., Bettler, B., Hertley, M., Sheppard, P. O., O'Hara, P. J., and Heinemann, S. F. (1994). A point mutation in the glutamate binding site blocks desensitization of AMPA receptors. *Neuron* 21, 907-918.
- Sun, Y.-J., Wang, B.-C., and Hsiao, D.-D. (1998). The structure of glutamine-binding protein complexed with glutamine at 1.94 Å resolution: comparison with other amino acid binding proteins. *Journal of Molecular Biology* 278, 219-229.

- Tate, C. G., and Blakely, R. D. (1994). The effect on *N*-linked glycosylation on activity of the Na<sup>+</sup> and Cl<sup>-</sup>-dependent serotonin transporter expressed using recombinant baculovirus in insect cells. *The Journal of Biological Chemistry* 269, 26303-26310.
- Unwin, N. (1993). Neurotransmitter action: opening of ligand-gated ion channels. *Cell* 72 Suppl., 31-41.
- Unwin, N. (1995). Acetylcholine receptor channel imaged in the open state. *Nature* 373, 37-43.
- Verdoorn, T. A., Burnashev, N., Monyer, H., Seeburg, P. H., and Sakmann, B. (1991). *Science* 252, 1715-1718.
- Wenthold, R. J., Petralia, R. S., Blahos, J., and Niedzielski, A. S. (1996). Evidence for multiple AMPA receptor complexes in hippocampal CA1/CA2 neurons. *Journal of Neuroscience* 16, 1982-1989.
- Wenthold, R. J., Yokotani, N., Doi, K., and K., W. (1992). Immunochemical characterization of the non-NMDA glutamate receptor using subunit-specific antibodies. *The Journal of Biological Chemistry* 267, 501-507.
- Wo, Z. G., and Oswald, R. E. (1995). Unraveling the modular desing on glutamate-gated ion channels. *Trends in Neurosciences* 18, 161-168.
- Zamanillo, D., Sprengel, R., Hvalby, O., Jensen, V., Brunashev, N., Rozov, A., Kaiser, K. M. M., Köster, H., Borchardt, T., Worley, P., *et al.* (1999). Importance of AMPA receptors for hippocampal synaptic plasticity but not for spatial learning. *Science* 284, 1805-1811.
- Zhou, Y., Morais-Cabral, J. H., Kaufman, A., and MacKinnon, R. (2001). Chemistry of ion coordination and hydration revealed by K<sup>+</sup> channel-Fab complex at 2.0 Å resolution. *Nature* 414, 43-48.

## **2. STRUCTURAL BIOLOGY BY ELECTRON MICROSCOPY**

This chapter evaluates the potential of electron microscopy and explains the basics of image formation. In a second part it describes the approach of the software package IMAGIC, which was used in combination with electron microscopy for the structural analysis of isolated GluR-B molecules.

### **2.1. ELECTRON MICROSCOPY**

#### **2.1.1. POTENTIAL OF ELECTRON MICROSCOPY**

Structural analysis at the level of atomic resolution by X-ray crystallography requires three-dimensional (3D) crystallization of proteins. To a homogeneous protein solution nuclear magnetic resonance (NMR) spectroscopy can be applied. This method can even capture dynamic changes in the protein structure. For technical reasons the molecular mass of protein structures solved by NMR so far was not higher than ca. 30 kD. Presently these limits are being pushed and structural analysis of proteins with a molecular weight of ca. 100 kD seems realistic (P. Güntert, personal communication). X-ray and NMR are powerful techniques, but both require milligram amounts of protein. A third method, electron microscopy (EM), is the only technique that permits the analysis of both single protein molecules and two-dimensional crystalline protein structures. Image analysis of single biomacromolecular complexes (called “single particles”) has been successfully used to reveal the symmetry of oligomeric proteins and resolve subunit boundaries. The 3D reconstructions resulting from electron microscopic analysis can be fitted with available known high-resolution domain substructures, which have been solved by X-ray crystallography (Luo et al., 1999).

The inherent problem of electron microscopy in the field of structural biology is the low contrast. In the absence of a contrast agent proteins can be imaged with very low contrast only. The scattering densities of atoms in biological samples and of the water atoms are closely matched resulting in extremely low contrast. Since biological samples are sensitive to radiation in cryo-electron microscopy contrast enhancement cannot be achieved by applying higher electron intensities. To prevent beam damage micrographs of biological samples are taken under low dose conditions. To enhance contrast in cryo-electron microscopy micrographs can be taken at larger defocus (see paragraph 2.1.3.). In addition, contrast-enhancement can be achieved by energy filtering (Schröder et al., 1990), (Schröder et al.,

1993). This approach considers that inelastically scattered electrons cause a decrease in the signal to noise ratio. The energy-filter consists of a system of magnets, which separates electrons spatially according to their energies. Using a slit, inelastically scattered electrons can be eliminated. Only those electrons, which have lost marginal amounts of energy (0-15 eV) pass through.

In negatively stained specimen the contrast is higher. The stain uranyl acetate scatters electrons more strongly than the atoms of the protein sample. It has a fixative effect on the sample and combines strong contrast enhancement with moderate radiation sensitivity. Since the stain forms an amorphous supportive layer, in which single particles are embedded, the protein molecules appear in negative contrast; the specimen is called “negatively stained”. For an ideal preservation of the protein structure the stain layer should be as thick as the height of the protein molecule thus the stain can occupy hydrated regions in and around the molecule. The analysis of negatively stained single protein molecules can even be performed with microgram amounts of protein and is therefore ideal for structural analysis of isolated proteins like GluR-B. However, negative staining often shows artifacts such as partial staining (Cejka et al., 1992), which can result in an incomplete preservation of the protein structure.

Compared to the negative staining technique cryo-electron microscopy (Dubochet et al., 1988) supports the preservation of internal protein structures much better since proteins are vitrified in their buffer. For two decades cryo-electron microscopy has been the only technique for the structural analysis of the *Escherichia coli* ribosome (Penczek et al., 1992), (Stark et al., 1997). It could reveal the arrangement of tRNAs in pre- and posttranslocational ribosomes at resolution of 20 Å (Stark et al., 1997). Despite the recent high-resolution X-ray structures of the complete *Thermus thermophilus* 70S ribosomal subunit at 5.5 Å resolution (Yusupov et al., 1999) and the structure of the large 50S ribosomal subunit from the bacterium *Haloarcula marismortui* at a resolution of 2.4 Å (Ban et al., 2000) the cryo-EM technique is still a very attractive technique for structural analysis of the ribosome since it can give insights into the dynamic nature of the cell’s protein factory (Stark et al., 2001). At present the technical limits of single particle cryo-electron microscopy are being pushed to yield structures at higher resolution. Beside the analysis of single particles electron microscopy permits the structural analysis of thin two-dimensional (2D) crystals formed by proteins. This approach is called “electron-crystallography”. Using electron-crystallography,

atomic or near atomic resolution has been achieved for proteins like bacteriorhodopsin (Henderson et al., 1990), the light-harvesting complex (Kühlbrandt et al., 1994), aquaporin (Walz et al., 1997) and the cytoskeletal protein tubulin (Nogales et al., 1998).

### 2.1.2. ELECTRON MICROSCOPY – TECHNICAL PRINCIPLES

As the name implies, in transmission electron microscopy (TEM)<sup>1</sup> electrons pass through the specimen. However, the electron wave with the wave-length  $\lambda$  interacts with the protein sample before the electrons strike the photographic plate. The components (magnetic lenses and diaphragms) of a typical EM are described in a schematic drawing of an EM in Figure 2.1.2.A.

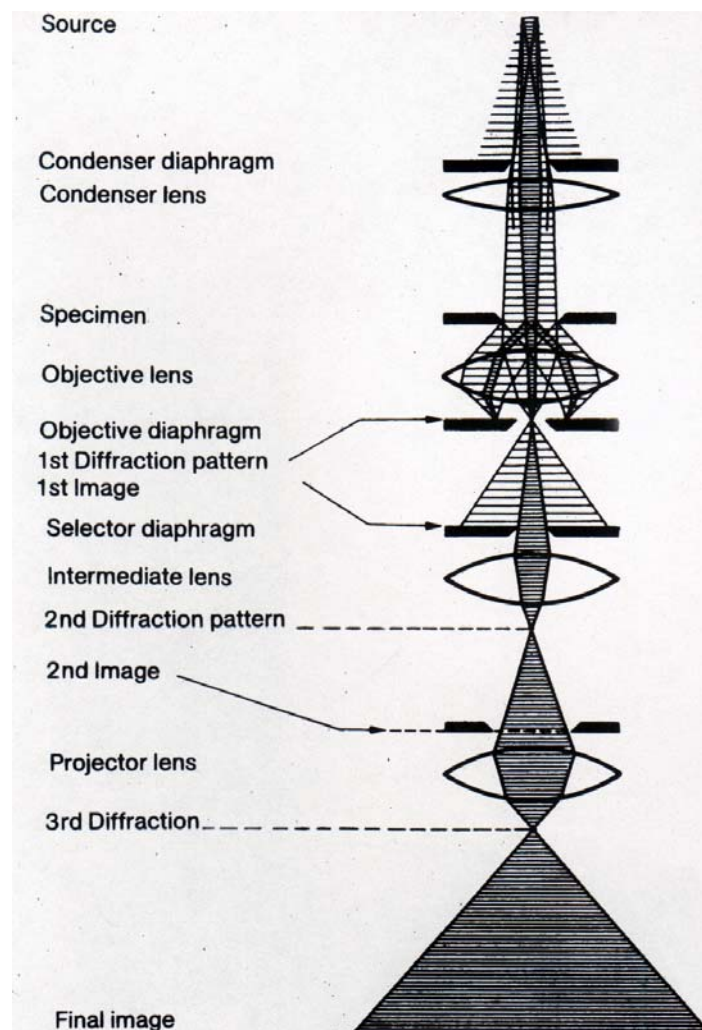


Figure 2.1.2.A.: Ray diagram for a transmission EM according to (Reimer, 1989).

Electrons are emitted by thermionic emission from a heated tungsten filament or from a single crystal of lanthanum hexaboride. An alternative electron source producing highly coherent electrons is the field emission gun. Here electrons are released from unheated metal surfaces

<sup>1</sup> In this work TEM will be referred to as electron microscopy (EM).

that are exposed to a high potential of several kV by the tunneling effect. The electron source is of major importance for the coherence of illumination. Emitted electrons are accelerated towards the anode by a high voltage (80-400 kV) before they hit the sample.

For image formation two types of interaction between the sample and the incident electron wave are important: inelastic and elastic scattering. During elastic scattering the electrons interact coulombically with the nuclei in the sample (electron-nucleus interaction), whereas inelastic scattering is an electron-electron interaction with the electrons in the sample. Inelastically scattered electrons that pass the objective diaphragm increase the background noise. (The theory of electron scattering is explained in more detail in the book of L. Reimer (Reimer, 1989).) Both, inelastic and elastic scattering cause image contrast. However, elastic scattering, which creates the phase contrast is the fundamental scattering process in EM since scattered and unscattered electrons are coherent. After elastic scattering the amplitude of an electron wave is modulated and its phase is shifted. This phase shift  $\chi(\alpha)$  is a function of the scattering angle  $\alpha$ . The phase contrast is produced by the interference of the scattered electron wave that passes through the objective diaphragm with the wave of unscattered primary electrons. Those electrons, which were elastically scattered at very large angles are eliminated by the objective diaphragm and thus create amplitude contrast.

After transmission of the radiation through the object the first diffraction pattern is formed in the back focal plane of the objective lens. Mathematically, the diffraction pattern formed by an ideal lens is described by the Fourier transform of the object transmission function (Slayter and Slayter, 1992). However, this Fourier transform is always modified by additional functions like the aperture function, which accounts for the fact that the transform is incomplete when some radiation leaves the object at very large scattering angles (see Figure 2.1.3.A).

### 2.1.3. ELECTRON MICROSCOPY – IMAGE FORMATION

Contrast enhancement in electron microscopy is essential for the interactive selection of the protein molecules and their alignment during image analysis. In cryo-electron microscopy image contrast is dominated by the phase contrast, whereas in negative stain experiments a strong scatterer like the heavy atom salt uranyl acetate is increasing amplitude contrast. Although in this project only the data of negative stain experiments were used for image analysis (see 4.4.3.) in the following the principles of image formation are described for cryo-electron microscopy since the evaluation of cryo-data covers the aspects of image formation more completely.

By defocusing the range of contrast can be extended. Therefore in cryo-electron microscopy micrographs are deliberately taken slightly under focus. By changing the focus ( $\Delta f$ ) of the objective lens (and by spherical aberration) the phase of the scattered wave components is additionally shifted and thus phase contrast is enhanced. The corresponding phase shift  $\chi(\alpha)$  was derived in 1949 by O. Scherzer and is described by the wave aberration function in (1).

$$\chi(\alpha) = 2\pi / \lambda \left[ -\frac{1}{4} C_s \alpha^4 + \frac{1}{2} \Delta f \alpha^2 \right] \quad (1)$$

The phase shift  $\chi(\alpha)$  is a function of the angle of elastic scattering ( $\alpha$ ).  $C_s$  is the coefficient of spherical aberration, which is caused by the difference in focal lengths between the axial and marginal zones of a lens. The electron's wavelength corresponds to  $\lambda$ .

When both amplitude and phase contrast contribute to the image, the Fourier transform of this image can be described by equation (2), which was derived by Erickson and Klug (Erickson and Klug, 1971).

$$T_{tot}^i(\alpha, \phi) = -T^0(\alpha, \phi) A(\alpha) f(\alpha) [\sin \chi(\alpha) + Q(\alpha) \cos \chi(\alpha)] \quad (2)$$

$T^0(\alpha, \phi)$  in equation (2) is the Fourier transform of the object given in polar coordinates. (In polar coordinates the reciprocal radial coordinate corresponds to  $\alpha/\lambda$  and the azimuthal coordinate is  $\phi$ . The spatial frequency is the reciprocal resolution of object details, which contribute to the object transform  $T^0(\alpha, \phi)$ .) The modulation of phase contrast and amplitude

contrast in Fourier space is described by the sin- respectively the cos-function. The term  $\sin\chi(\alpha)$  is the phase-contrast transfer function and the term  $\cos\chi(\alpha)$  is the amplitude-contrast function. Factor  $Q(\alpha)$  in equation (2) gives the ratio of amplitude to phase contrast. Since the image contrast is dominated by the phase contrast,  $Q(\alpha)$  is  $< 1$  in cryo-electron microscopy. Factor  $A(\alpha)$  is a function, which accounts for the effects of the objective aperture and  $f(\alpha)$  is the atomic scattering factor that accounts for elastic scattering of electrons by a single atom. The influence of different defocus values ( $\Delta f$ ) on the phase-contrast function,  $-\sin\chi(\alpha)$ , is illustrated in Figure 2.1.3.A.

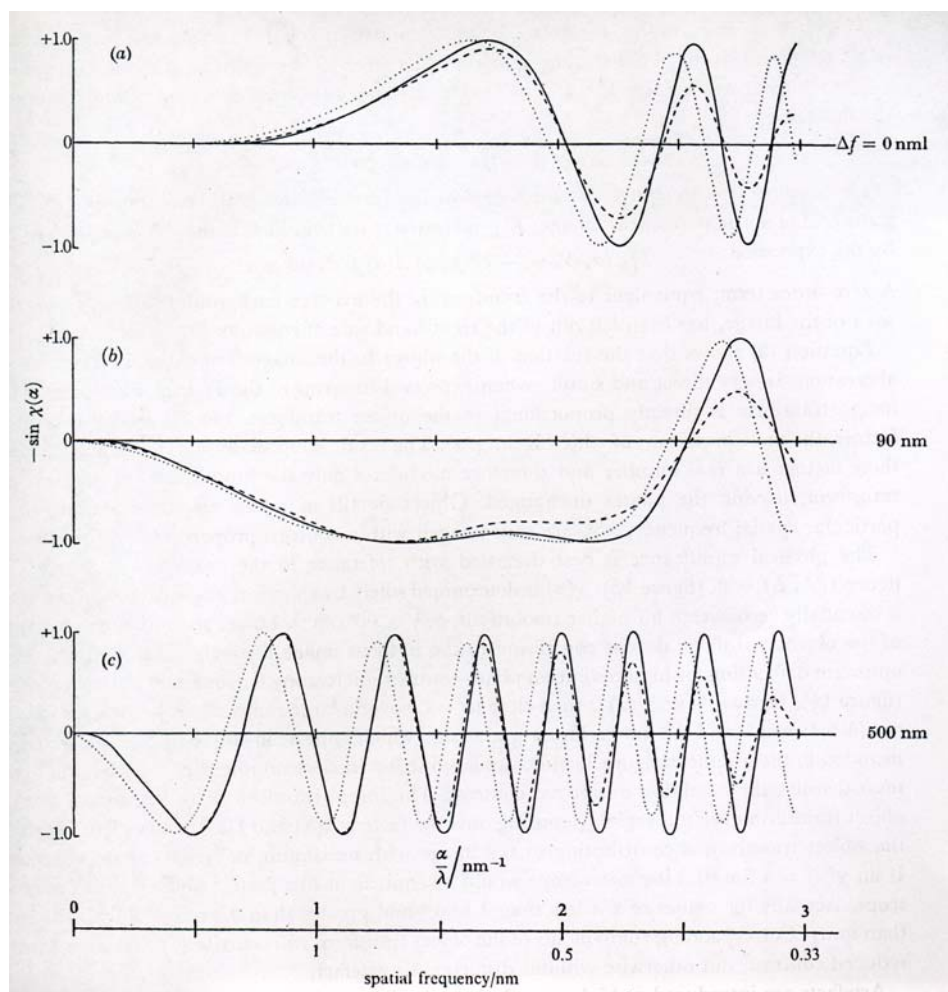


**Figure 2.1.3.A:** The phase-contrast transfer function,  $-\sin\chi(\alpha)$ , plotted as a function of  $\alpha/\lambda$ , in  $\text{nm}^{-1}$ , for  $\lambda=0.0042 \text{ nm}$ ,  $C_s=1.3 \text{ mm}$  and for the indicated values of  $\Delta f$ . The solid curves are for pure phase contrast. The dashed curves are corrected for the effects of chromatic aberration with normal electric instabilities, by averaging over a range of  $\pm 20 \text{ nm}$ . When the phase-contrast function  $\sin\chi(\alpha)$  is corrected for the effects of chromatic aberration and for the effects of the partial coherence of the electron source its amplitude is damped (see dashed curves and dotted curves). Taken from (Erickson and Klug, 1971).

When  $\Delta f = 0$  (see Figure 2.1.3.A. (a))  $\chi(\alpha)$  is determined by spherical aberration only. For values of  $\alpha/\lambda$  lower than 0.75 there is no phase contrast. For the conditions of Figure 2.1.3.A. the defocus for high-resolution phase-contrast microscopy is around 90 nm under focus. As Figure 2.1.3.A. (b) shows in this situation  $-\sin\chi(\alpha)$  is close to -1 over a large range of resolutions, i.e. for values of  $\alpha/\lambda$  between 1 and  $2.3 \text{ nm}^{-1}$ . Over this area the contribution of phase contrast to the image contrast is maximal. At larger under focus values (as shown in Figure 2.1.3.A. (c) with  $\Delta f = 500 \text{ nm}$ ) the peak of normal phase contrast becomes sharper and moves to lower values for the spatial frequency. When  $\sin\chi(\alpha)$  changes its sign the contrast is reversed. This means that image details of corresponding reciprocal spacing will be dark where they should be light. The contrast reversals are a source for artifacts and require CTF correction when zero-crossings are present within the processed data (Frank et al., 1995).

Specimens for electron microscopy include a continuous range of spacings. In principle, however, these spacings can be divided into individual periodicities or spatial frequencies, of which each corresponds to constructive interference between electron rays leaving the specimen at an appropriate angle  $\alpha$  (Slayter and Slayter, 1992). The spatial frequencies contained in the sample are projected into the micrograph. Closely spaced details, i.e. details in the protein structure are represented by high spatial frequencies, whereas comparably coarse details like the overall shape protein complex are represented by low spatial frequencies. The value of the contrast transfer function (CTF) describes the extent to which the spatial frequencies are transmitted by the electronic lens.

To facilitate the alignment and classification of particles raw-data are band-pass filtered. The low-frequency cut-off (LFCO) parameter of the band-pass filter should be adjusted to the size of the protein particle, whereas its high-frequency cut-off (HFCO) parameter should consider the first zero-crossing, if no CTF corrections was made. When a CTF correction was made the HFCO is chosen according to the expected resolution of the data. The term resolution refers to the minimum separation of points actually observed in the image of a given specimen. The cut-off parameters applied in the image analysis software IMAGIC (see paragraphs 2.2. and 4.4.3.) have no dimension. They are given as the fraction ( $f$ ) of the Nyquist frequency with values from 0 to 1. When  $P$  corresponds to the pixel size the Nyquist frequency is  $1/(2 \times P)$ . Therefore each fraction  $f$  between 0 and 1 corresponds to the spatial frequency  $f/(2 \times P)$ .

## 2.2. 3D RECONSTRUCTION BY ANGULAR RECONSTITUTION

Digitization of micrographs and subsequent image processing of single protein molecules (called “single particles”) form the second part in the structural analysis of a non-crystalline protein by electron microscopy. The goal of image processing in structural biology is the reconstruction of a three-dimensional model using noisy two-dimensional raw-data. In this project the images of single GluR-B molecules were processed using the software package IMAGIC-5 (Imagic Science Software GmbH, Berlin) (v. Heel et al., 1996), (v. Heel et al., 2000). The image processing procedure followed in this project is summarized in Figure 2.2.A.

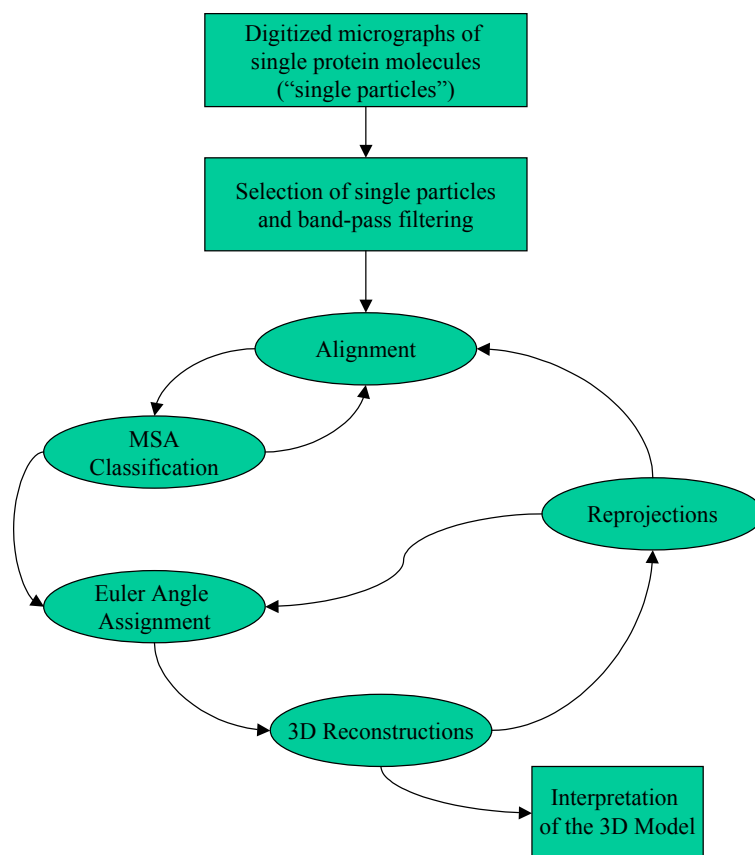


**Figure 2.2.A:** Scheme for the 3D reconstruction of single protein molecules with IMAGIC according to (Serysheva et al., 1995).

After digitization of micrographs single protein molecules are selected on the computer screen and are stored in a separate file. By the subsequent band-pass filtering the structurally irrelevant background is removed. To improve the signal to noise ratio (SNR) a large number of selected single particles is aligned, sorted and averaged in homogeneous groups called “class averages”. For a better understanding of the alignment procedure and the subsequent

classification some general aspects of data acquisition will be explained first. In the electron microscope the three-dimensional structure of protein molecules in different orientations is projected along the electron beam ( $z$ ) to the two-dimensional plane of the micrograph. Because of this projection protein particles on the micrograph have only the two “in-plane” translational degrees of freedom ( $x, y$ ) instead of three ( $x, y, z$ ). The molecule’s three rotational degrees of freedom are represented by the Euler angles  $\alpha$ ,  $\beta$  and  $\gamma$ . While  $\alpha$  represents the in-plane degree of rotational freedom the angles  $\beta$  and  $\gamma$  correspond to rotations of the molecules in directions out of the plane. Differences in these “out-of-plane” rotations ( $\beta, \gamma$ ) characterize fundamentally different projections and thus provide three-dimensional (3D) information of the protein molecule. During the initial alignment the in-plane degrees of freedom ( $x, y$  and  $\alpha$ ), which characterize the in-plane differences between otherwise identical particles are used to bring the particles into a common orientation and position. The subsequent classification procedure is used to find different characteristic views of the protein molecules associated with the two out-of-plane degrees of freedom. In the following it will be explained how these basic procedures and the Euler angle assignment were implemented in the IMAGIC software.

The 3D reconstruction approach of IMAGIC is based on the angular reconstitution (AR) method (v. Heel, 1987), which exploits the random orientations of protein molecules. The potential of the AR approach was first demonstrated by the reconstruction of the skeletal muscle calcium release channel (Serysheva et al., 1995) and the reconstruction of *Lumbricus terrestris* Hemoglobin (Schatz et al., 1995). Within the IMAGIC procedure two sub-procedures (see Figure 2.2.A) are applied iteratively:

- I.) Alignment, classification and averaging of many images to improve the signal to noise ratio (SNR).
- II.) Assignment of Euler angles to a set of two-dimensional input projections and generation of a 3D model.

The band-pass filtered images are centered by translational alignment in several iterative cycles relative to the rotational sum of all particles. The subsequent alignment is a cross-correlation-based procedure, which does not need a reference and thus avoids a possible reference bias problem. Aligned and classified images can be averaged and thus have an improved SNR, which facilitates the subsequent data processing. The alignment is refined by iterative cycles of the multi-reference alignment (MRA) (v. Heel and Stöffler-Meilicke,

1985). During the MRA procedure class averages of one cycle are references for the following cycle. Subsequently the multivariate statistical analysis (MSA) classification procedure is applied. This technique considers images as a linear combination of the main eigenvectors (=eigenimages) of the data set and thus reduces the total amount of data (v. Heel and Frank, 1981). The averaging after each classification helps to improve the signal to noise ratio. New class averages are used as references for the following MRA/MSA classification round. By this iterative procedure the internal variance of the classes (“intra-class variance”) are minimized and at the same time the inter-class variances between class averages are maximized. The final class averages are characteristic projection views of the three-dimensional protein molecule. The complexity of the MSA output is considerably reduced compared to that of the initial data set. A high SNR in the projection views is of great importance for an accurate assignment of Euler angles.

During assignment of Euler angles with the angular reconstitution (AR) algorithm (v. Heel, 1987) the orientation of projection views relative to each other (differences in the “out-of plane rotations”  $\beta$  and  $\gamma$ ) are assigned *a posteriori*. The AR technique is based on the common line projection theorem (CLP). According to the CLP theorem any two 2D projections of the same three-dimensional object share at least one one-dimensional projection, which is a line. By searching for the common line projections the spatial relationships, i.e. the angles between different projection views can be determined. It requires at least three different projections of an asymmetric particle to find the relative Euler angle orientations of the projection views (v. Heel, 1987). After the assignment of Euler angles to projection views a first 3D reconstruction is calculated using the exact-filter back projection algorithm (Harauz and v. Heel, 1986), (Radermacher et al., 1987). From this first 3D model reprojections can be calculated. A good correspondence between input projections and reprojections illustrates how well the input class averages fit the 3D volume of the model. While poor images are eliminated from the refined set of class averages the other projections are used for further multi-reference alignments followed by MSA classification and Euler angle assignment. Therefore they are called “anchor sets”. The whole procedure is done iteratively and is therefore called “anchor set refinement”. After some cycles the results stabilize and the 3D map shows no further improvements. By Fourier Shell Correlation (FSC) (Harauz and v. Heel, 1986) the resolution of a 3D reconstruction is determined.

**REFERENCES OF CHAPTER 2**

- Ban, N., Nissen, P., Hansen, J., Moore, P. B., and Steitz, T. A. (2000). The complete atomic structure of the large ribosomal subunit at 2.4 Å resolution. *Nature* 289, 905-920.
- Cejka, Z., Kleinz, J., Santini, C., Hegerl, R., and Ghirelli Magaldi, A. (1992). The Molecular architecture of the extracellular hemoglobin of ophelia bicornis: analysis of individual molecules. *Journal of Structural Biology* 109, 52-60.
- Dubochet, J., Adrian, M., J., C. J., C., H. J., Lepault, J., McDowell, A. W., and Schultz, P. (1988). Cryo-electron microscopy of vitrified specimens. *Quarterly Review of Biophysics* 21, 129-228.
- Erickson, H. P., and Klug, F. R. S. (1971). Measurement and composition of defocusing and aberrations by fourier processing of electron micrographs. *Philosophical Transactions of the Royal Society of London Series B* 261, 105-118.
- Frank, J., Zhu, J., Penczek, P., Li, Y., Srivastava, S., Verschoor, A., Radermacher, M., Grassucci, R., Lata, R. K., and Agrawal, R. K. (1995). A model of protein synthesis based on cryo-electron microscopy fo the *E. coli* ribosome. *Nature* 376, 441-444.
- Harauz, G., and v. Heel, M. (1986). Exact filters for general geometry three dimensional reconstruction. *Optik* 73, 146-156.
- Henderson, R., Baldwin, J. M., Ceska, T. A., Zemlin, F., Beckmann, E., and Downing, K. H. (1990). Model for the structure of bacteriorhodopsin based on high-resolution electron cryo-microscopy. *J Mol Biol* 213, 899-929.
- Kühlbrandt, W., Wang, D. N., and Fujiyoshi, Y. (1994). Atomic model of plant light-harvesting complex by electron crystallography. *Nature* 367, 614-621.
- Luo, R. Z.-T., Beniac, D. R., Fernandes, A., Cecil, C. Y., and Ottensmeyer, F. P. (1999). Quaternary structure of the insulin-insulin receptor complex. *Science* 285, 1077-1080.
- Nogales, E., Wolf, S., and Downing, K. H. (1998). Structure of the ab tubulin dimer by electron crystallography. *Nature* 391, 199-203.
- Penczek, P., Radermacher, M., and Frank, J. (1992). Three-dimensional reconstruction of single particles embedded in ice. *Ultramicroscopy* 44, 33-53.
- Radermacher, M., Wagenknecht, T., Verschoor, A., and Frank, J. (1987). Three-dimensional reconstruction from a single-exposure, random conical tilt series applied to the 50S ribosomal subunit of *Echerichia coli*. *Journal of Microscopy* 146, 113-136.
- Reimer, L. (1989). Transmission electron microscopy (Heidelberg, Springer).
- Schatz, M., Orlova, E. V., Dube, P., Jäger, J., and v. Heel, M. (1995). Structure of *Lumbricus terrestris* hemoglobin at 30 Å resolution determined using angular reconstitution. *Journal of Structural Biology* 114, 28-40.
- Schröder, R. R., Hofmann, E., and Menetret, J. F. (1990). Zero-loss energy filtering as improved imaging mode in cryo-electron microscopy of frozen-hydrated specimens. *Journal of Structural Biology* 105, 28-34.
- Schröder, R. R., Manstein, D. J., Jahn, W., Holden, H., Rayment, I., Holmes, K. C., and Spudich, J. A. (1993). Three-dimensional atomic model of F-actin decorated with *Dictyostelium* myosin S1. *Nature* 364, 171-174.

- Serysheva, I. I., Orlova, E. V., Chiu, W., Sherman, M. B., Hamilton, S. L., and v. Heel, M. (1995). Electron cryomicroscopy and angular reconstitution used to visualize the skeletal muscle calcium release channel. *Structural Biology* 2, 18-24.
- Slayter, E. M., and Slayter, H. S. (1992). Light and electron microscopy, Cambridge University Press).
- Stark, H., Dube, P., Lührmann, R., and Kastner, B. (2001). Arrangement of RNA and proteins in the spliceosomal U1 small nuclear ribonucleoprotein particle. *Nature* 409, 539-542.
- Stark, H., Orlova, E. V., Jutta, R.-A., Jünke, N., Mueller, F., Rodnina, M., Wintermeyer, W., Brimacombe, R., and v. Heel, M. (1997). Arrangement of tRNAs in pre- and posttranslational ribosomes revealed by electron cryomicroscopy. *Cell* 88, 19-28.
- v. Heel, M. (1987). Angular reconstitution: a posteriori assignment of projection directions for 3D reconstruction. *Ultramicroscopy* 21, 111-124.
- v. Heel, M., and Frank, J. (1981). Use of multivariate statistics in analysing the images of biological macromolecules. *Ultramicroscopy* 6, 187-194.
- v. Heel, M., Gowen, B., Matadeen, R., Orlova, E. V., Finn, R., Pape, T., Cohen, D., Stark, H., Schmidt, R., Schatz, M., and Patwardhan, A. (2000). Single-particle electron cryomicroscopy: towards atomic resolution. *Quarterly Review of Biophysics* 33, 307-369.
- v. Heel, M., Harauz, G., Orlova, E. V., Schmidt, R., and Schatz, G. (1996). A new generation of the IMAGIC image processing system. *Journal of Structural Biology* 116, 17-24.
- v. Heel, M., and Stöffler-Meilicke, M. (1985). Characteristic views of *E. Coli* and *B. stearothermophilus* 30S ribosomal subunits in the electron microscope. *The EMBO Journal* 4, 2389-2395.
- Walz, T., Hirai, H., Murata, K., Heymann, B. J., Mitsuoka, K., Fujiyoshi, Y., Smith, B., Agre, P., and Engel, A. (1997). The three-dimensional structure of aquaporin-1. *Nature* 387, 624-627.
- Yusupov, M. M., Yusupova, G. Z., Baucom, A., Lieberman, K., Earnest, T. N., Cate, J. H. D., and Noller, H. F. (1999). Crystal structure of the ribosome at 5.5 Å resolution. *Science* 292, 883-896.

### 3. MATERIALS AND METHODS

#### 3.1. PRIMARY STRUCTURE OF GLUR-B

The full-length flop isoform of the ionotropic glutamate receptor subunit B from rat (SWISS-PROT accession number P19491, ref. 4 or EMBL genebank accession number M36419) was used for cloning. The first 21 amino acids, coded by the sequence, form the signal peptide. The following 862 amino acids form one subunit of GluR-B. The final cloning construct corresponds to residues 1-861 since it omits the native C-terminal Ile residue of GluR-B<sub>flop</sub>.

1	MQKIMHISVL	LSPVLWGLIF	GVSSNSIQIG	GLFPRGADQE	YSAFRVGMVQ
51	FSTSEFRLTP	HIDNLEVANS	FAVTNAFCSQ	FSRGGVYAIFG	FYDKKSVNTI
101	TSFCGTLHVS	FITPSFPTDG	THPFVIQMRP	DLKGALLSLI	EYYQWDFKAY
151	LYDSDRGLST	LQAVLDSAAE	KKWQVTAINV	GNINNDKKDE	TYRSLFQDLE
201	LKKERRVILD	CERDKVNDIV	DQVITIGKHV	KGYHYIIANL	GFTDGDLLKI
251	QFGGANVSGF	QIVDYDDSLV	SKFIERWSTL	EEKEYPGAHT	ATIKYTSALT
301	YDAVQVMTEA	FRNLRKQRIE	ISRRGNAGDC	LANPAVPWGQ	EIERALKQ
351	VQVEGLSGNI	KFDQNGKRIN	YTINIMELKT	NGPRKIGYWS	VDKMVVTLT
401	ELPSGNDTSG	LENKTVVWTT	ILESPYVMK	KNHEMLEGNE	YEGYCVDLA
451	AEIAKHCQFK	YKLTIVGDGK	YGARDADTKI	WNGMVGELVY	GKADIAIAPL
501	TITLVREEVI	DFSKPFMSLG	ISIMIKKPQK	SKPGVFSFLD	PLAYEIW <b>MC</b> I
551	<b>VFAYIGVSVV</b>	<b>LFLVSRFSPY</b>	EWHTTEEFEDG	RETQSSESTN	FGIFNSLWF
601	<b>SLGAFMRQGC</b>	<b>DISPRSLSGR</b>	<b>IVGGVWVFFT</b>	<b>LIISSTAN</b>	<b>LAAFLTVERM</b>
651	VSPIESAEDL	SKQTEIAYGT	LDSGSTKEFF	RRSKIAVFDK	WTYMRSAEP
701	SVFVRTTAEG	VARVRKSKGK	YAYLLESTMN	EYIEQRKPCD	KVGGNLDS
751	KGYGIATPKG	SSLGNAVNLA	VLKLNEQGLL	DKLKNKWWYD	KGECGSGGGD
801	SKEKTSALSL	<b>SNVAGVFYIL</b>	<b>VGGLGLAMLV</b>	ALIEFCYKSR	AEAKRMKVAK
851	NPQNINPSSS	QNSQNFATYK	EGYNVYGIES	VKI	

**Figure 3.1.A: Native GluR-B<sub>flop</sub> Proteinsequenz; the N-terminal signal peptide is followed by the X-domain, which comprises amino acids 1-380, the ligand-binding domain consists of S1 (381-524) and S2 (623-789). Amino acids forming the four hydrophobic transmembrane domains are printed in bold letters.**

Purification of the GluR-B protein is facilitated by a FLAG-epitope formed by 8 amino acids following the signal sequence at the N-terminus and a hexahistidine tag at the C-terminus.

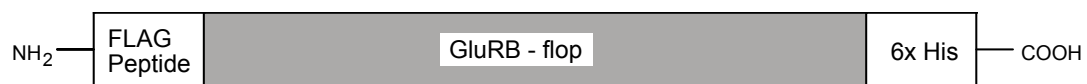


**Figure 3.1.B: Modifications to facilitate protein purification of GluR-B**

Including these affinity epitopes the construct consists of 897 amino acids. In the N-terminal domain and in the S1-domain there are potential locations for glycosylation. According to the amino acid sequence the molecular weight of one GluR-B subunit is 98.4 kD, or 104 kD for a glycosylated subunit.

### 3.2. EXPRESSION OF GLUR-B IN INSECT CELLS

In this project the baculovirus-mediated expression of GluR-B and the expression of GluR-B protein in stable cell lines was applied. The principles of both systems are summarized in the APPENDIX. The cultivation of cells in both systems was comparable although different media were used.

#### 3.2.1. CULTIVATION OF INSECT CELLS

Virus induced expression of GluR-B involved three cell lines: *Spodoptera frugiperda* (Sf) Sf9 cells were used for virus amplification and Sf21 were used for virus titration. For protein expression High5 insect cells were used. High5 cells are derived from the insect *Trichoplusia ni*. *Trichoplusia ni* cells are commonly used for protein expression since the yield can be up to five times higher compared with Sf9 cells. Cells were passaged continuously and used for  $\leq$  60 passages. Low passage number stocks were stored in liquid nitrogen.

For protein expression *Trichoplusia ni* High5 insect cells were grown in suspension culture and infected with recombinant baculovirus at a cell density of ca.  $2.0 \times 10^6$  cells/mL. The multiplicity of infection (MOI) was five plaque forming-units (PFU) per cell. The corresponding ratio between volumes of High5 cells and virus solution varied between 7:1 and 4:1. After incubation at 27°C for ca. 90 hours, the cells were harvested at 4°C. Insect cells have to be handled in a sterile environment. The use of a higher percentage (10%) of fetal calf serum (FCS) is recommended for procedures like freezing of cells, for storage in liquid nitrogen and plaque assays. Cell culture media and supplements used for cultivation of insect cells are listed in Table 3.2.1.A.

Type of cell	Cell culture medium
Sf21	Sf-900 II SFM (Gibco BRL) medium was supplemented with 1% antibiotic/antimycotic (add 10 ml of 100x to 1000 mL medium)
Sf9	Grace's Insect Medium (Gibco BRL) was supplemented with 2.25 $\mu$ g/mL Amphotericin (Sigma), 9.10 $\mu$ g/mL Gentamycin (Sigma), 0.1% Pluronic F 68 (Gibco BRL) and 10% fetal calf serum
High5	Ex-Cell 400 <sup>TM</sup> plus L-glutamine (JRH-Bioscience)
Stable Cells	Express Five SFM (Gibco BRL) plus 100x Glutamax (Gibco BRL)

**Table 3.2.1.A: Cell culture media.**

### **3.2.2. FREEZING OF INSECT CELLS**

Cells were grown in confluent layers in 75 cm<sup>2</sup>-cell culture flasks before freezing for long-term storage. After removal of the supernatant medium cells were rinsed off the plastic with fresh 27° C medium. Cell suspensions were centrifuged for 10 minutes at 1000× g and the supernatant was discharged. The cell pellet was resuspended in the cell-type specific medium (Table 3.2.2.A), which was supplemented with 10 % DMSO. High5 cells were resuspended at a density of 3 x 10<sup>6</sup> cells/mL; Sf9 and Sf21 cells at 6 x 10<sup>6</sup> cells/mL. 1 mL aliquots were cooled down in the following step-wise manner: incubation for 1 hour at -20°, incubation for 24 hours at -80° and finally storage at -196° in liquid nitrogen.

### **3.2.3. THAWING OF INSECT CELLS**

Long-term storage conditions were identical for all cells. 1 mL aliquots containing ca. 2-3 × 10<sup>6</sup> cells were stored in cryo vials (Greiner) under liquid nitrogen (-196 ° C). For thawing tubes were gently rocked at room temperature. When the cells suspension began to thaw it was transferred to a 25 cm<sup>2</sup>-cell culture flasks containing 4 mL ice cool medium. Cryo tubes were washed with ethanol before opening. Cells were incubated at 27° C. After ca. 30 minutes vital cells attached to the bottom of the plastic flask. Floating cells were removed with the supernatant medium. 4 mL fresh medium, warmed to 27° C, was added immediately.

### **3.2.4. VIRUS AMPLIFICATION**

Baculoviruses were amplified in Sf9 cells. At a density of ca. 1.5 × 10<sup>6</sup> cells/mL cells were infected with 0.1 multiplicity of infection (MOI) and incubated for 13 days in shaker flasks. The corresponding ratio between volumes of Sf9 cells and virus stock varied (500:1 to 400:1). Infection with a low MOI allows further amplification and thus produces a knock-on-effect: Initially only 10% of the cells are infected but during a second cycle of infection newly amplified Sf9 cells will be infected. The result is a higher virus titer.

### **3.2.5. VIRUS TITRATION**

In the baculovirus expression system a high and stable virus titer is essential for high protein yields. Thus virus titration is important for the optimization of protein expression. Sf 21 cells cultured in Sf-900 II SFM (Gibco BRL) medium supplemented with antibiotics and fetal calf serum proved to be most useful for plaque-assays. In plastic Petri dishes (35 mm diameter) for

these assays per dish  $1-1.5 \times 10^6$  Sf 21 cells were plated out. Cells were rocked on a Certomat TC2 (Braun Biotec International). After incubation at  $27^\circ\text{C}$  for one day cells were semi confluent. Using Sf-900 II SFM medium a dilution series of the virus ( $10^{-1}$ - $10^{-8}$ ) was prepared. Dilutions between ( $10^{-5}$ - $10^{-8}$ ) were used to infect a pair of dishes. After the supernatant medium was removed from the semi-confluent cell layer  $100\ \mu\text{L}$  virus solution, diluted in  $2\ \text{mL}$  Sf-900 II SFM medium, was added. Hundred  $\mu\text{L}$  of medium were used as a negative control. Dishes were incubated for 15 minutes gently rocked. Removal of the virus inoculum was preceded by the preparation of agarose (2%) mixed with the same volume of Sf-900 II SFM medium.  $2\ \text{ml}$  of this agarose overlay was added to the edge of each dish. This step is crucial for the vitality of the cells: the agarose must not be warmer than  $30^\circ\text{C}$ . After the agarose set  $1.5\ \text{mL}$  Sf-900 II SFM medium were added. Dishes were placed in a plastic box and incubated at  $27^\circ\text{C}$  for 3-4 days.



**Figure 3.2.5.A: Titration of a GluR-B virus stock; top left shows the  $10^{-6}$  dilution, top right shows the  $10^{-5}$ , bottom right shows  $10^{-4}$ , bottom left shows the virus-free control. The titer of the virus is ca.  $0.3 \times 10^8$ .**

Plaques were stained with 0.33 % neutral red solution (Gibco BRL) diluted 1:20 in PBS buffer.  $1\ \text{mL}$  of the diluted neutral red solution was added to each dish. After incubation for 2 hours the supernatant was poured off and the dishes were inverted. Plaques were left to clear

in the dark for 2 hours. For evaluation of the virus titer dishes with 10 to 20 easily countable plaques were chosen. For virus amplification a virus stock solution was used. Titers of virus stock solutions shown in Figure 3.2.5.A were  $0.8 \times 10^8$  for the  $10^{-6}$  dilution,  $0.3 \times 10^8$  for the  $10^{-5}$  dilution and  $0.85 \times 10^7$  for the  $10^{-4}$  dilution. Staining of infected cells with trypan blue solution showed that the efficiency of infection in different flasks can fluctuate considerably.

### **3.2.6. TRYPAN BLUE DETECTION**

Viability of Hi5 cells after the virus infection was measured by trypan blue detection. Trypan blue, which cannot permeate live cells can permeate dead cells and stain them. To monitor the stage of infection 900  $\mu$ L of Hi5 cell suspension were incubated with 100  $\mu$ L 0.4 % trypan blue solution (Sigma). After incubation for 5 to 10 minutes stained and unstained cells were counted in a hemocytometer using a light microscope. On average 9 % of the cells died during the ca. 90 hours of infection. Controls of uninfected cells showed not more than 1% cells stained by trypan blue.

### **3.3. SOLUBILIZATION AND PURIFICATION OF GLUR-B**

#### **3.3.1 HARVEST AND SOLUBILIZATION OF GLUR-B**

Virally infected cells were harvested at 4°C using a Contifuge 20 S equipped with a flow through rotor 8684 (Heraeus). Stable insect cells were harvested at 1300× g for 25 min at 4°C using a JLA-9.100 rotor (Beckmann). During the following procedure cells were kept at 4°C. The cell pellets were resuspended in 20 mM HEPES pH 7.4, 150 mM NaCl (buffer I) and aliquoted into centrifuge tubes (Beckman). After centrifugation at 1500× g for 25 min cell pellets were resuspended twice in 10 mL aliquots of 20 mM HEPES pH 7.4, 5 mM EDTA, 0.1 mM phenylmethyl sulfinyl fluoride (PMSF) (Sigma) (buffer II = lysis buffer); in 1200 mL of buffer II one Complete protease inhibitor tablet (Roche Molecular Biochemicals) was dissolved. (To allow gentle and complete resuspension of the pellet during this and the following steps a paintbrush was used.) Cell suspensions were homogenized with a Polytron PT 3100 (Kinematica) for 3 × 10 sec at 14 000 RPM. After centrifugation tubes were filled with additional buffer II; membranes were pelleted at 37 000× g for 25 min. Finally pellets were resuspended in 10 mL aliquots of 20 mM HEPES pH 7.4, 200 mM NaCl, 0.5 mM EDTA (buffer III = washing buffer). After centrifugation at 30 000× g membrane pellets were resuspended in 20 mM HEPES pH 7.4, 200 mM NaCl, 10 % (v/v) glycerol, 0.1 mM PMSF (buffer IV = solubilization buffer) and pooled. The overall protein concentration of the cell homogenate suspension was typically 20-30 mg/mL. Prior to solubilization membranes were diluted with solubilization buffer to ca. 3 mg/mL. The protein concentration was determined by bicinchonic acid assay (BCA) (Pierce). For membrane solubilization the non-ionic detergent Triton X-100 (TX-100) (Roche Molecular Biochemicals) was added to this suspension at a final concentration of 1.5 % (v/v) and gently mixed for 90 minutes using a Reax-20 mixer (Heidolph). Finally, the nuclei and the unsolubilized components were pelleted at 185 000× g for 15 minutes).

#### **3.3.2. IMMOBILIZED METAL-CHELATE AFFINITY CHROMATOGRAPY**

For purification by immobilized metal-chelate affinity chromatography (IMAC) the Chelating Sepharose Fast Flow (Pharmacia) were used. It was charged with Zn(II) ions by washing the column with 5 column volumes (CV) of 100 mM solutions of zinc acetate and equilibrated in 20 mM HEPES pH 7.4, 1 M NaCl by adding the appropriate amount of solid NaCl. After membrane solubilization 5 mM imidazole was added to the pool of supernatants. To prevent

electrostatic interactions between solubilized proteins NaCl concentration of the suspension was adjusted to 1M. Originally this suspension was pooled with zinc charged Sepharose and mixed for 12 hours using a Reax-20 mixer (Heidolph) (incubation-mode). By filtering the mixture through a glass frit (Schott, DURAN), porosity 2, the Sepharose was recovered and transferred to a 10 mL BioRad column. Initially 10 mL of Chelating Sepharose Fast Flow (Pharmacia) were used for 15-20 liters of insect cell suspension. In the course of optimization the volume of Sepharose was reduced to  $\leq 2$  mL Sepharose for 8 liters of insect cell suspension and the suspension containing all solubilized proteins was loaded directly (with up to 4 mL/min) on a column using a peristaltic pump (flow-through-mode). Loading in the flow-through-mode has a positive effect on the purity of eluates. (See paragraph 4.1.2.) After loading, the zinc charged Sepharose was washed with 10 CV of 20 mM HEPES pH 7.4, 10% glycerol, 0.1% Triton X-100 (buffer V), containing 1 M NaCl and 10 mM imidazole. For the next two washing steps the NaCl concentration in buffer V was reduced twice; after 2 CV of 200 mM NaCl the column was washed with 2 CV of 100 mM NaCl. Subsequently imidazole concentration in buffer V was increased twice while the NaCl concentration was 100 mM NaCl; the column was washed with 3 CV of buffer V containing 30 mM imidazole and 3 CV of buffer V containing 40 mM imidazole. To elute GluR-B protein in buffer V, containing 100 mM NaCl, the imidazole concentration was increased in three steps: 2 $\times$  10 CV containing 100 mM imidazole, 2 $\times$  10 CV containing 200 mM imidazole and 4 $\times$  10 CV containing 500 mM imidazole. Sodium dodecyl sulfate polyacrylamide gel electrophoresis (SDS-PAGE) (Laemmli, 1970) followed by silver staining and Western blotting showed that elution of GluR-B typically started at 100 mM imidazole and was finished after 7 CV at 500 mM imidazole (in total 18 CV).

### 3.3.3. IMMUNOAFFINITY CHROMATOGRAPHY

The receptor was further purified by immunoaffinity chromatography using immobilized anti-FLAG antibody. GluR-B containing IMAC eluates were pooled and CaCl<sub>2</sub> was added to a final concentration of 3 mM. The solution was loaded on 1 mL of M1  $\alpha$ -FLAG affinity gel (IBI Kodak/Sigma), which was equilibrated in TBS buffer containing 3 mM CaCl<sub>2</sub>, 0.1% Triton X-100. After that the column was washed with 10 CV of 20 mM TBS, 10% glycerol, 0.1% Triton X-100 (buffer VI), containing 3 mM CaCl<sub>2</sub>. GluR-B was eluted (20 CV) with TBS, containing 500 mM NaCl, 10% glycerol, 0.1% TX-100, 20 mM EDTA (buffer VII).

### 3.4. GENERAL METHODS

#### 3.4.1. SDS-PAGE

Sodium dodecyl sulfate polyacrylamide gel electrophoresis (SDS-PAGE) gels were prepared as described by Laemmli (Laemmli, 1970) and run with a Minigel-PAGE-System (Bio-Rad). The buffer for the preparation of separation gels consisted of 1.5 M Tris-HCl, pH 8.8 and 0.4% SDS. For the preparation of two 10% gels (10 cm x 8 cm x 0.075 cm) 3.75 mL of separation gel buffer, 6.25 mL dd-H<sub>2</sub>O, 5 mL of 30% (w/v) of acrylamide and 0.8% (w/v) of *N, N'*-bis-methylene acrylamide, 70  $\mu$ L of 10% (w/v) ammoniumperoxodisulfate (APS) and 15  $\mu$ L *N,N,N',N'*-tetramethylethylene diamine (TEMED) were mixed. During polymerization the separation gel was covered with 70 % ethanol. The buffer for preparation of the stacking gel consisted of 0.5 M Tris-HCl, pH 6.8 and 0.4% SDS. For the preparation of two gels having ca. 1 cm stacking gel 1.25 mL stacking gel buffer, 3 mL dd-H<sub>2</sub>O, 0.75 mL of 30% (w/v) of acrylamid and 0.8 % (w/v) of *N, N'*-bis-methylene acrylamide, 30  $\mu$ L of 10% (APS) (w/v) and 12  $\mu$ L TEMED were mixed.

SDS-sample buffer (3 $\times$ ) consisted of 150 mM Tris-HCl, 6% SDS, 0.3% bromphenol blue, 30% glycerol. Prior to use 100  $\mu$ L  $\beta$ -mercaptoethanol was added per 1 mL SDS-sample buffer. GluR protein samples were diluted 2:1 with 3 $\times$  SDS-sample buffer and incubated at 95° C for 5 minutes. 10  $\mu$ L - 15  $\mu$ L of the denatured protein solution was loaded on the gel. For MW calibration 3  $\mu$ L of the Bench Mark protein ladder (Gibco-BRL) containing standard proteins were loaded for silver stained gels. For Westernblotting 7  $\mu$ L of ready to use prestained Bench Mark protein ladder (Gibco-BRL) were loaded. 10 $\times$  electrode buffer consisted of 250 mM Tris, pH 8.3, 2.5 M glycine and 1% SDS. Electrophoresis was performed at 200 V until the bromphenol blue reached the bottom of the gel (ca. 45 min.).

#### 3.4.2. SILVER STAINING

Silver staining of SDS-PAGE gels allow the detection of nanogram amounts of protein (Oakley et al., 1980). After electrophoresis the gel is incubated for 15 minutes in fixation solution, which consisted of 30% ethanol and 10% acetic acid. Subsequently the gel was incubated in 100 mL 30% ethanol, 0.1 M sodium acetate (pH 6.0), which was supplemented with 0.4 mM (100 mg) sodiumthiosulfate-pentahydrate freshly. The gel was washed 3 times for 5 minutes each, in dd-H<sub>2</sub>O and incubated in 0.1% silver nitrate (w/v) (to 50 mL 12.5  $\mu$ L

36.5% formaldehyde were added prior to use) for 15 minutes. Subsequently the gel was briefly washed in dd-H<sub>2</sub>O and developed in freshly prepared developer: 2.5% (w/v) sodium carbonate in 100 mL dd-H<sub>2</sub>O plus 12.5  $\mu$ L 36.5 % formaldehyde. In order to stop the development acetic acid was added.

### 3.4.3. WESTERN-BLOT ANALYSIS

SDS-PAGE gels were transferred to nitrocellulose membrane (Schleicher & Schuell) by semi-dry Western-blotting in a Transblot-B SD-Apparatus Semi-Dry Transfer Cell (Bio-Rad) (Towbin et al., 1979). The gel, the membrane and four sheets of GB 002 gel-blotting paper (Schleicher & Schuell) were incubated in blotting-buffer (25 mM Tris-HCl, pH 8.2, 192 mM glycine, 20% methanol) for two minutes. In the apparatus the membrane was placed on two filters. Before the gel was put on the membrane air bubbles were removed carefully. A plastic mask was used to limit the contact area of the electrodes to the size of the gel. Finally gels were covered by two filter papers. Gels were blotted for 20 minutes with 15V. To reduce the background caused by unspecific binding, membranes were incubated for 15 minutes in 50 mL TBS buffer containing 1.5 g milk powder (Fluka). After washing twice in TBS buffer for 5 minutes, the membrane was washed in TBS containing 3 mM CaCl<sub>2</sub> and 0.05 % Tween20 for 5 minutes. This was followed by incubation in M1-antibody (20  $\mu$ g/mL in TBS, 0.05 % Tween 20, 1 mM CaCl<sub>2</sub>) for 1 hour. The M1-antibody was recovered, sterile filtered and stored at 4° C. After washing 2 $\times$  for 5 minutes in TBS containing 3 mM CaCl<sub>2</sub> and 0.05 % Tween20 incubation for 30 minutes with anti-mouse IgG (Sigma), diluted 1:1000 in TBS, 0.05 % Tween 20 followed. After washing 2 $\times$  for 5 minutes in TBS containing 3 mM CaCl<sub>2</sub> and 0.05 % Tween 20 membranes were stained by NBT/BCIP (Sigma). One capsule was dissolved in 10 mL dd-H<sub>2</sub>O. Staining was stopped with dd-H<sub>2</sub>O.

### 3.4.4. AMIDO-BLACK ASSAY

The protein concentrations of pooled M1 eluates containing GluR-Bs were determined by Amido-Black assay (Bio-Rad). The Amido-Black assay allows detection of low protein amounts and is not influenced by the presence of lipids or detergents (Kaplan and Pedersen, 1989). Duplicates of GluR-B samples were diluted (1:10 and 1:4) to a final volume of 2 mL with dd-H<sub>2</sub>O. A dilution series of BSA standards (0.5  $\mu$ g/mL - 10  $\mu$ g/mL) was prepared. Two controls containing dd-H<sub>2</sub>O instead of protein were included. To each sample 200  $\mu$ L of 10 %

SDS, 300  $\mu\text{L}$  1 M Tris / 1% SDS, pH 7.5, and 600  $\mu\text{L}$  and 104 % (w/v) trichloroacetic acid (TCA) were added sequentially. After each addition, the reaction mixtures were vortexed carefully. After TCA addition samples were incubated for at least 3 minutes. Samples were transferred onto filters (Millipore HAWP 024 00), which was soaked in dd-H<sub>2</sub>O for 5 minutes and fastened into a sampling manifold (Millipore). Each sample was then filtered under vacuum and each filter was immediately washed with 2 mL 6 % TCA. Filters were removed and placed into beakers where the surface of each filter was covered by 250  $\mu\text{L}$  0.1% staining solution Amido-Black 10B (Bio-Rad) dissolved in methanol/glacial acetic acid and dd-H<sub>2</sub>O (45/10/45, v/v/v). The stain incubated for 1 minute. Subsequently each filter was washed twice for 3 minutes in 5 mL destain solution, which consisted of methanol/glacial acetic acid and dd-H<sub>2</sub>O (90/2/8, v/v/v). This was followed by a dd-H<sub>2</sub>O wash for 3 minutes. During all washing steps gentle stirring is recommended. To remove excess water filters were blotted with Kimwipes. To release the blue dye from the filter they were placed in plastic tubes containing 1 mL 25 mM NaOH, 0.05 mM EDTA and 50 % ethanol for 20 minutes. The absorbance was measured at a wavelength of 630 nm (DU-640 Spectrophotometer, Beckman).

#### **3.4.5. GLUR-B CONCENTRATION IN CENTRIFUGAL CONCENTRATORS**

After purification by immunoaffinity chromatography GluR-B concentration in the eluates was typically ca. 5  $\mu\text{g}/\text{mL}$ . Before detergent exchange (see paragraph 3.4.6.) TX-100 solubilized GluR-B was concentrated five-fold using Centriplus centrifugal concentrators (Amicon) with a 100 000 kD molecular weight cut off (MWCO). For subsequent crystallization experiments dodecyl- $\beta$ -D-maltoside (DDM) solubilized GluR-B protein was concentrated to protein concentrations of at least 200  $\mu\text{g}/\text{mL}$ .

#### **3.4.6. DETERGENT EXCHANGE**

For two-dimensional crystallization experiments Triton X-100 was replaced by dodecyl- $\beta$ -D-maltoside (DDM) (TX-100  $\rightarrow$  DDM). For this purpose immobilized metal chelate affinity chromatography (IMAC) was used. To reduce EDTA concentration samples were concentrated five-fold and rediluted in 20 mM Hepes pH 7.4, 500mM NaCl, 10 % glycerol and 0.1 % DDM before loading GluR-B samples on a chelating Sepharose Fast Flow (Pharmacia) column (1 mL Sepharose / 50  $\mu\text{g}$  GluR-B) samples. Thus EDTA concentrations were reduced from ca. 10 mM to ca. 2 mM. Such high EDTA concentrations might chelate

the Zn(II) ions releasing them from the Sepharose. After loading protein was washed with 20 CV 20 mM Hepes pH 7.4, 500mM NaCl, 10 % glycerol and 0.1 % DDM. The detergent exchange (decrease of TX-100) was monitored by measurement of the absorption of washes at 280 nm (DU-640 Spectrophotometer, Beckman). When the remaining TX-100 concentration was ca. 10× lower than its CMC the protein was eluted in 20 mM Hepes pH 7.4, 500mM NaCl, 10 % glycerol, 400 mM Imidazol and 0.1 % DDM.

#### 3.4.7. DDM-MONITORING

To determine the DDM concentration in the protein samples the method of Dubois (Dubois et al., 1956), which is based on oxidation of carbon hydrates by sulfuric acid was applied. In the presence of phenol a brown chromophore is formed, which is quantitated by absorption at 490 nm. This test was performed in triplicates. DDM standards with 3.6 mg/mL, 6 mg/mL and 12 mg/mL were prepared freshly in the exchange buffer. 2 µL of GluR-B or standard solution were added to 998 µL dd-H<sub>2</sub>O. Three detergent-free buffer controls were included. 50 µL of an aqueous 90 % (w/v) phenol solution (Riedel-de Haën) were added. Tubes were carefully mixed. Then 2.5 mL conc. H<sub>2</sub>SO<sub>4</sub> (Merck) were added, and the samples were mixed again and cooled in a water bath at 20°C. Absorption was measured at 490 nm.

#### 3.4.8. TWO-DIMENSIONAL CRYSTALLIZATION EXPERIMENTS

For two-dimensional crystallization of DDM solubilized GluR-B protein a method was tested, which was successful for the two-dimensional crystallization of the *Neurospora crassa* plasma membrane H<sup>+</sup>-ATPase (Scarborough, 1994). The standard procedure for the crystallization of the *Neurospora crassa* plasma membrane H<sup>+</sup>-ATPase was communicated by G. Scarborough and is described here.

The final protein concentration in the standard H<sup>+</sup>-ATPase crystallization mixture was 1 mg/mL and the final DDM concentration was 1.28 mg/mL. These conditions were found to yield the largest crystals (Scarborough, 1994). Therefore DDM concentration in the 50 µL crystallization mixture was adjusted to 1.28 mg/mL by adding the appropriate volume of a 10 mg/mL DDM solution in 30G buffer (30 % (w/v) glycerol, 1 mM EDTA, 1 mM DTT, 2 µg/mL chymostatin (Sigma), pH adjusted to 6.8 with TRIS). Subsequently to each setup 5 µL of 1 M ammonium sulfate in 30G buffer and 10.5 µL of 50% PEG 4000 (FLUKA) in 30G

buffer were added. Crystallization mixtures were prepared on ice. Samples were vortexed in the cold room and stored for one night at 4°C.

From the bottom of the tube 3  $\mu$ L were taken and placed on a standard glass microscope slide. The droplet was covered with a 0.75 cm square plastic cover slip. At magnification of 400 $\times$  the sample was screened for crystals or other periodic protein arrangements using a phase-contrast microscope. Afterwards the tube containing the microcrystal setup was centrifuged for 5 min. with ca. 16 000 $\times$  g. The supernatant fluid was transferred to a new Eppendorf tube. Covered with a large beaker, set at an angle to allow air circulation, the tube was set in cold room overnight 4°C. Slides were made and screened daily for at least a week.

(The two-dimensional crystallization experiments with GluR-B and results of these experiments are described in the APPENDIX, A.3.)

### **3.5. BIOCHEMICAL PROTEIN CHARACTERIZATION**

#### **3.5.1. FILTER-BINDING OF THE RADIOLIGAND [<sup>3</sup>H]-AMPA**

Ligand binding activity of GluR-B was tested by filter binding using radio labeled [<sup>3</sup>H]-AMPA (Dupont-NEN). During the test, which was performed in triplicate samples were stored on ice. Using AMPA Binding Buffer (ABB) (30 mM Tris, pH 7.2, 2.5 mM CaCl<sub>2</sub>, 100 mM KSCN, 0.1 % TX-100) a 300 nM [<sup>3</sup>H]-AMPA stock solution was prepared. To measure K<sub>D</sub>-values a series of AMPA concentrations, typically 1, 3, 10, 15, 30, 100 and 300 nM, were used. For concentrations higher than 100 nM the [<sup>3</sup>H]-AMPA was diluted 5× with non-radioactive AMPA. Setups had a final volume of 500 μL. To 425 μL ABB-buffer 50 μL GluR-B solution and 25 μL 300 nM [<sup>3</sup>H]-AMPA were added. GluR concentration was 5-20 μg/mL. Volumes were compensated with ABB-buffer. Two controls were prepared to estimate unspecific binding. In these controls to 375 μL ABB-buffer, 50 μL of flow-through protein from IMAC purification, 25 μL 300 nM [<sup>3</sup>H]-AMPA and 50 μL 10 mM L-glutamate were added. After addition of [<sup>3</sup>H]-AMPA samples were stored for 1 hour on ice in the dark. Samples were transferred onto 25 mm GF/B-filters (Whatman) fastened into a sampling manifold (Millipore) after they were soaked in 0.3% (w/v) polyethylenimin. Each sample was filtered under vacuum and immediately washed twice with 5 mL ABB-buffer. Each filter was placed in a scintillation tube. After addition of 5 mL scintillation liquid (Emulsifier Safe, Canberra-Packard) samples were incubated over night. Samples were counted in a Beckman LS 6500 Scintillation Counter according to the manufacturer's manual (User program No.2 (<sup>14</sup>C- and <sup>3</sup>H isotopes)).

#### **3.5.2. ELECTROPHYSIOLOGICAL ANALYSIS**

Whole-cell recordings were performed by B. Schupp and G. Köhr in the Neurobiology Department of our institute using patch pipettes filled with 140 mM CsCl, 2 mM MgCl<sub>2</sub>, 2 mM Na<sub>2</sub>ATP, 10 mM EGTA, 10 mM Hepes (pH adjusted to 6.3 with CsOH). To ensure rapid application of agonists via a piezo-driven double-barreled pipette cells were lifted from the cover slip. For whole-cell recordings 30 ml of the two stable cell lines (GluR-D(E1) and GluR-B(D9)) were cultivated in 100 mL spinner flasks. These cells were plated on cover slips at different densities. Cover slips with the attached cells were transferred to a bath containing 135 mM NaCl, 5.4 mM KCl, 1.8 mM CaCl<sub>2</sub> and 5 mM Hepes (pH adjusted to 6.3 with NaCl).

### 3.6. INDIRECT ANALYSIS OF THE OLIGOMERIC PROTEIN STRUCTURE BY CROSS-LINKING

Glutamate receptor heterooligomers in total rat brain lysate can be efficiently cross-linked by DTSSP (Osten, 2000). Despite the presence of lipids in brain lysate and the heteromeric nature of the glutamate receptors this natural sample was considered to be a good reference for cross-linking experiments with GluR-B. To prepare total rat brain lysate 100 mg brain tissue of a one month old rat were homogenized in brain lysate buffer 1 (25 mM Hepes pH 7.5, one Complete protease inhibitor tablet dissolved in 10 mL; Roche Molecular Biochemicals) and stored for 20 minutes on ice. The unhomogenized material was pelleted by centrifugation at  $1000\times g$  for 10 min at  $4^{\circ} C$ . The total protein concentration of the supernatant, determined by the Bradford method, was ca. 5.5 mg/mL. Aliquots of 200  $\mu L$  were frozen in liquid nitrogen and stored at  $-80^{\circ} C$ . Prior to cross-linking, freshly thawed samples were diluted 1:1 with brain lysate buffer 2 (25 mM Hepes pH 7.5, 300 mM NaCl, 2 % TX100, one Complete protease inhibitor tablet was dissolved in 10 mL; Roche Molecular Biochemicals).

Protein concentrations in purified GluR-B samples used for cross-linking experiments were between ca. 25  $\mu g/mL$ . For buffer exchange Tris buffered GluR-B samples were dialyzed using Slide-A-Lyzer Dialysis Cassettes (Pierce) with a MWCO of 10 000. 150-300  $\mu L$  volumes were dialyzed twice for 24 hours in 800 ml Hepes buffer (20 mM Hepes, 500 mM NaCl, 10% glycerol, 0.1% TX-100, 20 mM EDTA). Since DTSSP reacts with the primary amines of all molecules present cross-linking experiments with DTSSP should not be performed in Tris buffered solutions. An excess of Tris at pH 7.5 is used to stop the reaction. To remove Tris from protein samples 150  $\mu L$  volumes were dialyzed twice for 24 hours in 800 ml Hepes buffer (20 mM Hepes, 500 mM NaCl, 10% glycerol, 0.1% TX-100, 20 mM EDTA). DDM solubilized GluR-B samples (see detergent exchange) were in Hepes buffer already.

Different volumes of a 20 mM DTTSP stock solution, which has been prepared freshly in dd-H<sub>2</sub>O were added to 50  $\mu L$  or 100  $\mu L$  volumes of the protein samples. After incubation with cross-linker for 120 minutes samples were quenched with 50mM Tris, pH 7.5 for 30 minutes.

Two types of controls were prepared. The first control (minusCLcontrol) consisted of solubilized GluR-B to which sample buffer instead of DTSSP was added. The second control (DTT-Control) was a cross-linked sample that was subsequently reduced by the agent 1,4-Dithio-*DL*-threitol (DTT). For this DTT-Control 15  $\mu$ L of those protein samples containing the highest cross-linker concentration were incubated with 50 mM DTT for 5 minutes at 37° C. The 500 mM DTT stock solution in dd-H<sub>2</sub>O was freshly prepared. Finally 15  $\mu$ L of each sample and each control were mixed with 7.5  $\mu$ L SDS(3 $\times$ ) sample buffer. Samples were loaded on 8% PAA gels. For the characterization of larger oligomers commercial NuPAGE gradient gels (Novex) were used. For subsequent Western-blotting with 0.5  $\mu$ g/mL GluR2/3 primary antibody (CHEMICON) SDS-PAGE gels were wet blotted (tank-blotting) in a Mini Trans-Blot Transfer Cell (BioRad) for ca. 20 hours at 110 mA. Signals were detected by enhanced chemiluminescence (ECL). ECL protocols (Amersham) were applied. As a secondary antibody horseradish peroxidase labeled anti-rabbit Ig (Amersham) was used.

### 3.7. DIRECT ANALYSIS OF THE OLIGOMERIC PROTEIN

#### STRUCTURE BY ELECTRON MICROSCOPY

##### 3.7.1 NEGATIVE STAINING

Copper grids (300 mesh) (Plano GmbH) were coated with carbon film. Within 20 min, 3  $\mu$ L of GluR-B in buffer VII (TBS, containing 500 mM NaCl, 10% glycerol, 0.1% TX-100, 20 mM EDTA) were applied to the grid. Proper staining was achieved for single protein molecules at concentrations of GluR-B between 15 and 30  $\mu$ g/mL. After 3 min. the supernatant was blotted from the edge and specimens were washed twice with 25 mM Tris pH 7.4, 20 mM NaCl, 2mM EDTA. The grid was then washed with one droplet of stain. After blotting from the edge the grid was incubated for 1 minute in a second stain droplet. As shown in table 3A different stains were used.

Type of stain	Concentration
Uranyl acetate (Fluka)	2 % in dd-H <sub>2</sub> O
Aurothioglucose (Sigma)	1 %, 2 %, 4% in dd-H <sub>2</sub> O
Ammonium molybdate (Fluka) ( for cryo-negative staining)	0.8 g + 650 $\mu$ l dd-H <sub>2</sub> O + 125 $\mu$ l 10 M NaOH

**Table 3.7.1.A: Stains used for negative stain sample preparation.**

##### 3.7.2. CRYO-ELECTRON MICROSCOPY

For cryo-EM, grids carrying holey films were prepared as described (Jahn, 1995). To standardize conditions grids were glow discharged in the presence of tripropylamin (MERCK) or air glow discharged before use. Tweezers with a fixed grid were placed in a plunge-freeze apparatus before application of 4  $\mu$ L protein solution. After blotting with filter paper (Rundfilter 597) (Schleicher & Schuell) the grid was plunged in liquid ethane.

##### 3.7.3. CRYO-NEGATIVE STAINING

In cryo-negative staining the protein solution is mixed with stain on the holey grid prior to blotting and plunging (Adrian et al., 1998). Before 4  $\mu$ L of protein solution were incubated for 30 seconds on a grid carrying a holey film two droplets of 16 % ammonium molybdate were

prepared on a plastic film. First the grid was washed in one of the 100  $\mu\text{L}$  16 % ammonium molybdate droplets. Due to the presence of detergent in GluR-B samples the surface tension of the stain droplet was reduced considerably. Thus it was not possible to float the grid on the surface of the stain droplet. However, it was possible in most of the experiments to float the grid on the surface of the second stain droplet. If floating was not possible tweezers were used to stabilize the position of the grid in the middle of the droplet during the 60 seconds incubation time. After insertion of the tweezers plus grid in the holder of a plunge-freeze apparatus the grid was blotted and plunged in liquid ethane.

#### **3.7.4. ELECTRON MICROSCOPY**

Micrographs (Kodak SO-163) used for image processing were recorded at an electron optical magnification of 46000 $\times$  using a Philips EM400 electron microscope at 80 kV. Cryo-experiments were recorded at electron optical magnifications ranging from 3000 $\times$  to 50000 $\times$  using a Zeiss CEM 902 electron microscope operating at 80 kV and the corresponding Zeiss cryo-transfer system. Both electron microscopes were equipped with low-dose facilities, which were used during experiments with specimens negatively stained in aurothioglucose and cryo-experiments. Recordings were done at an electron dose  $\leq 10 \text{ e}^-/\text{\AA}^2$ , and 1 seconds exposure time at 0.5 - 0.8  $\mu\text{m}$  under focus. Micrographs were developed in full strength D19 developer (Kodak).

After the micrographs were checked for lens asymmetry and defocus values with an optical diffractometer they were digitized with a SCAI Precision Scanner (Zeiss) at a resolution of 14  $\mu\text{m}$ . Images of protein particles were selected from micrographs with similar defocus values and processed with the software package IMAGIC (Image Science Software GmbH, Berlin) (v. Heel et al., 1996). (The principles of IMAGIC are explained in paragraph 2.2.)

**REFERENCES OF CHAPTER 3**

- Adrian, M., Dubochet, J., Fuller, , and S. D., H., R. (1998). Cryo-negative staining. *Micron* 29, 145-160.
- Dubois, M., Gilles, K. A., Hamilton, J. K., Rebers, P. A., and Smith, F. (1956). *Analytical Chemistry* 28, 350-356.
- Jahn, W. (1995). Easily prepared holey films for use in cryo-electron microscopy. *Journal of Microscopy* 179, Pt 3, 333-334.
- Kaplan, R. S., and Pedersen, P. L. (1989). Sensitive protein assay in presence of high levels of lipid. *Methods in Enzymology* 172, 393-399.
- Laemmli, U. K. (1970). Cleavage of structural proteins during the assembly of the head of bacteriophage T4. *Nature* 227, 680-685.
- Oakley, B. R., Kirsch, D. R., and Morris, N. R. (1980). *Analytical Biochemistry* 105, 361.
- Osten, P. (2000). GluR crosslinking with DTSSP (personal communication).
- Scarborough, G. A. (1994). Large single crystals of the *Neurospora crassa* plasma membrane of H<sup>+</sup>-ATPase: an approach to the crystallisation of integral membrane proteins. *Acta Crystallographica Section D* 50, 643-649.
- Towbin, H., Staehelin, T., and Gordon, J. (1979). Electrophoretic transfer of proteins from polyacrylamide gels to nitrocellulose sheets: Procedure and some applications. *Proceedings of the National Academy of Science USA* 76, 4350-4354.
- v. Heel, M., Harauz, G., Orlova, E. V., Schmidt, R., and Schatz, G. (1996). A new generation of the IMAGIC image processing system. *Journal of Structural Biology* 116, 17-24.

## 4. RESULTS

### 4.1. GLUR EREXPRESSION IN STABLE INSECT CELLS

#### 4.1.1. ELECTROPHYSIOLOGICAL ANALYSIS OF GLUR-D AND GLUR-B

It has been shown previously by whole-cell recordings of virus infected cells that membrane-inserted heteromeric GluR-B/-D subunits recombinantly expressed in the baculovirus expression system assemble to functional AMPA receptor channels (Keinänen et al., 1994). In this project functionality of GluR-D and GluR-B homomers, constitutively expressed in stable cell lines, was tested for the first time using the same patch-clamp setup. Five different cells of a cell line, expressing the GluR-D subunit were measured, of which one showed an inward current triggered by 2 mM *L*-glutamate.

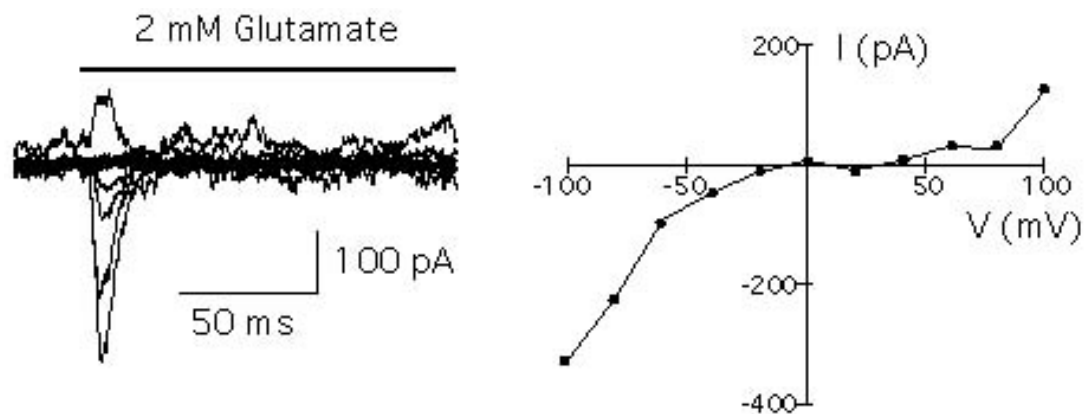


**Figure 4.1.1.A: Whole-cell recordings; current responses of GluR-D cells to 2 mM *L*-glutamate. The corresponding peak I-V relations are characteristic for the GluR-D subtype. *L*-glutamate was applied for 300 ms.**

The rectifying I-V curve shown in Figure 4.1.1.A is characteristic for homomeric GluR-D channels. I-V behavior and measured current signals were comparable to those of the GluR-D homomers expressed by the baculovirus expression system (Keinänen et al., 1994). Nine different GluR-B expressing cells were measured. None of these cells produced a signal in the presence of the agonist *L*-glutamate, which can be explained by the low conductivity of the B-type subunit.

#### 4.1.2. OPTIMIZATION OF IMAC PURIFICATION

Immobilized metal-chelate affinity chromatography (IMAC) purification for GluR-B was optimized during a series of five large-scale GluR-B preparations, starting with a volume of ca. eight liters of stable insect cell culture suspension. Several parameters were varied to reduce unspecific binding to the  $Zn^{2+}$ -charged Sepharose. The subsequent purification by M1  $\alpha$ -FLAG antibody affinity chromatography (immunoaffinity chromatography) was found to be more effective in combination with an optimized IMAC procedure.

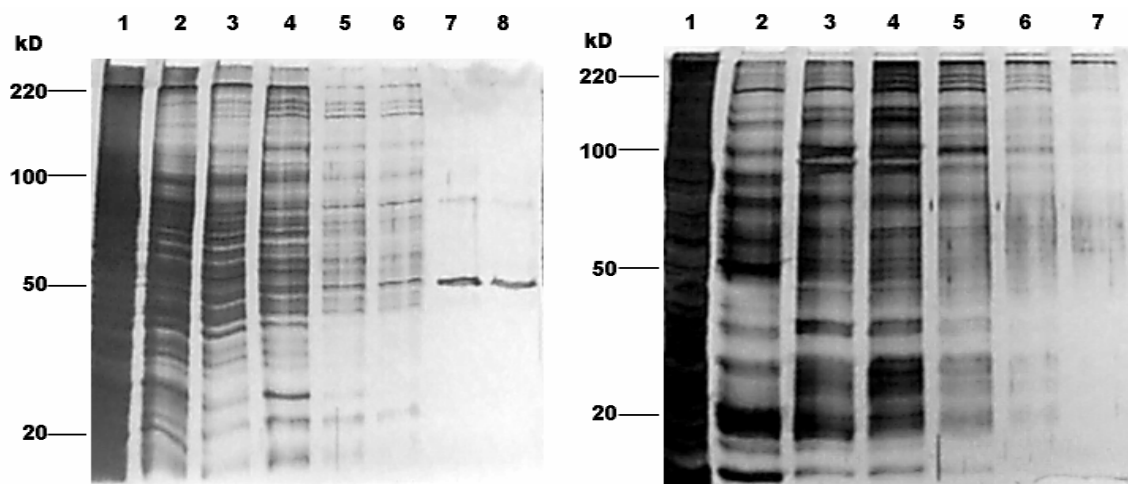


**Figure 4.1.2.A:** Silver stained SDS-PAGE gels of GluR-B IMAC purification (incubation mode); solubilized proteins were incubated with 5 mL  $Zn^{2+}$ -charged Sepharose overnight. After filtration through a glass frit, the Sepharose was transferred to a column and washed. Left side; samples were loaded as follows: lane 1, IMAC loading; lane 2 and 3, glass frit filtrate; lane 4 and 5, wash 1 (10 mM imidazol); lane 6, wash 2 (10 mM imidazol); lane 7, wash 3 (10 mM imidazol); lane 8, wash 4 (30 mM imidazol). Right side; samples were loaded as follows: lane 1, IMAC loading; lane 2, elution 1 (100 mM imidazol); lane 3, elution 2 (200 mM imidazol); lane 4 to 7, elution 3 (500 mM imidazol). Before loading proteins were incubated with SDS (3 $\times$ ) buffer in the ratio 2:1 for 5 minutes at 90 $^{\circ}$  C. Of each sample 20  $\mu$ L were loaded.

The incubation of Sepharose and solubilized proteins with gentle agitation over night (incubation-mode), as well as the immense protein binding capacity of chelating Sepharose (ca. 5 mg histidine-tagged protein per mL Sepharose charged with divalent cations) were considered as major sources of background binding. Considering that the yield of GluR-B protein in stable insect cells is 40-50  $\mu$ g receptor protein per liter cell suspension, the required volume of chelating Sepharose could be in principal less than 0.1 mL for eight liters of cell culture suspension.

Considering the high binding capacity of zinc charged Sepharose its volume was reduced from 5 mL to 1 - 2 mL and instead of batch incubation with Sepharose the solution containing all the detergent-solubilized proteins was loaded on a column prepacked with  $Zn^{2+}$ -charged Sepharose directly (flow-through-mode). Comparison of IMAC eluates on silverstained SDS-PAGE gels (see Figure 4.1.2.B right side and Figure 4.1.2.C right side) shows that the adjustment of column volume in combination with accelerated flow-through loading (flow-through-mode) considerably reduced background binding in the IMAC eluates yielding GluR-B protein of higher purity.

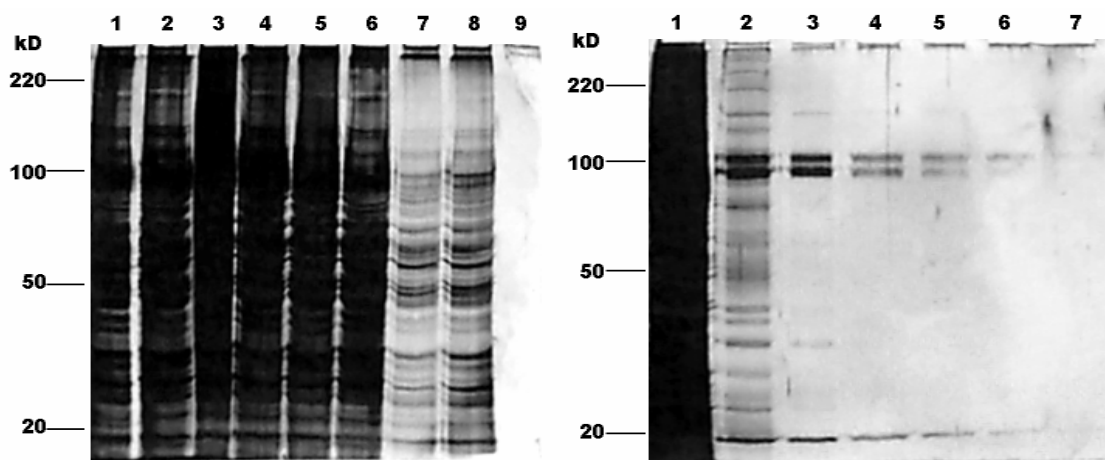


**Figure 4.1.2.B:** Silver stained SDS-PAGE gels of GluR-B IMAC purification (flow-through-mode); the solution containing the detergent solubilized proteins was loaded with 3-4 mL/minutes on a column prepacked with 1 mL  $Zn^{2+}$ -charged Sepharose using a peristaltic pump. Left side; samples were loaded as follows: lane 1, IMAC loading; lane 2 to 6, 150 mL flow-through; lane 7, wash 1 (10 mM imidazol); lane 8, wash 2 (10 mM imidazol); lane 9, wash 3 (10 mM imidazol). Right side; samples were loaded as follows: lane 1, IMAC loading; lane 2 to 4, elution 1 (100 mM imidazol); lane 5 and 6, elution 2 (200 mM imidazol), lane 7 elution 3 (500 mM imidazol). Before loading proteins were incubated with SDS (3 $\times$ ) buffer in the ratio 2:1 for 5 minutes at 90° C. Of each sample 20  $\mu$ L were loaded.

IMAC eluates (see Figure 4.1.2.B on the right side) contain two protein species with a molecular weight close to 100 kD, of which the one with a higher molecular weight represents GluR-B. This was shown by SDS-PAGE analysis of IMAC eluates and of immunoaffinity chromatography eluates, which were loaded on the same gel. The result is documented in Figure 4.1.2.C. Lane 4 shows the flow-through of immunoaffinity chromatography loading and clearly identifies the impurity. Immunolabeling of the same samples confirmed this.

Lanes 5 to 8 in Figure 4.1.2.C document that immunoaffinity chromatography yielded pure GluR-B protein. The smear at ca. 70 kD does not represent protein impurities. Most likely it can be attributed to the use of  $\beta$ -mercaptoethanol during sample preparation for SDS-PAGE.

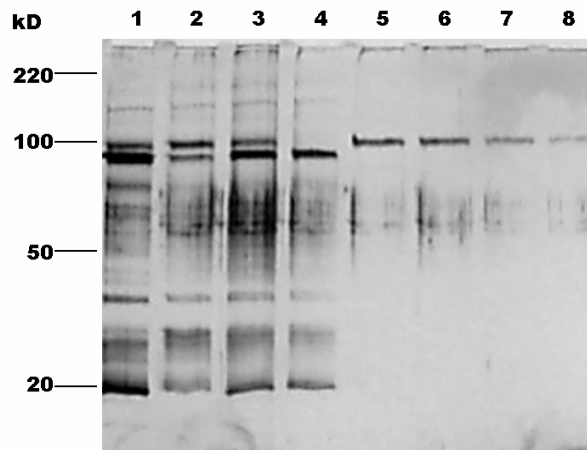


**Figure 4.1.2.C: Silver stained SDS-PAGE gel - summary of flow-through mode; samples were loaded as follows: lane 1 and 2, IMAC eluates; lane 3, load of immunoaffinity chromatography, lane 4, flow-through of affinity chromatography; lane 5 to 8, eluates of affinity chromatography. Before loading proteins were incubated with SDS (3 $\times$ ) buffer in the ratio 2:1 for 5 min at 90 $^{\circ}$  C. Of each sample 20  $\mu$ L were loaded.**

Recently the hexahistidine tag has been modified in our lab to a decahistidine tag to facilitate single-step purification by IMAC (Tarabin, 2000). Preliminary attempts showed that the protein could not be solubilized under the same conditions.

In the next paragraph the process of concentrating immunoaffinity purified GluR-B samples using centrifugal concentrators will be monitored.

#### 4.1.3. GLUR-B PROTEIN AT HIGHER PROTEIN CONCENTRATIONS

Prior to analysis by electron microscopy and 2D crystallization experiments, purified GluR-B samples were concentrated. GluR-B typically eluted from the immunoaffinity chromatography column at a protein concentration less than 10  $\mu\text{g}/\text{mL}$ . To investigate the behavior of GluR-B at higher protein concentrations concentration series were analyzed by SDS-PAGE. Figure 4.1.3.A shows a silverstained SDS-PAGE gel of a GluR-B concentration series. The unconcentrated GluR-B sample at a concentration of 4.3  $\mu\text{g}/\text{mL}$  (result of Amido-Black assay) was loaded on lane 1. Lanes labeled with even numbers (2-12) show GluR-B at increasingly higher concentrations. (The values of protein concentrations given here are calculated according to the volume reduction during the process of protein concentration and are therefore not exact.) Rediluted samples were loaded adjacent to the concentrated samples, on lanes with uneven numbers (3-13).

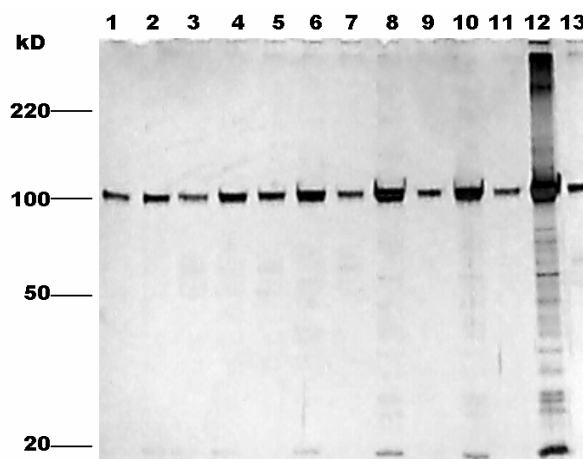


**Figure 4.1.3.A:** The Silver stained SDS-PAGE gel showing a concentration series of a GluR-B sample, which had been purified by affinity chromatography. Lanes labeled with even numbers show the concentration series. Lanes with uneven numbers show the samples of the concentration series rediluted to the initial protein concentration of 4.3  $\mu\text{g}/\text{mL}$ . Samples were loaded as follows: lane 1, GluR-B at 4.3  $\mu\text{g}/\text{mL}$  (50 mL) not concentrated; lane 2, GluR-B at ca. 8.6  $\mu\text{g}/\text{mL}$  (25 mL); lane 4, GluR-B at ca. 14.7  $\mu\text{g}/\text{mL}$  (14 mL); lane 6, GluR-B at ca. 32  $\mu\text{g}/\text{mL}$  (6 mL); lane 8, GluR-B at ca. 45  $\mu\text{g}/\text{mL}$  (3.5 mL); lane 10, GluR-B at 60  $\mu\text{g}/\text{mL}$  (2.3 mL); lane 12, GluR-B at 300  $\mu\text{g}/\text{mL}$  (0.4 mL). Before loading proteins were incubated with SDS (3 $\times$ ) buffer in the ratio 2:1 for 5 minutes at 90 $^{\circ}$  C. Of each sample 12  $\mu\text{L}$  were loaded.

At protein concentrations from 4.3  $\mu\text{g}/\text{mL}$  to 60  $\mu\text{g}/\text{mL}$  no GluR-B specific aggregations were detected. However, for the following concentration step (from 60  $\mu\text{g}/\text{mL}$  to 300  $\mu\text{g}/\text{mL}$ ) high molecular weight species were observed. Immunolabeling experiments confirmed that these aggregates were GluR-B specific (see Figure 4.1.3.B).

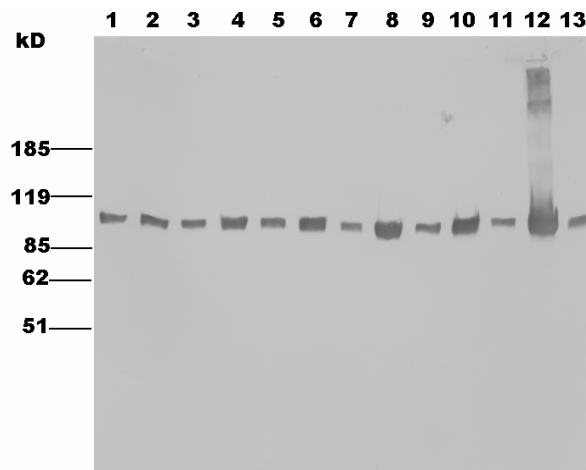


**Figure 4.1.3.B:** SDS-PAGE showing immunolabeling of a concentration series of a GluR-B sample, which had been purified by affinity chromatography. Lanes labeled with even numbers show the concentration series. Lanes with uneven numbers show the samples of the concentration series rediluted to the initial protein concentration of 4.3  $\mu\text{g}/\text{mL}$ . Samples were loaded as follows: lane 1, GluR-B at 4.3  $\mu\text{g}/\text{mL}$  (50 mL) not concentrated; lane 2, GluR-B at ca. 8.6  $\mu\text{g}/\text{mL}$  (25 mL); lane 4, GluR-B at ca. 14.7  $\mu\text{g}/\text{mL}$  (14 mL); lane 6, GluR-B at ca. 32  $\mu\text{g}/\text{mL}$  (6 mL); lane 8, GluR-B at ca. 45  $\mu\text{g}/\text{mL}$  (3.5 mL); lane 10, GluR-B at 60  $\mu\text{g}/\text{mL}$  (2.3 mL); lane 12, GluR-B at 300  $\mu\text{g}/\text{mL}$  (0.4 mL). Before loading proteins were incubated with SDS (3 $\times$ ) buffer in the ratio 2:1 for 5 min at 90° C. Of each sample 12  $\mu\text{L}$  were loaded.

After redilution the GluR-B specific aggregations in the 300  $\mu\text{g}/\text{mL}$  sample were not detected anymore (see lane 13). Although the immunodetection of these aggregations proved to be very sensitive, it is possible that the concentration of GluR-B specific aggregations in the rediluted sample was below the detection limit. At the same time it cannot be ruled out that the aggregation is reversible, which might indicate that it is not mediated by covalent interactions among GluR-B molecules.

Furthermore is it possible that the accumulation of the detergent Triton X-100 during the concentration of protein samples is critical for the stability of GluR-B homomers. It was found that concentration of the purified eluates by a factor of 4 was accompanied by an increase of Triton X-100 concentration by a factor of 2. The sample of lane 12 was concentrated by a factor of 125 (50 mL  $\rightarrow$  0.4mL).

## 4.2. BIOCHEMICAL CHARACTERIZATION OF GLUR-B

Electrophysiological whole-cell recordings had shown that GluR expressed in stable insect cells in principal form functional channels (see paragraph 4.1.1.). Conditions for reconstitution of purified receptor molecules in liposomes have not been established yet. Therefore ligand-binding was taken as a substitute to show that the isolated protein is not completely inactive.

### 4.2.1. RADIOLIGAND-BINDING

Binding activity of GluR-B was assayed by filter-binding experiments. Using the radioligand [ $^3\text{H}$ ]-AMPA, experiments were carried out with two different types of GluR-B samples, which were collected from two different protein preparations: a) membranes of the stable insect cells before solubilization and b) GluR-B protein after purification by immunoaffinity chromatography. (Prior to the filter-binding experiments both samples were stored at  $-80^\circ\text{C}$ .)

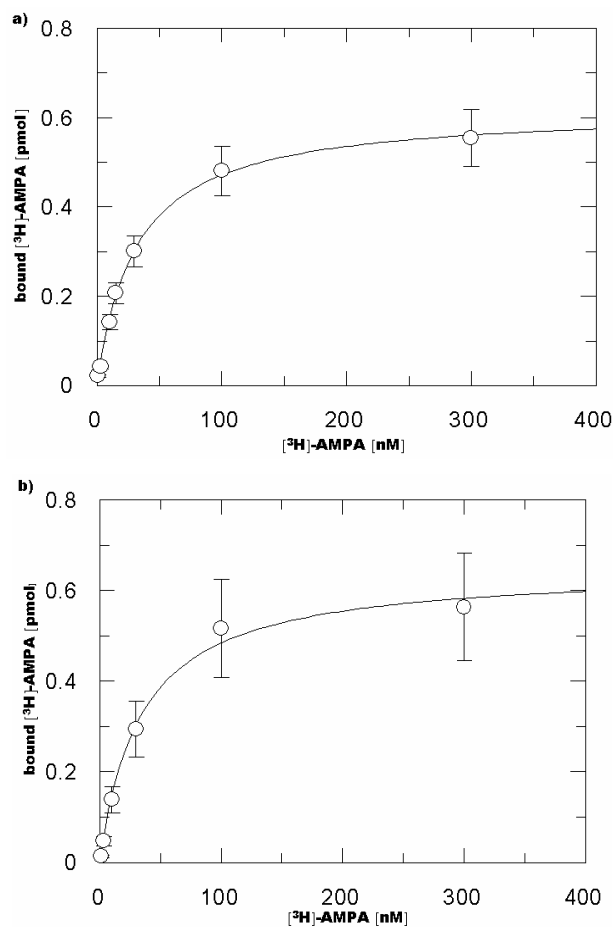


Figure 4.2.1.A: Saturation binding isotherms of specific binding; a) Binding of [ $^3\text{H}$ ]-AMPA to GluR-B containing membranes of stable insect cells and b) Binding of [ $^3\text{H}$ ]-AMPA to GluR-B solubilized in Triton X-100 after purification by affinity chromatography. Curves were fitted by a non-linear curve fitting assuming a single-binding site mechanism (GraFit, Erithacus Software; Prism, GraphPad Software).

The saturation curves obtained were used to determine values for the equilibrium dissociation constant ( $K_D$ -values) and values for the total amount of receptor/ligand complexes present ( $B_{max}$ -values). Non-linear curve fits confirm a single-binding site mechanism.

$K_D$ -values and  $B_{max}$ -values were calculated as listed. Values for GluR-B protein, which had been isolated from virus infected insect cells (Safferling et al., 2001) are listed for comparison. The comparison reveals that  $K_D$ -values differentiate by a factor of ca. 2. Higher binding capacities are plausible since protein yields for the virus-induced expression were ca. 100  $\mu\text{g}$  GluR-B per liter cell culture while the same volume of stable insect cells yielded only 40 to 50  $\mu\text{g}$  GluR-B protein.

<b>Stable insect cells</b>	<b>Dissociation constant (<math>K_D</math>)</b>	<b>Binding capacity (<math>B_{max}</math>)</b>
GluR-B membranes	31.4 +/- 1.7 nM	6.2 pmol/mg
Purified GluR-B solubilized in Triton X-100	34.0 +/- 4.6 nM	1298 pmol/mg
<b>Virus infected insect cells</b>		
Purified GluR-B solubilized in Triton X-100	18.2 +/- 0.9 nM	2140 pmol/mg

### 4.3. INDIRECT ANALYSIS OF THE OLIGOMERIC PROTEIN STRUCTURE BY CROSS-LINKING

Samples were cross-linked at increasing DTSSP concentrations and signals were detected by enhanced chemiluminescence (ECL). ECL Western blotting (Amersham) after SDS-PAGE of cross-linked and non-cross-linked samples revealed a pattern of four GluR-B specific bands. Monomeric and dimeric bands showed strong signal intensities compared to the putative trimeric and tetrameric bands. There was no pentamer or higher oligomer detectable. The four-band-pattern was observed in rat brain lysate samples and in purified GluR-B samples. By cross-linking of rat brain lysate samples it was possible to stabilize the GluR oligomer such that only the tetrameric band was detected. With purified GluR-B homomers the same experiment did not succeed. One possible explanation for this difference could be that glutamate receptors in rat brain lysate are heteromers, which offer more variability in side chains. However, in both samples the dimer seems to be a subassembly with a high biochemical stability.

#### 4.3.1. CROSS-LINKING OF PURIFIED GLUR-B HOMOMERS

Chemical cross-linking of recombinantly expressed and purified GluR-B protein molecules did not produce a distinct major cross-linking adduct. ECL Western blotting of cross-linked GluR-B proteins is shown in Figure 4.3.1.A.

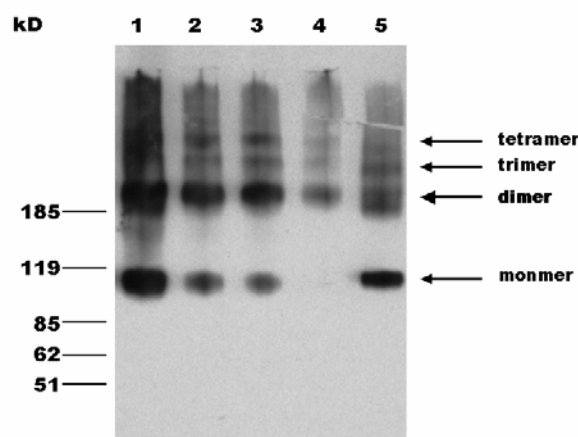


Figure 4.3.1.A: SDS-PAGE followed by ECL Western blotting of isolated and chemically cross-linked GluR-B protein; samples were loaded as follows: lane 1, minusCL control; lane 2, 1 mM DTSSP; lane 3, 3 mM DTSSP; lane 4, 5 mM DTSSP, lane 5, 5 mM DTSSP plus 10 %  $\beta$ -Mercaptoethanol. After addition of SDS (3 $\times$ ) sample buffer 12  $\mu$ L were loaded on a NuPAGE 3-8 % Tris-Acetate gradient gel (Novex).

In this experiment 100  $\mu$ l aliquots of GluR-B protein at a protein concentration of 26  $\mu$ g/ml, solubilized in Triton X-100, were cross-linked with 1 mM, 3 mM and 5 mM DTSSP (lane 2 to 4), incubated with SDS sample buffer and loaded on a NuPAGE 3-8 % Tris-Acetate gradient gel (Novex). At increasing concentrations of DTSSP the intensities of the monomeric and the putative dimeric bands decrease. However, this is not correlated with an increase in any other signal. At 5 mM DTSSP even the prominent putative dimeric band becomes faint.

An inverse relation of signal intensities among samples cross-linked with increasing concentration of DTSSP is not evident in Figure 4.3.2.1.A. Furthermore the total sum of signal intensities in the different lanes is not the same. It is conceivable that DTSSP produced higher protein conglomerates by **intermolecular** cross-linking. These conglomerates were possibly not detected since they could not enter the gel. (This is confirmed by the fact that reduction of cross-linked samples with  $\beta$ -mercaptoethanol reproduces the monomeric signals.) Beside the monomeric band and the putative dimeric band Figure 4.3.2.1.A. shows two additional bands specific for GluR-B. Most likely the two bands represent a GluR-B trimer and a GluR-B tetramer. Presumably 10%  $\beta$ -mercaptoethanol was not sufficient to reduce all the oligomers formed in the presence of 5 mM DTSSP. Although the monomeric signal in the reduced sample (lane 5) is more intense than those of the cross-linked samples it is obvious that the reduction by  $\beta$ -mercaptoethanol was not quantitative: Beside the signals for the higher oligomeric bands there is a strong dimeric band in the  $\beta$ -mercaptoethanol reduced samples.

#### **4.3.2. CROSS-LINKING OF TOTAL RAT BRAIN LYSATE**

Cross-linking experiments with total rat brain lysate were used as a control for experiments with purified GluR-B. Rat brain lysate was cross-linked at different DTSSP concentrations (Aliquots of 100  $\mu$ l rat brain lysate were incubated with 0.5 mM, 0.75 mM, 1 mM, 1.5 mM, 2 mM and 2.5 mM DTSSP.) Of these samples 10  $\mu$ l were incubated with 5  $\mu$ l SDS sample buffer as described and loaded on a 8% PAA gel. All samples were loaded with SDS sample buffer. The result of GluR-B/-C specific immunolabeling is shown in Figure 4.3.2.A. A concentration of 2 mM DTSSP (lane 6) is sufficient in this protein sample to cross-link GluR monomers quantitatively into the major GluR adduct. At 0.5 mM DTSSP (lane 2) the monomer band is still very intensive. Beside the GluR-specific monomeric band and the band of the major cross-link adduct every lane shows a band which could be attributed to a GluR dimer.

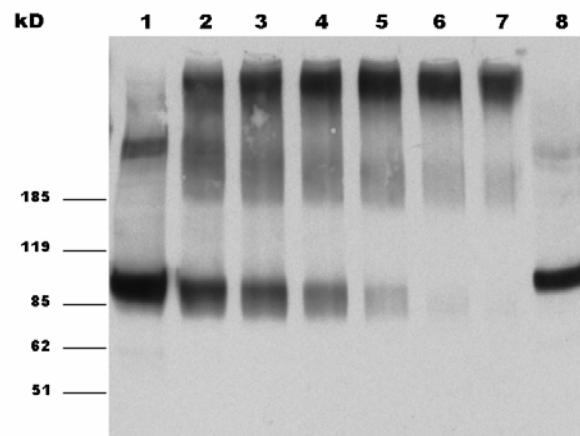


**Figure 4.3.2.A:** SDS-PAGE followed by ECL Western blotting of chemically cross-linked rat brain lysate; samples were loaded as follows: lane 1, minusCL-control; lane 2, 0.5 mM DTSSP; lane 3, 0.75 mM DTSSP; lane 4, 1 mM DTSSP, lane 5, 1.5 mM DTSSP; lane 6, 2 mM DTSSP; lane 7, 2.5 mM DTSSP, lane 8, 2.5 mM DTSSP plus 50 mM DTT. After addition of SDS (3 $\times$ ) sample buffer 12  $\mu$ L were loaded on a 8% PAA gel.

A reliable calibration of the GluR cross-linking adduct with the highest molecular weight band would require a membrane protein with a comparable molecular weight. The marker protein with the highest molecular weight used in these experiments corresponds to 185 kD. According to this the major adduct would have a molecular weight of ca. 420 kD (+/-50 kD). Since the band with the highest molecular weight, which represents most probably a tetramer, is not discrete the error of this calculation is considerable. (In this blot the trimeric band is missing. But it was successfully resolved in other experiments with rat brain lysate.) The monomeric band has a calculated molecular weight between 125 and 110 kD. At higher concentrations of DTSSP signals of the monomer and the putative dimer are less intense. Simultaneously the intensity of the putative tetrameric band is increasing. The inverse correlation between signal intensities of GluR specific bands can be considered as a successful test for the cross-linking technique in experiments with total brain lysate. The putative dimeric band is very prominent in the absence of reducing agents (see minusCL-control in lane 1) and in the presence of the reducing agent DDT (DTT-control) (see lane 8). Representing a protein with a MW between 240 and 180 kD this putative dimer shows an increasingly higher electrophoretic mobility at higher DTSSP-concentrations (see lane 2 to 7).

## 4.4. DIRECT ANALYSIS OF THE OLIGOMERIC GLUR-B STRUCTURE BY ELECTRONMICROSCOPY

### 4.4.1. CRYO-ELECTRON MICROSCOPY

Since proteins are vitrified in their buffer cryo-electron microscopy can be considered as a physiological technique compared to the negative stain approach (vitrification means that the buffer is amorphously frozen). Negative staining artifacts such as partial staining and deformation of protein structures are thus excluded. In Figure 4.4.1.A a frozen-hydrated preparation of GluR-B is shown at a magnification of 3000 $\times$ . The image illustrates that the amorphously frozen buffer forms ice-layers of variable thickness. The presence of the thin ice-layers is sometimes documented by black contaminations, which are lying on top of them.

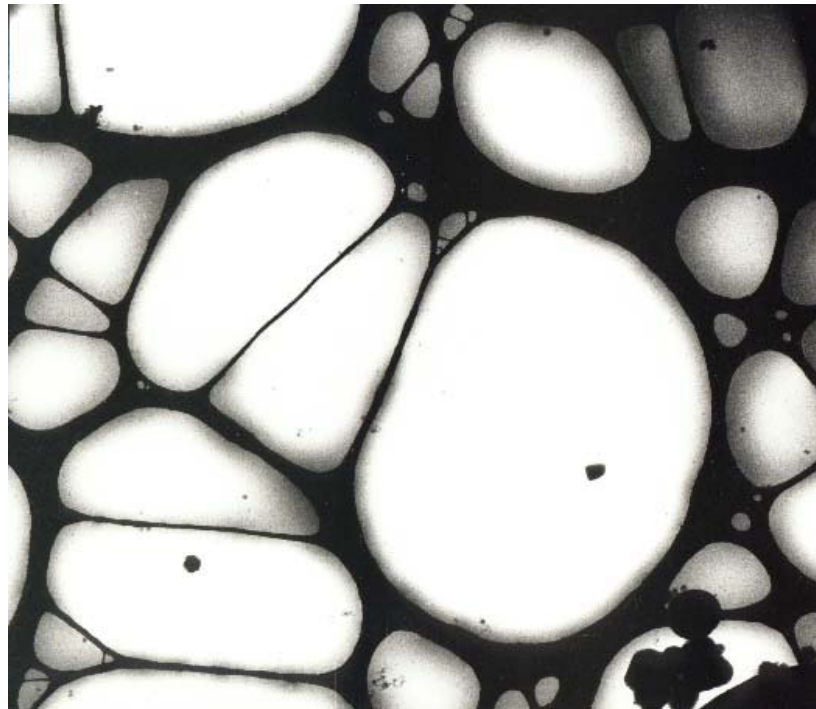


**Figure 4.4.1.A:** Cryo electron microscopy; shown is a frozen hydrated sample of a purified GluR-B sample at low magnification (3000 $\times$ ) prepared on a holey grid. Each hole is filled with vitrified buffer, which contained GluR-B protein.

To determine the thickness of ice layers the electron beam was used to burn small holes through the ice. By tilting the grid for 30 $^{\circ}$  to both sides it was possible to visualize the burn line and calculate the thickness of the ice, which was ca. 100 to 150 nm. In principle these conditions should allow the detection of smaller proteins like the glutamate receptor ion channel. Due to the low contrast in cryo-electron microscopy detection of larger macromolecules like TMV is easier. To facilitate the detection of smaller proteins their concentration should be at least in the mg/mL range.

At a GluR-B concentration of ca. 200  $\mu\text{g}/\text{mL}$  in theory the number of receptor molecules per hole with a diameter of 1  $\mu\text{m}$  would be lower than 30. To facilitate the detection of GluR-B ion channels we increased the protein concentration and prepared vitrified samples at 200, 330 and ca. 660  $\mu\text{g}/\text{mL}$  using air glow discharged grids. Since none of these experiments allowed the detection of the vitrified receptor protein in any form it was suspected that the protein was immobilized by the matrix of the grid and thus undetectable. To drive GluR-B protein to the holes, grids carrying the perforated film were glow discharged in an atmosphere of tripropylamine.

When it was clear that neither air glow discharged grids nor grids glow discharged in an atmosphere of tripropylamine allowed the detection of frozen hydrated GluR-B ion channels blotting conditions were varied using air glow discharged grids and grids glow discharged in an atmosphere of tripropylamine. However, neither of these pretreatments had a detectable influence on the quality of ice-layers. A slight difference was noticeable during blotting; the supernatants on grids glow discharged in an atmosphere of tripropylamine were removed more quickly by the same kind of filter paper.

By the use of filter papers having three different densities blotting conditions were further varied. In control experiments using air glow discharged grids it was relatively easy to vitrify TMV with each of the different filter papers. TMV was in the same buffer as the GluR-B protein. The amount of vitrified TMV was higher when the filter paper with the lowest density was used for blotting. The same effect was observed when the supernatant was plotted from the opposite site. However, these quantitative improvements for TMV did not facilitate the detection of vitrified GluR-B ion channels.

#### **4.4.2. CRYO-NEGATIVE STAINING**

The cryo-negative staining approach was shown to enhance contrast for several proteins under cryo conditions (Adrian et al., 1998). It was therefore considered as a promising method for the detection of GluR-B in vitrified samples. In an initial control experiment the potential of the cryo-negative staining method was tested successfully using the tobacco mosaic virus (TMV). Figure 4.4.2.A shows TMV rods embedded in a mixture of vitrified buffer and 16% ammonium molybdate stain. The rods are contrasted by the stain, which makes their detection easier. At reduced concentrations of ammonium molybdate, i.e. 10% and 2%, the contrast was found to be lower.

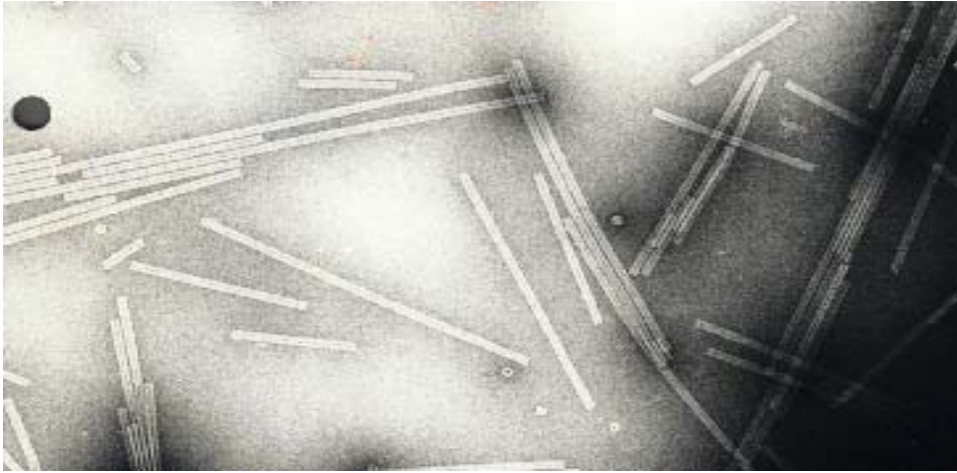


**Figure 4.4.2.A: Cryo-negative staining; TMV vitrified in a mixture of buffer and 16% ammonium molybdate at a magnification of 30 000 $\times$ .**

During cryo-negative staining experiments with GluR-B the variations described in paragraph 4.4.1. were repeated. Since the cryo-negative stain experiments were not done in parallel to the cryo-experiments the GluR-B samples originated from different protein preparations. The approximate GluR-B concentrations used for cryo-negative staining experiments were 80, 200 and ca. 600  $\mu\text{g}/\text{mL}$ . In a brute-force approach after intensive concentration (see paragraph 4.1.3.) the GluR-B concentration was even 1.7  $\text{mg}/\text{mL}$ . When ammonium molybdate was added to this relatively high concentration of GluR-B turbidity was detected in the mixture.

In addition to the variations, described in paragraph 4.4.1. different modes of stain incubation were tested. In one series the grid carrying the protein sample was placed on a 60  $\mu\text{L}$  droplet of 16% ammonium molybdate. However due to the presence of the detergent the grid did mostly not float on the stain droplet. Therefore in another series ca. 3  $\mu\text{L}$  of stain were added to the protein sample prior to plunging in liquid nitrogen. To evaluate a possible harmful effect of the high stain concentration the experiments were repeated with 10% ammonium molybdate. The suggested incubation time was 60 seconds. Here 30 and 120 seconds of incubation were tested alternatively. Beside the front blot, blotting from the back and from both sides simultaneously was tested (control experiments with TMV had shown that more TMV molecules were detectable in the holes when the grid was blotted from both sides). However, none of the variations allowed the detection vitrified GluR-B oligomers.

### 4.4.3. NEGATIVE STAINING

In parallel to cryo-electron microscopy techniques possible improvements of the negative staining for GluR-B were considered. Other investigators had found in initial experiments that aurothioglucose could be a promising stain for membrane proteins (B. Böttcher, personal communication).

#### 4.4.3.1. GLUR-B NEGATIVELY STAINED IN AUROTHIOGLUCOSE

Negative staining in uranyl acetate, which is only soluble in a low pH range (3-4) and embedding in aurothioglucose (pH: 6-7) for the extracellular hemoglobin of *Ophelia bicornis* had been compared earlier by three-dimensional reconstruction, using random conical tilting (Cejka et al., 1992). Uranyl acetate stained samples showed about 60% of the original height of the molecule due to flattening and incomplete embedding in stain. In contrast to this, the specimen embedded in aurothioglucose showed no flattening. Considering the deep-stain effect of aurothioglucose GluR-B protein specimen were recorded according to the random conical tilt approach using the low dose facility of the Philips EM400 microscope. For the random conical tilt technique (RCT) the same area has to be imaged twice; first in a tilted position with the plane of the grid  $50^\circ$  from the horizontal and subsequently the untilted position. (For the reconstruction of a 3D model with the RCT technique images of the tilted position are used while for the initial classification particles from untilted images are taken. See 2.5.2.) One tilt pair is shown in Figure 4.4.3.1.A.



**Figure 4.4.3.1.A:** GluR-B negatively stained in aurothioglucose at magnification of 46000 $\times$ ; the image on the left side shows the grid tilted by  $50^\circ$  relative to the electron beam. On the right side the same area was imaged in an untilted position. The black contaminant illustrates the effect of tilting.

The changed shape of the black contaminant illustrates the effect of tilting. It is obvious from these images that aurothioglucose is a low contrast stain. In total 3400 pairs of protein particles were selected from 15 image pairs using the IMAGIC software package.

#### 4.4.3.2. IMAGE PROCESSING OF GLUR-B STAINED IN AUROTHIOGLUCOSE

Aurothioglucose (ATG) stained specimen were characterized by the granularity of the stain and low contrast. Images were band-pass filtered first. Compared with 0.01 and 0.05 the low-frequency cut-off (LFCO) value 0.03 produced the highest contrast. The high-frequency-cut off value during band-pass filtering was 0.16 and the value of the remaining low-frequency transmission was 0.005.

The cut-off parameters applied in IMAGIC have no dimension. They are given as the fraction ( $f$ ) of the Nyquist frequency with values from 0 to 1. When  $P$  corresponds to the pixel size the Nyquist frequency is  $1/(2 \times P)$ . Therefore each fraction  $f$  between 0 and 1 corresponds to the spatial frequency  $f/(2 \times P)$ . Since the pixel size is  $3 \text{ \AA}$  0.03 (LFCO) corresponds to a spatial frequency of  $1/200 \text{ \AA}^{-1}$ , whereas 0.3 (HFCO) corresponds to a spatial frequency of  $1/37.5 \text{ \AA}^{-1}$ .

In total 3440 protein particles like those shown in Figure 4.4.3.2.A. were centered by the iterative alignment procedure.

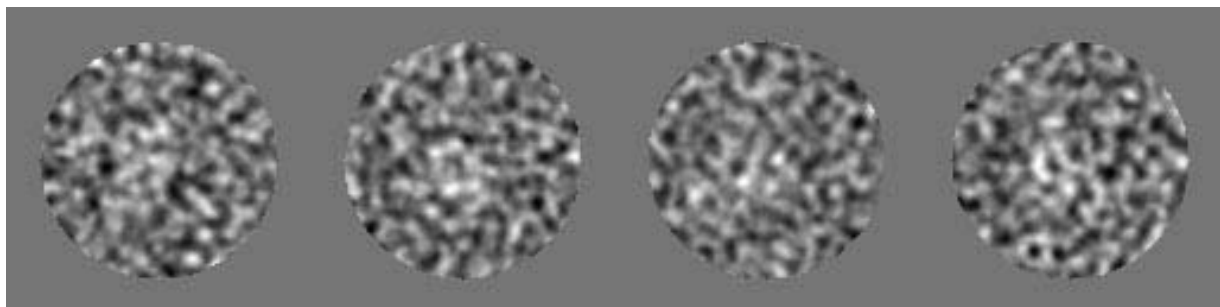


**Figure 4.4.3.2.A: GluR-B negatively stained in aurothioglucose; aligned GluR-B molecules. The edge of one frame corresponds to 97 nm.**

The average image of each alignment cycle, which is the total sum of all particles served as a new reference. Figure 4.4.3.2.B shows that the third cycle of iterative alignment produced rings around the central density. This untypical feature, which might be caused by the granularity of the stain is even more obvious in the images of the rotational sums (shown in Figure 4.4.3.2.C) and is meant to illustrate the problem with the classification of ATG stained GluR-B particles.

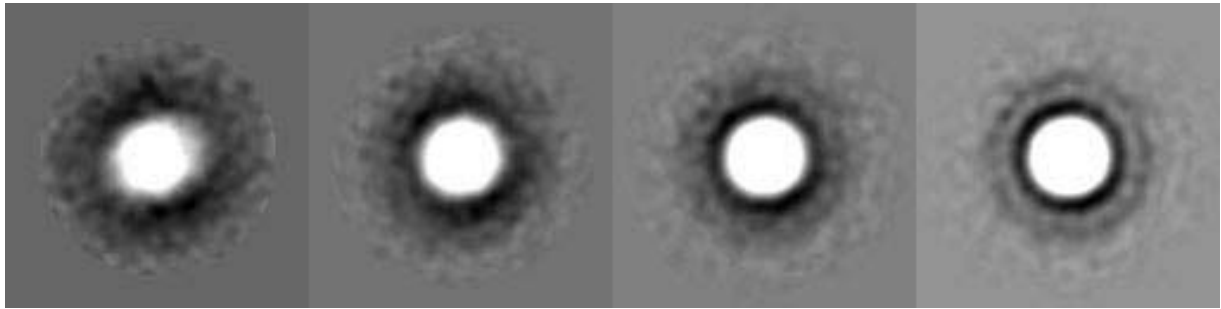


**Figure 4.4.3.2.B: GluR-B negatively stained in aurothioglucose; total sums after 3 steps of iterative alignment. The edge of one frame corresponds to 97 nm.**

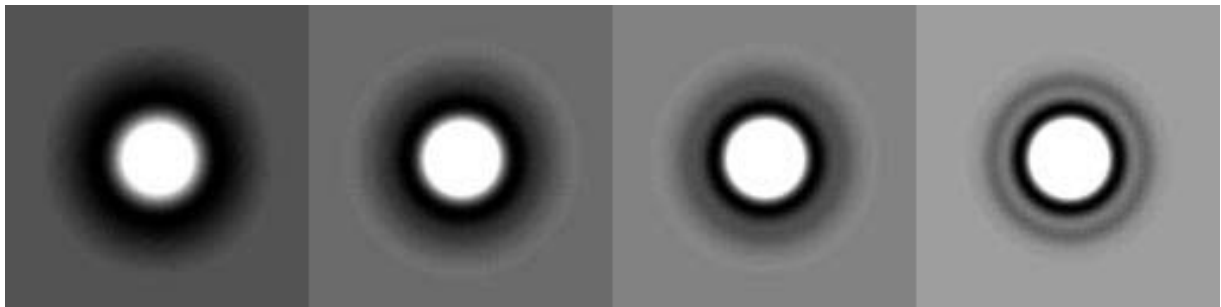


**Figure 4.4.3.2.C: GluR-B negatively stained in aurothioglucose; rotational sums after 3 steps of iterative alignment. The edge of one frame corresponds to 97 nm.**

The subsequent classification procedure resulted in very similar looking classes. The sum of one class is called “class average”. Neither size nor shape characterized these class averages (see Figure 4.4.3.2.D). Due to the low contrast enhancement of aurothioglucose characteristic features of the GluR-B protein were not detectable. However, recognition of such features is essential for classification and subsequent image processing.

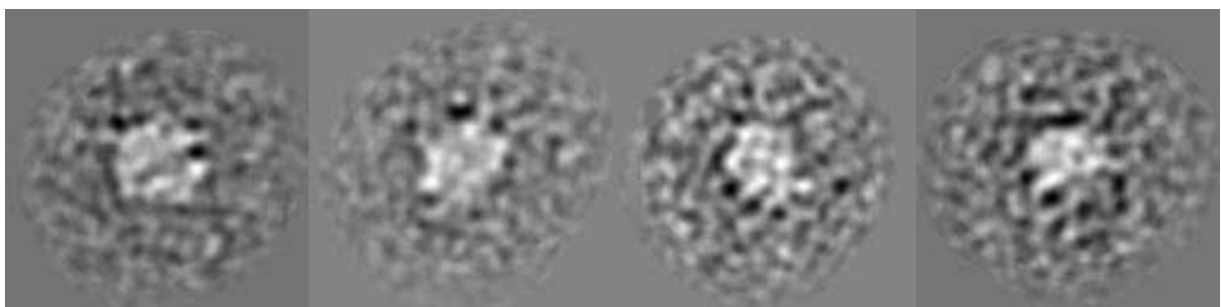


**Figure 4.4.3.2.D: GluR-B negatively stained in aurothioglucose; particles were classified into 220 classes, of which four are shown. The edge of one frame corresponds to 97 nm.**

Since 3D reconstruction is based on the successful classification of a data set image processing of GluR-B molecules negatively stained in aurothioglucose was not continued.

#### 4.4.3.3. GLUR-B STAINED IN URANYL ACETATE

For routine negative staining experiments receptor molecules were absorbed to a thin carbon film supported by a copper grid and air-dried. GluR-B has a high affinity for air glow discharged hydrophilic carbon films. Air glow discharging of the carbon films was applied to improve fixation of receptor molecules, which was tight enough to allow double washing of the grid with a detergent-free buffer. However, on freshly fished carbon films without previous glow discharging areas were found where the stain layer of 2% uranyl acetate showed variable thickness. Although the absolute thickness of these stain layers was not calibrated during these experiments it was assumed that the preservation of GluR-B should be best in the thickest stain layers. Figure 4.4.3.3.A shows an extended area of these receptor molecules imaged at a magnification of 46000 $\times$  with a Philips EM 400 electron microscope.

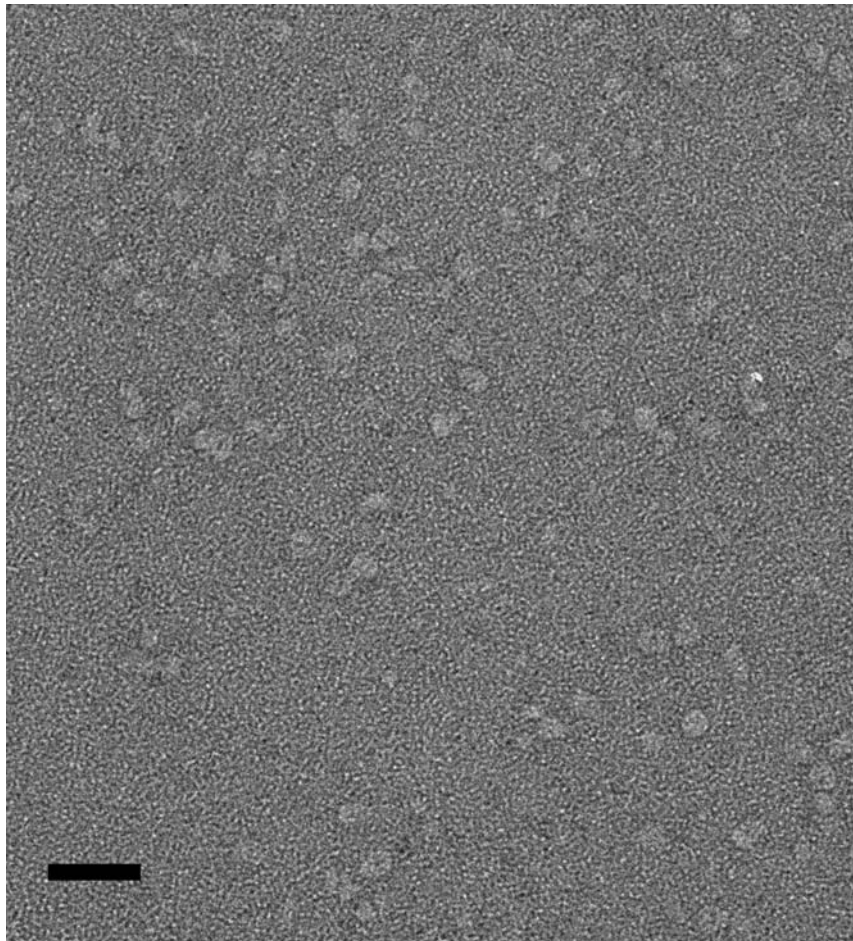


**Figure 4.4.3.3.A: GluR-B molecules negatively stained in 2 % uranyl acetate as they were selected for image processing. The bar corresponds to 50 nm.**

Most of the GluR-B molecules in Figure 4.4.3.3.A are homogeneous in size, while some molecules are too small to be complete oligomers; they were not selected for image processing.

#### 4.4.3.4. SINGLE PARTICLE ANALYSIS AND 3D RECONSTRUCTION OF GLUR-B

To evaluate the putative positive effect on GluR-B preservation 500 protein molecules, of which four are shown in Figure 4.4.3.4.A were processed using the image software package IMAGIC. Of the initially selected 665 particles 165 were excluded. Their location was too close to other proteins, which can prevent their correct alignment.

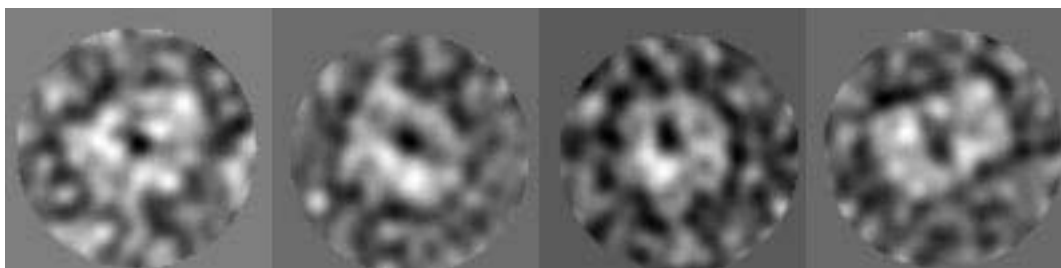


**Figure 4.4.3.4.A: Electron microscopic images of GluR-B homomers negatively stained with 2% uranyl acetate. The edge of one frame corresponds to 30 nm.**

The projection images showed that molecular dimensions of the most elongated projections of the GluR-B protein molecules were as long as ca. 180 Å, while the shortest projections were ca. 100 Å. During initial band-pass filtering the lower limit, called the low-frequency cut-off (LFCO) of the Gauss filter was varied to optimize the contrast and to achieve optimal adjustment to the size of the GluR-B molecule as suggested by the manual of IMAGIC. Thus the variation of the LFCO parameter resulted in five different classifications, which are listed with the corresponding spatial frequencies in Table 4.4.3.4.A.

Classification #	Low-frequency cut-off (LFCO)	Spatial Frequency [ $\text{\AA}^{-1}$ ]	Name of the 3D model
1	0.005	1/1200	GluR-BI
2	0.01	1/600	not calculated
3	0.02	1/300	not calculated
4	0.03	1/200	GluR-BII a/ b
5	0.05	1/120	GluR-BIII

**Table 4.4.3.4.A.: The variation of the low-frequency cut-off (LFCO) parameter, resulted in five different classifications.**

For all classifications the value for the high-frequency cut-off (HFCO) was 0.16, which corresponds to a spatial frequency of  $1/37.5 \text{ \AA}^{-1}$  since pixel size is 3 Å. The residual transmission was 0.005 for all.

---

After alignment of particles the five sets were classified independently. Particles of each classification were grouped into 20 classes yielding on average 25 protein particles per class. The class averages of each classification were displayed in a gallery. Visual inspection of the five galleries showed that the elimination of low frequency information reduced contrast in the images. Furthermore it became obvious that class averages of different low-frequency cut-offs were notably different, although some class averages in one gallery had very similar-looking counterparts in other galleries. (See now Figure 4.4.3.4.B. on the next page.)

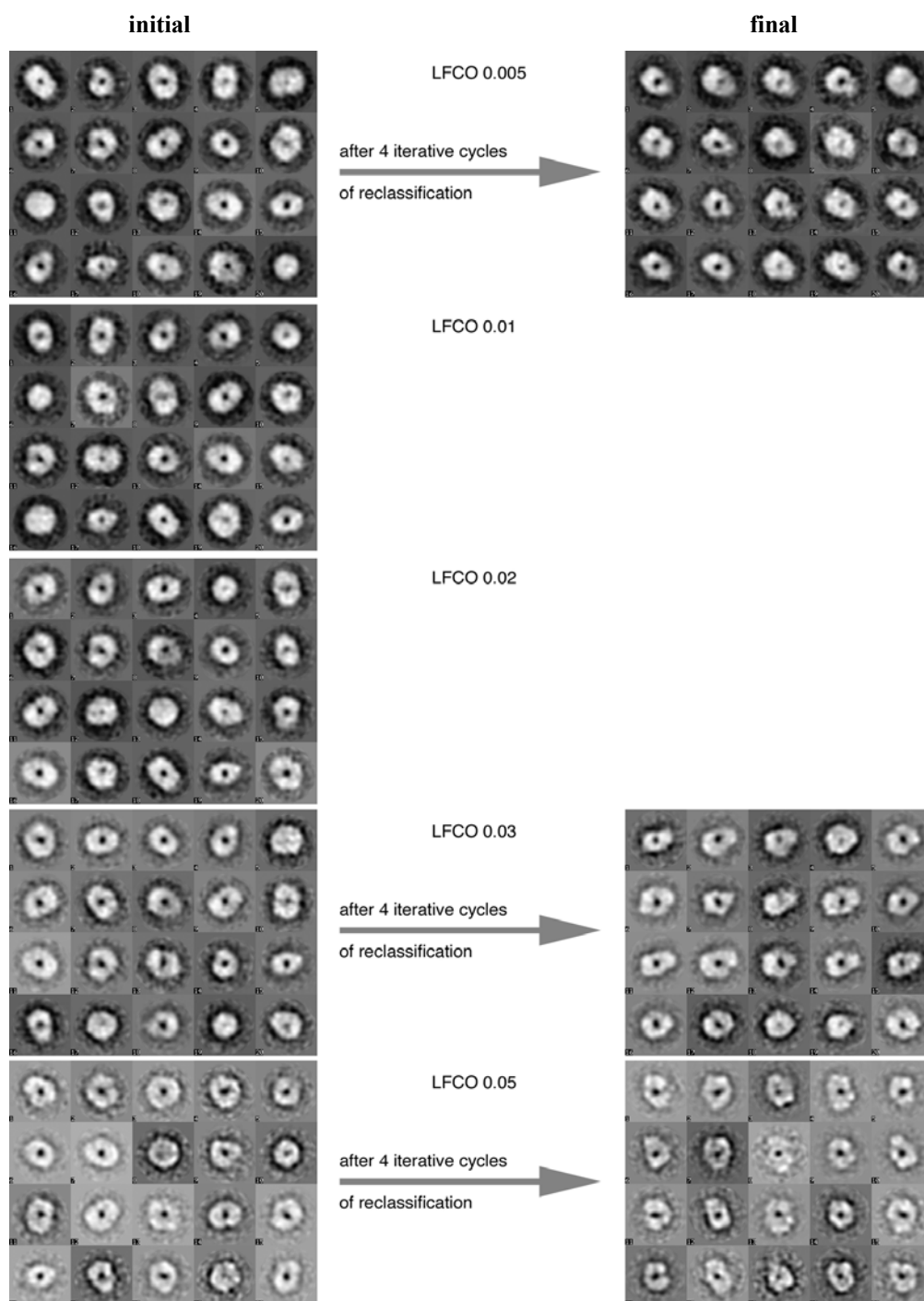


**Figure 4.4.3.4.B: Influence of the low-frequency cut-off (LFCO) on particle classification. Each classification consists of 20 class averages. Left side from top to bottom: LFCO 0.005 (classification #1), LFCO 0.01 (classification #2), LFCO 0.02 (classification #3), LFCO 0.03 (classification #4) and LFCO 0.05 (classification #5). The classifications #1, #4 and #5, which were selected for further image processing are shown on the right side after 4 iterative cycles of reclassification. The edge of one image frame corresponds to 30 nm.**

After visual inspection of the galleries it was postulated that similar looking class averages have a large number of identical particles in common. This postulate was checked by pair wise analysis of the different classifications (in total 10 combinations were possible). If more than 50 % of particles forming a class average in one classification were identical to the

particles forming a class averages in a different classification and *vice versa* they were considered to be equivalent. The maximum number of equivalent class averages is 20 since each set consists of 20 class averages. The results of this comparative analysis, i.e. the total number of equivalent class averages for all 10 pairs were visualized in a 3D plot, which is shown in Figure 4.4.3.4.C. The diagram illustrates the influence of the LFCO on the alignment and on the initial classification of GluR-B receptor molecules suggesting that the consistency of the initial classification is higher among those classifications that have more low-frequency information in common. For example classification #1 (LFCO 0.005) and classification #2 (LFCO 0.01) have 15 equivalent class averages and thus more low-frequency information in common than any other combination. Whereas the analog comparison of LFCO 0.05 (classification #5) with parameter sets #1, #2, #3 and #4 produced a very low rate of equivalent class averages for all four possible combinations.

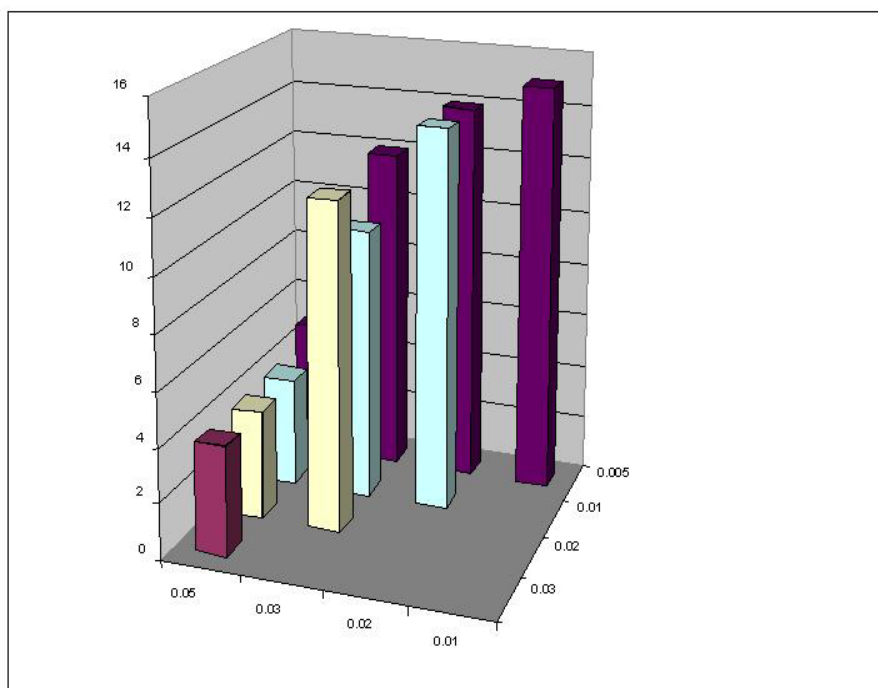


**Figure 4.4.3.4.C: Pair wise comparison of class averages after initial classification; the vertical axis of the diagram measures the degree of identity between two compared classifications. For each of the 10 possible combinations the number of class averages, which showed more than 50% particle-identity to a class averages of a different classification, and *vice versa* is plotted. The two in-plane axes indicate the low-frequency cut-off values, which characterize the five classifications (see Table 4.4.3.4.A.).**

As shown in Table 4.4.3.4.A the spatial frequency of LFCO 0.03 (classification #4) is close to the largest molecular dimensions of GluR-B protein molecules, which was found to be ca. 180 Å according to the projection views. Classification #4 shares with #1 (LFCO 0.005) and #3 (LFCO 0.02) 12 class averages each with more than 50% particle-identity. Since the

analysis showed that all possible combinations with classification #5 (LFCO 0.05) have less than 6 class averages with more than 50% particle-identity it was concluded at this stage that spatial frequencies between  $1/120 \text{ \AA}$  and  $1/200 \text{ \AA}$  have a strong influence on the initial classification of GluR-B particles.

For further image processing classification #1 (LFCO 0.005), #4 (LFCO 0.03) and #5 (LFCO 0.05) were selected: Compared to the other classifications #1 contains the maximum of low-frequency information, classification #4 was selected because the LFCO of this classification fits the dimension of GluR-B molecule best. Classification #5 was chosen to allow a final evaluation of the LFCO 0.05, which appeared distinct. The classification of these three sets was optimized in four iterative cycles; the final class averages are input projections for the subsequent 3D reconstruction. For each iterative cycle of reclassification references from the previous cycle were selected.

The iterative optimization of class averages relative to selected references was accompanied by a considerable improvement of the variance per member value and a significant reclassification of particles: after the first iteration the comparative analysis of classification #4 (LFCO 0.03) and classification #1 (LFCO 0.005) showed that both had only one class average with more than 50% particle-identity. The preference for certain projection views could be one explanation for the significant reclassification of particles. For each iterative cycle of reclassification references from the previous cycle were selected. After the final 4<sup>th</sup> cycle classification #4 (LFCO 0.03) and #1 (LFCO 0.005) still had only one pair of class averages with more than 50% particle-identity (see Figure 4.4.3.4.D). At the same stage the two other combinations e.g. comparison of classification #1 with #5 and comparison of classification #4 with #5 had no class averages in common showing more than 50% particle-identity. These results are illustrated by Figure 4.4.3.4.D. The differences in the final class averages of each classification may result from the references, which were selected after the initial classification from the previous cycle of the same classification.

In Figure 4.4.3.4.E the improvement of the variance per member by iterative reclassification is documented. The three plots A, B and C show the decrease of the variance per member value during the course of iterative reclassification for LFCO 0.005 (A), LFCO 0.03 (B) and LFCO 0.05 (C). Interestingly the variance values of the classification with LFCO 0.05 were

below 0.4 right after the initial classification. The two other classifications reach this level only after the first cycle of iterative reclassification.

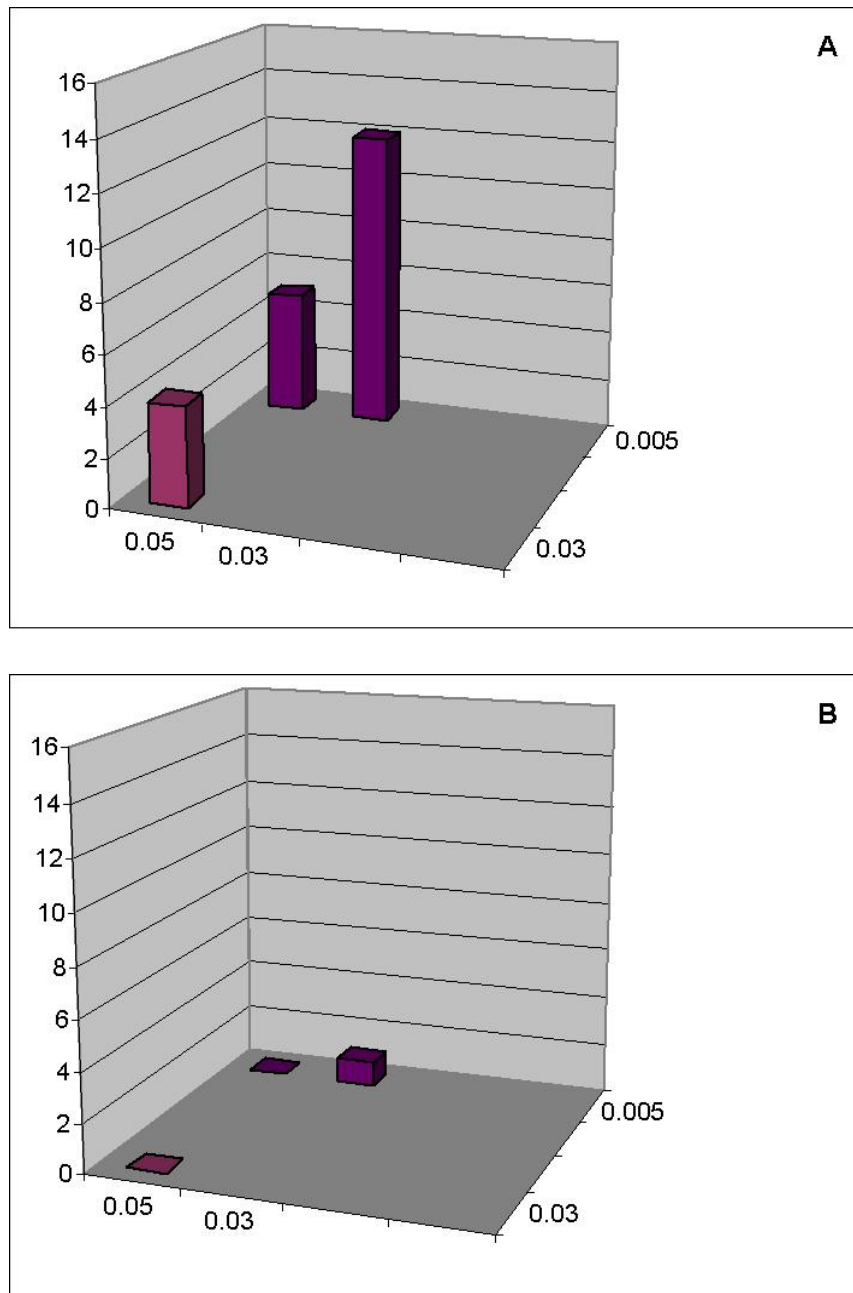


**Figure 4.4.3.4.D:** Pair wise comparison of class sums; the vertical axis measures the degree of identity between two compared class averages. Diagram A shows selectively the results of the comparative analysis after initial classification for those classifications, which were selected for further image processing. (These results are among those, which were already shown and explained in Figure 4.4.3.4.C.) Diagram B shows that the initial correlation among class averages belonging to different classifications after the first classification does not exist anymore after four cycles of iterative reclassification. The two in-plane axes indicate the low-frequency cut-off values, which characterize the classifications (see Table 4.4.3.4.A.).

The variance per member for all three classifications was below 0.3 after the 4<sup>th</sup> cycle of reclassification. Interestingly the final cycle continued to reduce the variance in #1 (LFCO 0.005), while values of the two other classifications were quite stable after the 1<sup>st</sup> cycle of reclassification. To have comparable conditions, i.e. 4 cycles for all sets the reclassification for #1 was not continued.

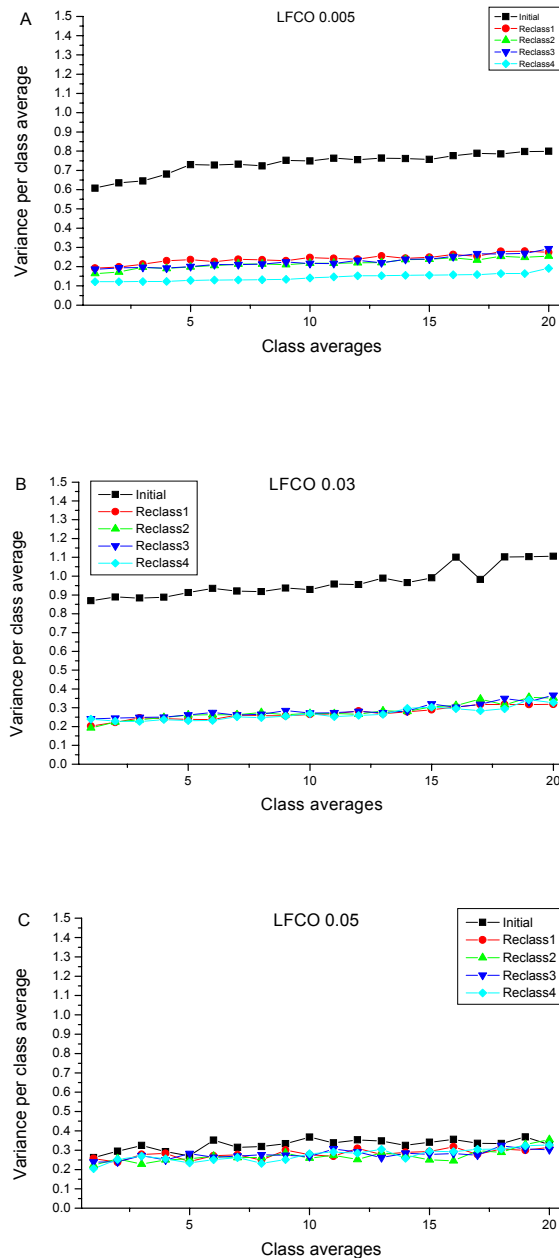


**Figure 4.4.3.4.E:** The three plots A, B and C show the decrease of the variance per member value during the course of iterative reclassification for LFCO 0.005 (A), LFCO 0.03 (B) and LFCO 0.05 (C). Despite differences after the initial classification the variance per member for all three parameter sets is below 0.3 after the 4<sup>th</sup> cycle of reclassification.

In Figure 4.4.3.4.F values for the variance per class average after the 4<sup>th</sup> cycle of iterative reclassification are summarized for all three classifications (LFCO 0.005 (A), LFCO 0.03 (B)

and LFCO 0.05 (C)). The LFCO 0.005 classification has the lowest values, while values of classification #4 (LFCO 0.03) and #5 (LFCO 0.05) are comparable. However, when variance values are compared it has to be considered that the variance is influenced by different factors like resolution and contrast. The obviously strong contrast in classification #1 (LFCO 0.005), see Figure 4.4.3.4.B, could be one explanation for its low variance values.

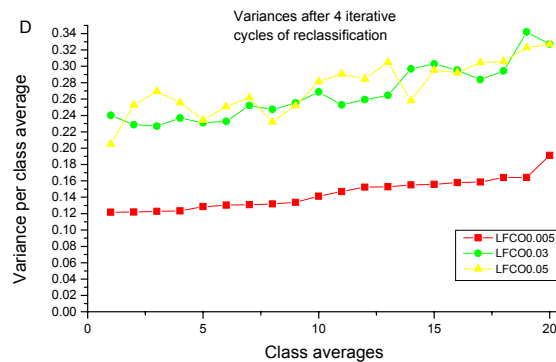


**Figure 4.4.3.4.F:** This plot summarizes the series of plot A, B and C. It shows the values for variance per class average after the fourth cycle of iterative reclassification.

Before assignment of Euler angles those class averages with the highest variance values were excluded in each classification (see Figure 4.4.3.4.F.). In classification #1 (LFCO 0.005 / red line) the last class average was excluded. In classification #4 (LFCO 0.03 / green line) the first thirteen class averages were selected since their variance values seemed to form a homogeneous group, i.e. there was no extreme among them. In classification #5 (LFCO 0.05 / yellow line) only the two class averages with the highest variance values were excluded.

After Euler angle assignment to these projections a first 3D model was calculated for each classification. Two views of each low-resolution model are shown in the following figures together with the input projections and the reprojections of the corresponding model. To evaluate the three models their input projections were compared with the corresponding reprojections, which can be calculated from the 3D model. An obvious similarity in shape and size between the input projection and the corresponding reprojection indicates that the correlation between the 3D model and its input projections is good. To quantitate this similarity the correlation coefficients (CC) were calculated for each image pair using the cross-correlation function of the software package SPIDER (Frank et al., 1996). To standardize the image contrast in each classification all images were filtered with LFCO 0.05 before the correlation coefficients were calculated. (The correlation coefficients are listed below the reprojections in the following figures.)

The 3D model of classification #1, GluR-BI, was calculated on the basis on 19 input projections. This rather compact model shows a central cavity and a hole. Its density is attributed to the strong contrast of the input projections. For image pair No.15 the CC value is highest, which is confirmed by the optical similarity of the input projection and the corresponding reprojection. However, most of the image pairs, like No.16, are not similar. Therefore this model is not likely to represent the GluR-B ion channel correctly.

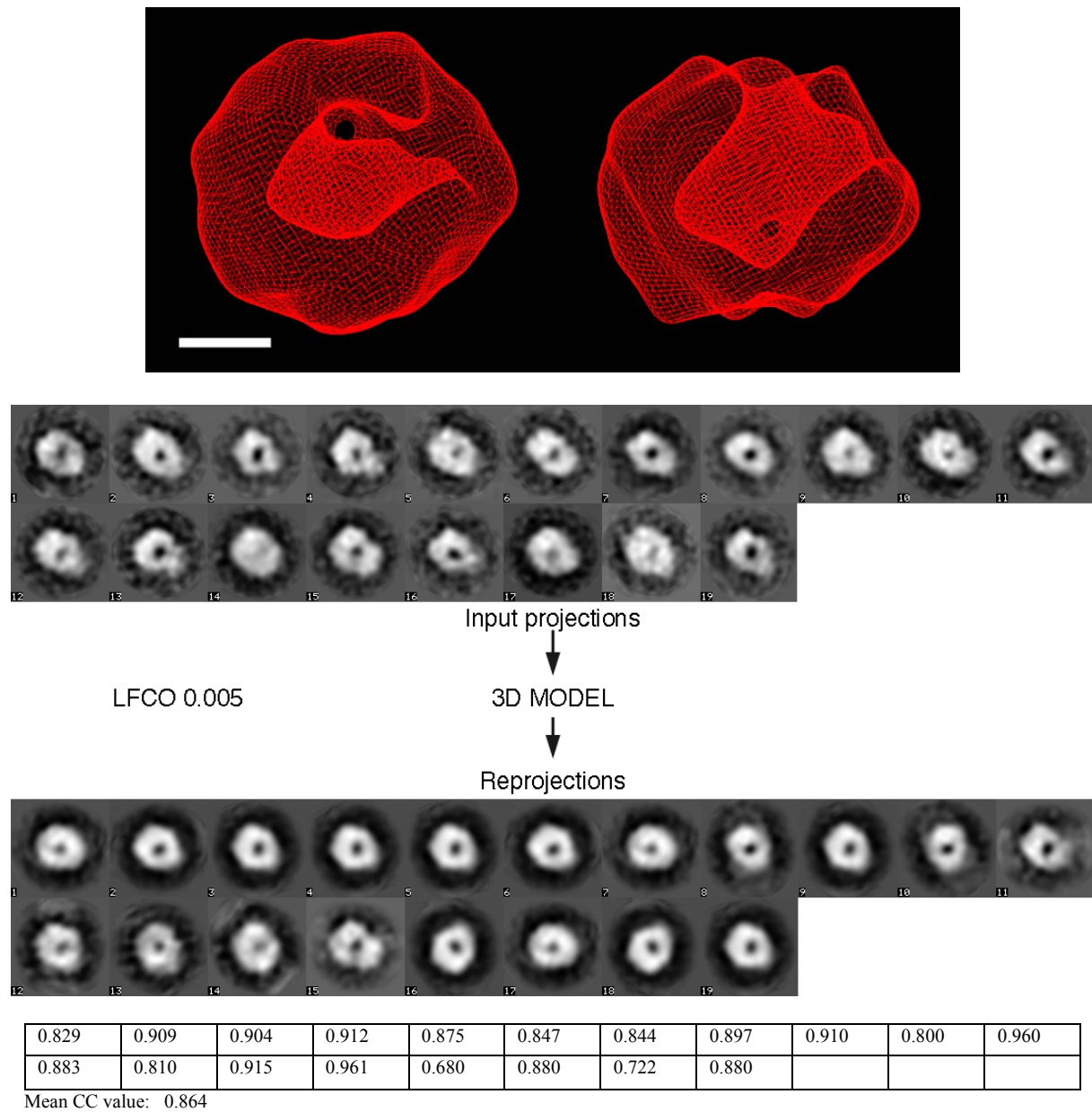


**Figure 4.4.3.4.G: Influence of the low-frequency cut-off parameter on the 3D reconstruction of GluR-BI: 3D model of classification #1 (LFCO 0.005).** Shown are a top and a side view of the same model. (The white bar corresponds to 5 nm.) The input projections of the model and its reprojections are shown as small images. (The edge of one image frame corresponds to 30 nm.) The table shows the cross correlation coefficients (CCs) between input projections and the corresponding reprojections.

The 3D model of classification #4 (LFCO 0.03), GluR-BII/a, is based on 13 input projections. It allowed the calculation of reprojections, which are all recognizable as the corresponding input projections (see CC values, which show a high mean value). This elongated model shows a closed but relatively open ring. It seems that GluR-B molecules used for this reconstruction were preserved in their oligomeric state in the negatively stained specimen.

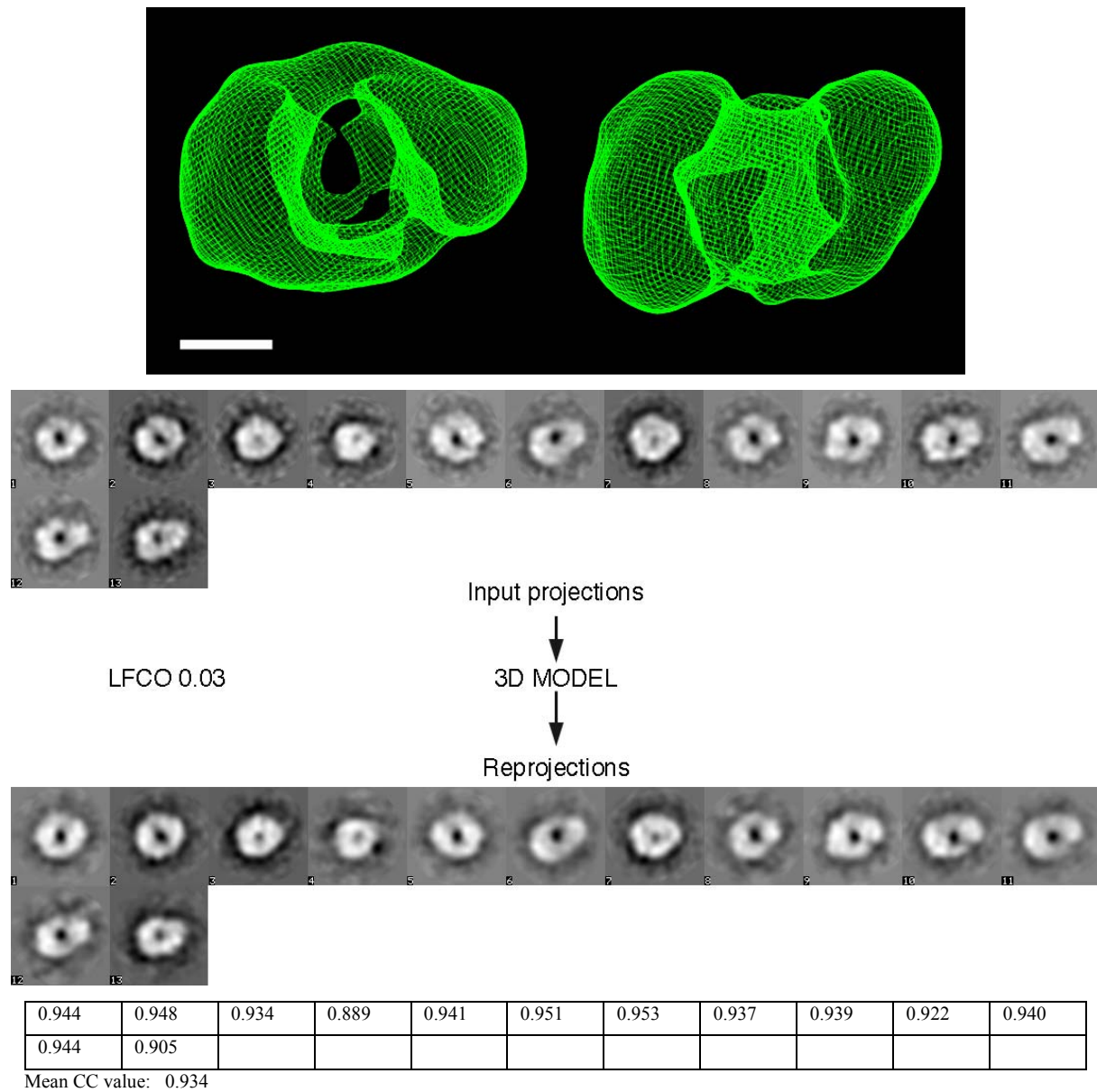


**Figure 4.4.3.4.H:** Influence of the low-frequency cut-off parameter on the 3D reconstruction of GluR-BII/a: 3D model of classification #4 (LFCO 0.03), which corresponds to a spatial frequency of  $1/200 \text{ \AA}^{-1}$ . Shown are a top and side view of the same model. (The white bar corresponds to 5 nm.) The input projections of the model and its reprojections are shown as small images. (The edge of one image frame corresponds to 30 nm.) The table shows the cross correlation coefficients between input projections and the corresponding reprojections.

A 3D reconstruction of more than 5000 negatively stained GluR-B molecules on air glow discharged carbon films, filtered with a LFCO that also corresponded to a spatial frequency of  $1/200 \text{ \AA}^{-1}$ , confirmed model GluR-BII/a (W. Tichelaar, personal communication).

The 3D model of classification #5 (LFCO 0.05), GluR-BIII, was calculated on the basis of 18 input projections.

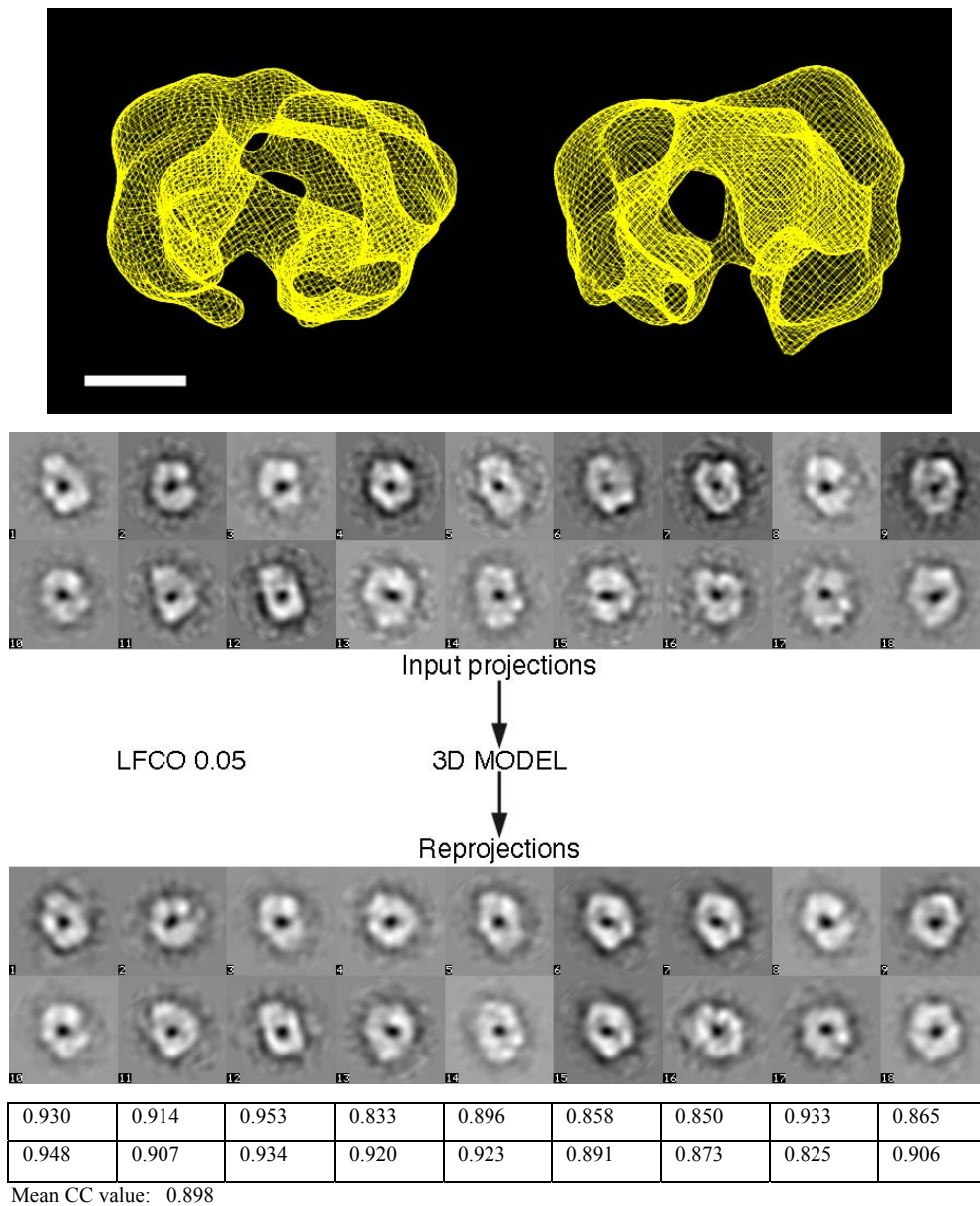


**Figure 4.4.3.4.I: Influence of the low-frequency cut-off parameter on the 3D reconstruction of GluR-BIII: 3D model of classification #5 (LFCO 0.05).** Shown are a top and a side view of the same model. (The white bar corresponds to 5 nm.) The input projections of the model and its rejections are shown as small images. (The edge of one image frame corresponds to 30 nm.) The table shows the cross correlation coefficients between input projections and the corresponding rejections.

Despite partial correspondence between input projections and rejections the model looks choppy. The loss of connectivity is attributed to the low contrast caused by the suppression of low frequencies. Model GluR-BIII can give less insight into the putative structure of the GluR-B ion channel than model GluR-BI although the input projections here have more similarly looking counterparts among their rejections (see No. 3, 10 and 12) than in model GluR-BI. The CC mean value for model GluR-BIII is slightly higher than for model GluR-BI,

which has a mean CC value of 0.864. The shape of model GluR-BIII might indicate that spatial frequencies below  $1/120 \text{ \AA}$  are essential for the correct assignment of Euler angles to the input projections.

Since input projections and rejections of model GluR-BII/a (LFCO 0.03, classification #4) showed the best agreement this classification was submitted to one further step of anchor set refinement. The two class averages with the highest standard deviations were excluded before the remaining 11 class averages were used to calculate the refined model, GluR-BII/b. In Figure 4.4.3.4.J this model, which has the dimensions  $18 \text{ nm} \times 14 \text{ nm} \times 11 \text{ nm}$  is shown. The red lines display the perspectives of Euler angles assigned to the input projections, i.e. they indicate the variety of available perspectives.

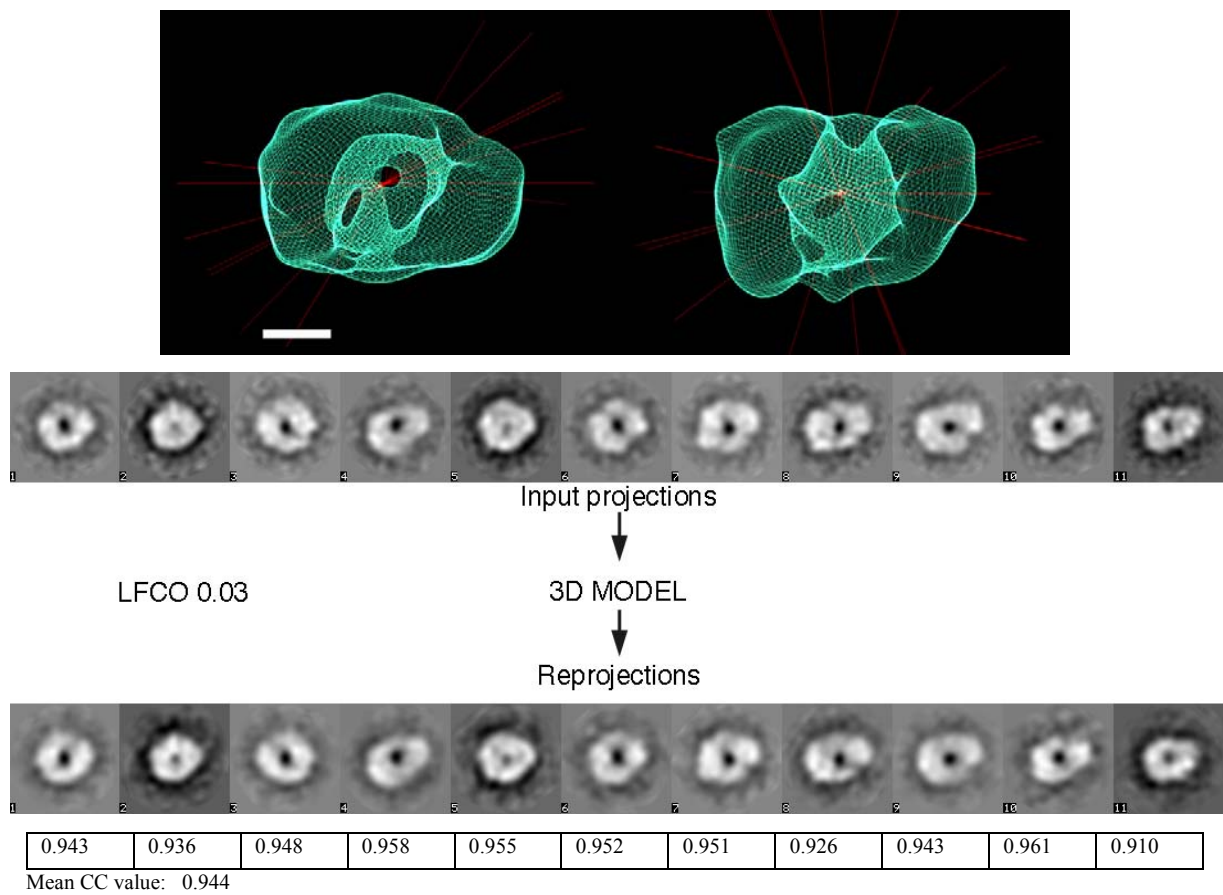


**Figure 4.4.3.4.J: Refinement of classification #5 (LFCO 0.05) GluR-BII/b.** Shown are a top and a side view of the same model. The red lines show the distribution of Euler angles. The missing cone where no angles were assigned due to missing perspectives of the protein molecules is estimated to be ca.  $115^\circ$ . (The white bar corresponds to 5 nm.) The input projections of the refined model and its rejections are shown as small images. (The edge of one image frame corresponds to 30 nm.) The table shows the cross correlation coefficients between input projections and the corresponding rejections.

The area where red lines are absent is called the “missing cone”, which is  $115^\circ$  wide (see top view in Figure 4.4.3.4.J). However, like model GluR-BII/a the top view of this refined model

GluR-BII/b shows an oval with an approximately two-fold symmetry, which is consistent with the “pair of dimer-model”, proposed as an explanation of the GluR architecture by the Stern-Bach group (Ayalon and Stern-Bach, 2001). Further refinement of model GluR-BII/b was not considered since the data set is relatively small. A larger data set could only yield more information if some of the perspectives missed in the data set analyzed here were included.

## References in Chapter 4

- Adrian, M., Dubochet, J., Fuller, , and S. D., H., R. (1998). Cryo-negative staining. *Micron* 29, 145-160.
- Ayalon, G., and Stern-Bach, Y. (2001). Functional assembly of AMPA and kainate receptors is mediated by several discrete protein-protein interactions. *Neuron* 31, 103-113.
- Cejka, Z., Kleinz, J., Santini, C., Hegerl, R., and Ghiretti Magaldi, A. (1992). The Molecular architecture of the extracellular hemoglobin of ophelia bicornis: analysis of individual molecules. *Journal of Structural Biology* 109, 52-60.
- Frank, J., Radermacher, M., Penczek, P., Zhu, J., Li, Y., Ladjadj, M., and Leith, A. (1996). SPIDER and WEB: processing and visualization of images in 3D electron microscopy and related fields. *Journal of Structural Biology* 116, 190-199.
- Keinänen, K., Köhr, G., Seeburg, P. H., Laukkanen, M. L., and Oker-Blom, C. (1994). High-level expression of functional glutamate receptor channels in insect cells. *Bio/Technology* 12, 802-806.
- Safferling, M., Tichelaar, W., Kümmerle, G., Jouppila, A., Kuusinen, A., Kainänen, K., and Madden, D. R. (2001). First images of a glutamate receptor ion channel: oligomeric state and molecular dimensions of GluRB homomer. *Biochemistry* 40, 13948-13953.
- Tarabin, V. (2000). Subklonierung der AMPA-Rezeptor-Untereinheit. Diplomarbeit, Fachhochschule Mannheim.

## 5. DISCUSSION AND OUTLOOK

The isolation of single-milligram quantities of biochemically homogeneous GluR-B ion channels from the baculovirus-expression system had been established recently (Safferling et al., 2001). The 3D reconstruction of this protein is shown in Figure 1.4.A. In the project discussed here stable insect cells were used as an alternative protein source. Their potential for the expression of homomeric GluR-B ion channels was evaluated biochemically and by the reconstruction of a new 3D model. For the isolation of the protein the previously established protocol (Safferling et al., 2001) has been applied and further optimized. The discussion of the protein's biochemistry in the next section (5.1.) is structured in two parts: *Expression of the GluR-B membrane proteins* and *Oligomeric state of GluR-B*. In the second section (5.2.) of this chapter electron microscopy experiments are discussed. This section is structured into the parts: *Sample preparation* and *3D reconstruction of GluR-B*.

### 5.1. DISCUSSION OF BIOCHEMICAL RESULTS

*Expression of the GluR-B membrane proteins.* During the generation of cell lines that constitutively express GluR-B and GluR-D homomers Dr. S. Coleman (Viikii Biocenter, University of Helsinki, Finland) used Fab7 live staining for the selection of cell lines (see Appendix A.2.2. for more details). Thereby it was noticed that expression levels among different cells of the same cell line were not uniform; some cells did not express GluR-B at all (David Mottershead, personal communication), i.e. the two cell lines are not monoclonal. In addition Fab7 staining of permeabilized and non-permeabilized cells showed that the level of cell-surface expression was low compared to the overall expression level. The activity of membrane inserted GluR-D homomers was tested by whole cell recordings. They showed signal intensities were comparable to those measured for the baculovirus-mediated expression of GluR-D homomers (Keinänen et al., 1994). While this confirmed the functionality of plasma membrane-inserted GluR-D receptors, the functionality of those GluR-D homomers accumulated in the endoplasmatic reticulum of stable cells was not confirmed by this experiments. GluR expression in stable insect cells can be further optimized. The continued selection of stable cell lines for cells with good surface expression will be essential for the optimization of this GluR expression system.

Given the low conductivity of the GluR-B(R) subunit it has to be accepted that the functionality of GluR-B(R) homomers cannot be characterized effectively by electrophysiological means. To evaluate the functionality of GluR-B protein ligand-binding experiments were applied. Filter binding experiments with the radioligand [ $^3\text{H}$ ]-AMPA confirmed the binding activity of the isolated GluR-B protein. Comparable  $K_D$ -values were measured for GluR-B containing cell membranes ( $K_D$ : 31.4 +/- 1.7 nM) and for the purified protein ( $K_D$ : 34 nM +/- 4.6 nM). The difference in the binding capacities ( $B_{\text{max}}$ ) between GluR-B containing cell membranes (6.2 pmol/mg) and purified GluR-B protein (1298 pmol/mg) can be attributed to the increase in GluR-B purity. For the baculovirus mediated expression of GluR-B protein a  $K_D$  of  $18.2 \pm 0.9$  nM and a  $B_{\text{max}}$  of 2140 pmol/mg GluR-B was determined previously (Safferling et al., 2001). The high ligand-binding activity of this protein shows that the virus infection does not affect the ligand-binding activity of GluR-B.

The yields of GluR-B (ca. 50  $\mu\text{g}$  protein per liter cell suspension) isolated from stable insect cells were about 50% of the yields in the baculovirus-mediated GluR-B expression (Safferling et al., 2001). Microgram amounts of protein are sufficient for negative stain experiments and subsequent single particle analysis, while cryo-electron microscopy and two-dimensional crystallization experiments require milligram amounts of protein, which are in principle accessible with baculovirus-mediated GluR-B expression (Safferling et al., 2001). The lower yields in stable insect cells are acceptable since the labor intensive and expensive virus amplification is not required here. To isolate microgram amounts of GluR-B protein from stable cells per protein preparation it would be in principle possible to double the volume of cultured cells. It is estimated that the subsequent isolation procedure would then require ca. 30% more time.

The initial IMAC purification in the GluR-B purification protocol was considerably improved by applying flow-through loading. It was shown that flow-through loading of  $\text{Zn}^{2+}$ -charged Sepharose improved the purity of GluR-B IMAC eluates, whereas overnight batch incubation of solubilized proteins with  $\text{Zn}^{2+}$ -charged Sepharose was accompanied by considerable background binding. In both cases GluR-B did bind quantitatively to the  $\text{Zn}^{2+}$ -charged Sepharose.

When the isolated membrane protein is used for single particle analysis stable cell lines have a further advantage: Their use eliminates the risk of virus specific contaminations (Hewat et al., 1992) and (Beaton and Filshie, 1976) and thus eliminates one source of contaminations, which can complicate selection of single particles for image processing. The detection of virus capsids (see Appendix A.2.1.) in doubly purified GluR-B samples showed that the isolates of a baculovirus-mediated expression must be assessed carefully when they are used for single particle analysis. Other EM groups using the baculovirus expression system found similar virus capsids in purified samples (T. Ruiz, personal communication). The interactive selection of single particles before image processing would be considerably more complicated when virus-specific protein particles and the protein molecules of interest are similar in size. It can be concluded at this stage that both insect cell expression systems have a main disadvantage; yields in stable insect cells are lower than in the baculovirus expression system, for which the presence of virus-specific contaminants, even in doubly purified samples, cannot be ruled out completely.

To overcome such problems in future the use of yeast cells could be considered. Yeast cells are unicellular eukaryotes, in which proteins are modified post-translationally. They have been used successfully for the expression of membrane proteins. At the moment the yeast system is probably the most promising alternative system for the expression of GluR-B. According to Grishammer and Tate the potential of yeast strains for obtaining large amounts of correctly folded and functional membrane proteins used to be underestimated (Grishammer and Tate, 1995). The P-glycoprotein, a multidrug resistance protein, (Mao and Scarborough, 1997) and the human cystic fibrosis transmembrane conductance regulator (Huang et al., 1996) were recombinantly expressed in *Saccharomyces cerevisiae*. A further yeast species, *Neurospora crassa*, allowed the isolation of the plasma membrane  $H^+$ -ATPase (Scarborough, 1994). While the human cystic fibrosis transmembrane conductance regulator is a promising candidate for single particle analysis (G. Scarborough, personal communication), the  $H^+$ -ATPase protein produced thin 3D and large 2D crystals in three-dimensional crystallization experiments (Scarborough, 1994). The 2D  $H^+$ -ATPase crystals were well suited for electron crystallography (Auer et al., 1998). Due to the intensive research on the molecular biology of yeast cells in the past and at present yeast vector constructs are among the most developed eukaryotic vectors. This can be a considerable advantage for structural biologists, who want to establish eukaryotic protein expression.

*Oligomeric state of GluR-B.* In 1996 other investigators had applied the combination of hydrodynamic behavior analyses and cross-linking experiments to suggest that the GluR has a tetrameric structure (Wu et al., 1996). Density-gradient centrifugations of Triton TX-100 solubilized GluR-B channels, which were isolated from virus-infected insect cells yielded a single peak confirming the uniformity of the oligomeric assembly. Assuming that one ~ 80 kD micelle is bound per GluR-B homomer, the observed 495 kD molecular mass of the complex corresponds well to the molecular mass expected for a tetrameric molecule ( $4 \times 104 \text{ kD} + 80 \text{ kD} = 496 \text{ kD}$ ) (Safferling et al., 2001). The oligomeric state of GluR-B ion channels isolated from stable insect cells was evaluated by cross-linking experiments using DTSSP as a cross-linker. It has been shown that DTSSP can conjugate glutamate receptor proteins in hippocampal lysate into a single oligomeric species (Osten, 2000). Enhanced chemiluminescence (ECL) detection after SDS-PAGE analysis of cross-linked GluR-B samples revealed a pattern of four GluR-B specific bands with a very prominent dimeric band at ca. 200 kD and two further oligomeric species with molecular weights clearly higher than 200 kD. Since the uncrosslinked control showed the same pattern it has to be assumed that the oligomeric species were not formed by conjugation of GluR-B subunits with DTSSP molecules. Wu and coworkers have noticed already that a significant proportion of AMPA receptor subunits were linked into oligomers up to the tetramer under non-reducing conditions in the absence of a cross-linker when they performed Western-Blot analysis of synaptic junctions (Wu et al., 1996). The signal intensities of the four bands in the minusCL control (see Figure 4.3.1.A.) might reflect the stability of oligomeric states in a non-crosslinked sample. Since the intensity of the dimeric band was lower in the presence a reducing agent it is attributed to disulfide bonds, which covalently conjugate monomers in the AMPA receptor. The dominance of the dimeric band is consistent with a model, which postulates that glutamate receptors are formed by dimers of dimers (Ayalon and Stern-Bach, 2001).

As a control cross-linking experiments were repeated with hippocampal rat brain lysate. Results of these experiments clearly showed that an increase in the concentration of DTSSP correlated with the formation of a higher oligomeric band, which most probably represents a GluR tetramer. How can it be explained that cross-linking experiments with hippocampal rat brain lysate generated a single oligomeric species, while purified GluR-B samples could not be conjugated by DTSSP? Two points have to be considered in this respect: First, rat brain lysate samples contain mainly GluR heteromers (Wenthold et al., 1992), while purified GluR-B samples consist of GluR oligomers formed exclusively by the B-type subunit. The various

GluR subunits are characterized by their specific amino acid sequence, i.e. each subunit exposes different side chains available as reaction partners for the cross-linker DTSSP. It is possible that the cross-linking reaction is governed by the type and position of certain side chains. Embedded in the lipid bilayer the position of these side chains is probably more fixed than in the solubilized receptor. It has been noticed earlier that there are differences in the structure of the AMPA receptors in the “solubilized” and in the “native” states, which documents that the membrane environment influences the properties of AMPA receptors (Hall et al., 1992) and (Wu et al., 1996). Second, during solubilization of overexpressed GluR-B homomers the natural lipids, which saturate hydrophobic transmembrane domains were replaced at least partially by detergent molecules. It has been shown previously that the presence of phospholipids during purification supports the activity of isolated acetylcholine receptors for lipid reconstitution (Huganir and Racker, 1982). It is possible that the delipidation might affect the potential of a membrane protein for cross-linking experiments in a similar way.

## 5.2. DISCUSSION OF ELECTRON MICROSCOPY RESULTS

*Sample preparation.* The preservation of a protein sample is an important factor for structural analysis by electron microscopy. To prevent possible artifacts of the negative staining approach, like partial staining and limited stain penetration (Cejka et al., 1992) for the structural analysis of GluR-B different methods of sample preservation were tested during this project. Cryo-electron microscopy was applied first, since it allows protein preservation under almost physiological conditions. The reconstruction of the spliceosomal U1 small nuclear ribonucleoprotein particle with a molecular mass of ca. 240 kD (Stark et al., 2001) shows that a complete GluR-B tetramer (ca. 496 kD) is in principle large enough for cryo-detection. However, in experiments with GluR-B the contrast was too low to allow the detection of the ion channel protein. Cryo-experiments in the presence of a carbon film, which was meant to have a fixative effect on the proteins did not facilitate its detection either (R. Schröder, personal communication).

To enhance contrast a recently developed technique, cryo-negative staining, seemed to be an ideal approach. However the detection of vitrified GluR-B molecules in the presence of ammonium molybdate was not achieved. It is likely that the protein was not longer in the oligomeric state in the presence of ammonium molybdate. Investigators who developed cryo-

negative staining have showed the contrast enhancement in experiments with robust proteins like TMV and pointed out that negative effects of sample-stain interaction, prior to vitrification, must be carefully assessed for each protein (Adrian et al., 1998). While it was possible to reproduce the cryo-negative staining experiments with TMV in control experiments, it is likely that the detection of GluR-B did not succeed due to the harmful effect of high stain concentrations. Since the introduction of cryo-negative staining in 1998 there are only few published results by other groups based on this new method. One example is a heptameric protease, which tolerated cryo-negative staining (16% ammonium molybdate, pH 7.0) after previous cross-linking with 0.1 % glutaraldehyde. The resolution of the corresponding 3D reconstruction was reported to be better than that of the cryo-electron microscopy approach (Stahlberg et al., 1999).

In his book “Three-Dimensional Electron Microscopy of Macromolecular Assemblies” J. Frank listed some proteins as examples to illustrate that efforts to obtain a 3D reconstruction of vitrified protein samples almost always involve a negatively stained specimen as the first step, “sometimes with a delay of several years” (Frank, 1996). The proteins he refers to are the 50S ribosomal subunit, the nuclear pore complex, the calcium release channel and hemocyanin; the delay for the first three proteins was 5 years and 2 years for hemocyanin. Certainly the same applies for the GluR ion channel; analysis of cryo-electron microscopy data will be facilitated if there is a first low-resolution model available.

To obtain a reliable model of GluR-B the options for an improved negative stain approach were considered: Beside uranyl acetate the potential of two other stains, sodium silico tungstate and phosphotungstate, for negative staining of GluR-D had been evaluated previously. However, both tungstate stains were found to be not suitable for negative stain experiments with GluR-D (D. Madden, personal communication.) Therefore, in this project the potential of the low-contrast stain aurothioglucose (ATG) was evaluated by image processing of GluR-B particles. However, due to the granularity of ATG it was not possible to classify protein particles. Another group used ATG to stain two different ATPases. Single particle analysis of a ATG stained F-type ATPase did not generate a reliable 3D reconstruction (B. Böttcher, personal communication) whereas the same experiments with plant V-ATPase produced recently a three-dimensional map at a resolution of 22 Å (Domgall et al., 2002).

It has been shown that negative staining of protein molecules in thicker stain layers reduces partial staining and has a positive effect on the preservation of single protein molecules (Cejka et al., 1992). The Radermacher group recently managed to get a 3D structure of the  $V_1$ -ATPase from *Manduca Sexta*, which consists of eight subunits with varying molecular masses (Radermacher et al., 2001) using a deep-staining technique (Stoops et al., 1992). After 8792 particles were classified into 21 class averages it was obvious that only 13% of the images corresponded to projections of a full  $V_1$ -ATPase molecule. The other 87% were projections of partial complexes containing only a subset of subunits. However, the largest and thus the most complete particles were concentrated in only two class averages. The two class averages consisted of 483 respectively 633 protein particles. When the two of them were combined a common reconstruction at a resolution of 18 Å was the result. To facilitate deep-staining of GluR-B molecules freshly floated carbon-films without glow discharging (Michael Radermacher, personal communication) were used. During experiments with GluR-B and uranyl acetate it was found that the thickness of uranyl acetate layers on freshly floated carbon films without previous glow discharging varied locally. This effect was observed sometimes on air-dried carbon films too, but freshly floated carbon films were found to facilitate the local accumulation of stain much stronger. A possible explanation for this could be that the elasticity of dry carbon films is lower than the elasticity of freshly floated carbon films. In addition to the effect of charging such wrinkles in the carbon film might support the local accumulation of stain. By visual judgment the preservation of protein particles in thicker uranyl acetate layers was considered to be better. The putative positive effect was evaluated by image analysis of 500 GluR-B molecules. The results of this analysis are discussed in the next section (*3D reconstruction of GluR-B*).

The recent work of M. Radermacher is discussed here because of two reasons: first, the  $V_1$ -ATPase protein molecules were negatively stained using a deep-staining technique (Stoops et al., 1992). Second, due to the elimination of 87% of the projections finally only ca. 1100 molecules of the  $V_1$ -ATPase generated the 3D reconstruction of the complete complex at a resolution of 18 Å.

To illustrate that the number of particles used for a 3D reconstruction does not necessarily limit the resolution in Table 5.2.A. some recent 3D reconstructions of membrane proteins are summarized. All the proteins listed in table 5.2.A are membrane proteins with molecular weight not higher than 600 kD. The MW of the GluR-B ion channel is ca. 496 kD.

To allow a limited evaluation of these reconstructions the way of sample preparation, i.e. negative stain vs. cryo-electron microscopy and the resolution of each reconstruction is included. (The protein quality and protein stability of these examples, which are certainly the first prerequisite for EM sample preparation are not discussed here.)

Protein	MW in kD	Sample preparation	Number of classified individual images	Resolution in Å	Reference
<b>Multidrug Resistance Protein 1</b>	190	Negatively stained in uranyl acetate	600	22	(Rosenberg et al., 2001)*
<b>Multidrug Resistance P-glycoprotein</b>	170	Negatively stained in uranyl acetate	621	25	(Rosenberg et al., 1997)*
<b>V<sub>1</sub>-ATPase</b>	554	Negatively stained in methyl-amine tungstate	1116	18	(Radermacher et al., 2001)*
<b>Voltage-gated potassium channel</b>	400	Negatively stained in uranyl acetate	6000	25	(Sokolova et al., 2001)
<b>Voltage-sensitive sodium channel</b>	300	Cryo-electron Microscopy	12000	19	(Sato et al., 2001)

**Table 5.2.A: Reference table for single particle analysis of different proteins. \* For the analysis of these proteins the random conical tilt approach (Radermacher, 1988), (Frank et al., 1996) was applied. Both channel proteins were analyzed by IMAGIC.**

The multidrug resistance proteins, which can both be reconstituted in liposomes, are based on less than 1000 protein particles. They are of special interest for this project since the model of the GluR-B ion channel is based on 500 molecules. Single particle analysis of the multidrug resistance protein 1 was exclusively based on detergent-solubilized single particles, whereas the interpretation of the single particle analysis of the 621 detergent-solubilized P-glycoprotein particles involved three separate approaches (3D analysis of the detergent-solubilized proteins, analysis of lipid-reconstituted proteins and analysis of small 2D ordered arrays of the protein. (In addition lectin-gold labeling was applied to evaluate the orientation and oligomeric state of the protein.)) The three approaches gave consistent results.

For the last two examples listed in Table 5.2.A the influence of the particle number cannot be separated from the influence of the sample preparation. It is likely that both support the high resolution of the voltage-sensitive sodium channel (Sato et al., 2001). However, the model of the voltage-gated potassium channel (Sokolova et al., 2001) provided a remarkable insight into the structure of this tetrameric ion channel although negatively stained samples were used.

*3D reconstruction of GluR-B.* The comparative classification of a data set consisting of 500 GluR-B protein particles, negatively stained in uranyl acetate on freshly floated carbon films, resulted in three different 3D models. The comparison showed the influence of low spatial frequency information on the initial classification of particles. Low spatial frequencies represent coarse structural details like the overall shape of the protein. The iterative optimization of class averages by reclassification coincided as expected with a considerable improvement of the variance among the members of a class averages. At the same time, however, the pair wise comparison of class averages showed that low spatial frequency information did not continue to exert any influence on the reclassification. In order to evaluate this inconsistency the 3D reconstruction was calculated for three different classifications.

The analysis of the models showed that the 3D reconstruction is most consistent when the frequencies below  $1/200 \text{ \AA}^{-1}$  were eliminated (see model GluR-BIIa and GluR-BIIb). The choppy structure of model GluR-BIII shows clearly that a low-frequency cut-off, which corresponds to  $1/120 \text{ \AA}^{-1}$ , eliminates too much structural information. The consistency of each model was evaluated by visual comparison of input projections and corresponding reprojections of each 3D reconstruction. One explanation for the quality of the model GluR-BIIa and GluR-BIIb is that the LFCO fits the size of the GluR-B particle. The refined model GluR-BII/b has the dimensions  $18 \text{ nm} \times 14 \text{ nm} \times 11 \text{ nm}$ . Its top view shows a closed oval, which has a central hole that is likely to represent the ion channel of the GluR-B protein. First of all this model confirms that the selected GluR-B molecules were still in their oligomeric state after purification and negative staining. The first 3D reconstruction of GluR-B, which is based on 10 000 virus-mediated GluR-B molecules (see Figure 1.4.A.) has nearly identical dimensions ( $17 \text{ nm} \times 14 \text{ nm} \times 11 \text{ nm}$ ). It shows several internal solvent accessible volumes instead of one central channel and does not have a distinct overall shape. Since hydrodynamic experiments confirmed a tetrameric structure for this protein (Safferling et al., 2001) it is unlikely that the protein was not in its oligomeric state. The comparison of the models might indicate that the sample preparation on freshly floated carbon films has a positive effect on the preservation of GluR ion channels.

Model GluR-BII/b does not show a clearly tetrameric architecture. Its two-fold symmetry, however, is consistent with the biochemical (Ayalon and Stern-Bach, 2001) and structural (Armstrong et al., 1998) evidence, which revealed the importance of a dimeric motif in architecture of the putative tetrameric glutamate receptor. Since the number of input

projections for GluR-BII/b was only 11 a Fourier Shell Correlation (FSC), which could indicate the resolution of the 3D reconstruction was not considered. The missing cone of model GluR-BII/b measures ca.  $115^\circ$ . A small missing cone indicates that the input projections covered a high number of different perspectives of the protein molecule. Considering that a relatively small number of particles contributed to the model a missing cone of  $115^\circ$  is acceptable.

In general one should assume that the diversity of input projections is proportional to the number of particles. Since most of the GluR-B particles show stain-filled cavities it is likely that their top-view orientation is preferred in negative staining. However, negatively stained protein particles are often not randomly orientated because of preferred association of different faces of the protein with the electrostatically charged carbon film (v. Heel and Stöffler-Meilicke, 1985). The classification of 600 images of the multidrug resistance protein 1 showed that this protein clearly has a preferred top-view orientation under negative stain conditions (Rosenberg et al., 2001), whereas voltage-gated potassium channel *Shaker* molecules from *Drosophila* prefer a side view orientation (Sokolova et al., 2001). In cryo-electron microscopy the diversity of views is usually higher. The class averages of GluR-B, calculated during this project suggest that the ion channel has a preference for the top-view orientation. It is therefore unlikely that image analysis of 5000 or more negatively stained GluR-B particles would reveal considerably more perspectives, i.e. side-views of the ion channel. The best approach to get the maximum variety of perspectives is vitrification and imaging under cryo-conditions. Once the experiments are established and a data set of GluR-B particles is available the reprojections of model GluR-BII/b could be used as references for the alignment of the vitrified molecules.

### 5.3. OUTLOOK

Since vitrification of single protein molecules usually gives the highest number of different orientations of the molecules cryo-electron microscopy GluR-B should be reconsidered as soon as the isolation of homogeneous protein GluR samples at 2-5 mg/mL concentrations has been established. Then the potential of the protein for its detection under cryo-conditions can be evaluated by making specimens of a dilution series. Subsequently conditions for the detection of isolated particles are optimized at the appropriate protein concentrations.

The use of holey grids, coated with a thin (ca. 2nm) carbon film, might help to fix protein particles and thus facilitate their detection by cryo-electron microscopy (Harris et al., 2001). Antibodies, which bind to a specific docking site could show the subunit stoichiometry of the glutamate receptor and could also reveal the orientation of the GluR channel relative to the membrane (Sato et al., 2001). In addition, larger complexes between GluR-B and antibodies could make detection of the protein in vitrified samples easier.

The long-term goal of structural analysis of full-length GluRs is to correlate structure with function. To answer the question how conformational changes in the transmembrane helices, induced by extracellular agonist binding, cause channel gating it will be essential to manipulate the functional states of reconstituted channels before they are freeze-trapped by vitrification. To achieve reconstitution in liposomes the purified membrane has to be homogeneous and stable. The stability of purified GluR-B oligomers is likely to improve when its delipidation during solubilization and purification is reduced. The presence of phospholipids during purification was shown to have a positive effect on the reconstitutive activity of the acetylcholine receptor (Huganir and Racker, 1982). Alternatively, a reduction of the delipidation might be achieved by establishing a single-step purification protocol using a C-terminal decahistidine tag. In addition the use of short chain phospholipids and lysophospholipid detergents could allow a gentle solubilization, which might improve the stability of the isolated GluR protein.

**REFERENCES OF CHAPTER 5**

- Adrian, M., Dubochet, J., Fuller, , and S. D., H., R. (1998). Cryo-negative staining. *Micron* 29, 145-160.
- Armstrong, N., Sun, Y., Chen, G.-Q., and Gouaux, E. (1998). Structure of a glutamate-receptor ligand binding core in complex with kainate. *Nature* 395, 913-917.
- Auer, M., Scarborough, G. A., and Kühlbrandt, W. (1998). Three-dimensional map of the plasma membrane H<sup>+</sup>-ATPase in the open conformation. *Nature* 392, 840-843.
- Ayalon, G., and Stern-Bach, Y. (2001). Functional assembly of AMPA and kainate receptors is mediated by several discrete protein-protein interactions. *Neuron* 31, 103-113.
- Beaton, C. D., and Filshie, B. K. (1976). Comparative ultrastructural studies of insect granulosis and nuclear polyhedrosis viruses. *Journal of General Virology* 31, 151-161.
- Cejka, Z., Kleinz, J., Santini, C., Hegerl, R., and Ghiretti Magaldi, A. (1992). The Molecular architecture of the extracellular hemoglobin of ophelia bicornis: analysis of individual molecules. *Journal of Structural Biology* 109, 52-60.
- Domgall, I., Venzke, D., Luttge, U., Ratajczak, B., and Böttcher, B. (2002). Three-dimensional map of plant V-ATPase based on electron microscopy. *Journal of Biological Chemistry (in press)*.
- Frank, J. (1996). Three-dimensional electron microscopy of macromolecular assemblies, Academic Press).
- Frank, J., Radermacher, M., Penczek, P., Zhu, J., Li, Y., Ladjadj, M., and Leith, A. (1996). SPIDER and WEB: processing and visualization of images in 3D electron microscopy and related fields. *Journal of Structural Biology* 116, 190-199.
- Grisshammer, R., and Tate, C. G. (1995). Overexpression of integral membrane proteins for structural studies. *Quarterly Review of Biophysics* 28, 315-422.
- Hall, R. A., Kessler, M., and Lynch, G. (1992). Evidence that high and low-affinity DL-amino-3-hydroxy-5-methylisoxazole-4-propionic acid (AMPA) binding sites reflect membrane-dependent states of a single receptor. *Journal of Neurochemistry* 59, 1997-2004.
- Harris, R. J., Hoeger, U., and Adrian, M. (2001). Transmission electron microscopical studies on some haemolymph proteins from the marine polychaete *Nereis virens*. *Micron* 32, 599-613.
- Hewat, E., Booth, T. F., Wade, R. H., and Roy, P. (1992). 3-D reconstruction of bluetongue virus tubules using cryoelectron microscopy. *Journal of Structural Biology* 108, 35-48.
- Huang, P., Stroffekova, K., Cuppoletti, J., Mahanaty, S. K., and Scarborough, G. A. (1996). Functional expression of the cystic fibrosis transmembrane conductance regulator in yeast. *Biochimica et Biophysica Acta* 1281, 80-90.
- Huganir, R. L., and Racker, E. (1982). Properties of proteoliposomes reconstituted with acetylcholine receptor from *Torpedo californica*. *The Journal of Biological Chemistry* 257, 9372-9378.
- Keinänen, K., Köhr, G., Seeburg, P. H., Laukkanen, M. L., and Oker-Blom, C. (1994). High-level expression of functional glutamate receptor channels in insect cells. *Bio/Technology* 12, 802-806.
- Mao, Q., and Scarborough, G. A. (1997). Purification of functional human P-glycoprotein expressed in *S. cerevisiae*. *Biochimica et Biophysica Acta* 1327, 107-118.

- Osten, P. (2000). GluR crosslinking with DTSSP (personal communication).
- Radermacher, M. (1988). Three-dimensional reconstruction of single particles from random and non-random tilt series. *Journal of Electron Microscopy Techniques* 9, 359.
- Radermacher, M., Ruiz, T., Wiczorek, H., and Grüber, G. (2001). The structure of the V1-ATPase determined by three-dimensional electron microscopy of single particles. *Journal of Structural Biology* 135, 26-37.
- Rosenberg, M. F., Callaghan, R., Ford, R. C., and F., H. C. (1997). Structure of the multidrug resistance P-glycoprotein to 2.5 nm resolution determined by electron microscopy and image analysis. *The Journal of Biological Chemistry* 272, 10685-10694.
- Rosenberg, M. F., Mao, Q., Holzenburg, A., Ford, R. C., Deeley, R. G., and Cole, S. P. C. (2001). The structure of the multidrug resistance protein 1 (MRP1/ABCC1). *The Journal of Biological Chemistry* 276, 16076-16082.
- Safferling, M., Tichelaar, W., Kümmerle, G., Jouppila, A., Kuusinen, A., Kainänen, K., and Madden, D. R. (2001). First images of a glutamate receptor ion channel: oligomeric state and molecular dimensions of GluRB homomer. *Biochemistry* 40, 13948-13953.
- Sato, C., Ueno, Y., Asai, K., Takahashi, K., Sato, M., Engel, A., and Fujiyoshi, Y. (2001). The voltage-sensitive sodium channel is a bell-shaped molecule with several cavities. *Nature* 409, 1047-1051.
- Scarborough, G. A. (1994). Large single crystals of the *Neurospora crassa* plasma membrane of H<sup>+</sup>-ATPase: an approach to the crystallisation of integral membrane proteins. *Acta Crystallographica Section D* 50, 643-649.
- Sokolova, O., Kolmakova-Partensky, L., and Grigorieff, N. (2001). Three-dimensional structure of a voltage-gated potassium channel at 2.5 nm resolution. *Structure* 9, 215-220.
- Stahlberg, H., Kutejova, E., Kitaru, S., Wolpensinger, B., Lustig, A., Schatz, G., Engel, A., and Suzuki, C. K. (1999). Mitochondrial lon of *Saccharomyces cerevisiae* is a ring-shaped protease with seven flexible subunits. *Proceedings of the National Academy of Science, USA* 96, 6787-6790.
- Stark, H., Dube, P., Lührmann, R., and Kastner, B. (2001). Arrangement of RNA and proteins in the spliceosomal U1 small nuclear ribonucleoprotein particle. *Nature* 409, 539-542.
- Stoops, J. K., Kolodziej, S. J., Schroeter, J. P., and Breaudiere, J.-P. (1992). Structure-function relationships of the yeast fatty acid synthase: Negative-stain, cryo-electron microscopy, and image analysis studies of the end views of the structure. *Proceeding of the National Academy of Science, USA* 89, 6585-6589.
- v. Heel, M., and Stöffler-Meilicke, M. (1985). Characteristic views of *E. Coli* and *B. stearothermophilus* 30S ribosomal subunits in the electron microscope. *The EMBO Journal* 4, 2389-2395.
- Wenthold, R. J., Yokotani, N., Doi, K., and K., W. (1992). Immunochemical characterization of the non-NMDA glutamate receptor using subunit-specific antibodies. *The Journal of Biological Chemistry* 267, 501-507.
- Wu, T.-Y., Liu, C.-I., and Y.-C., C. (1996). A study of the oligomeric state of the  $\alpha$ -amino-3-hydroxy-5-methyl-4-isoxazopropionic acid-preferring glutamate receptors in the synaptic junction of porcine brain. *Biochemical Journal* 319, 731-739.

## 6. ZUSAMMENFASSUNG

Diese Zusammenfassung ist in zwei Abschnitte gegliedert. Im Abschnitt 6.1. wird die physiologische Bedeutung der Glutamatrezeptoren (GluR) und ihr biologischer Hintergrund kurz erklärt. Am Ende dieses Abschnitts wird der Stand der Strukturanalyse des GluR-B Ionenkanals zu Beginn des Projektes zusammengefasst. Im nachfolgenden Abschnitt 6.2. sind die wesentlichen Ergebnisse der hier vorgelegten Arbeit zusammengefasst.

### 6.1. Die Bedeutung von Glutamatrezeptoren -

#### Stand der Strukturanalyse zum Beginn dieser Arbeit

Die Kommunikation zwischen Nervenzellen erfolgt vorwiegend an hochspezialisierten Kontaktstellen – den chemischen Synapsen. Der enge Raum zwischen sendender und empfangender Nervenzelle wird auch als synaptischer Spalt bezeichnet. Der Prozess der synaptischen Übertragung beruht auf der präsynaptischen Freisetzung von chemischen Botenstoffen, sogenannten Neurotransmittern in den synaptischen Spalt. Die Aminosäure L-Glutamat (Glu) ist der wichtigste erregende Neurotransmitter im menschlichen Gehirn und Rückenmark. Dementsprechend bedeutend ist die Rolle der ionotropen Glutamatrezeptoren (iGluRs)<sup>1</sup>, die sie bei der elektrochemischen Erregungsübertragung am synaptischen Spalt spielen (Seeburg, 1993), (Hollmann and Heinemann, 1994), (Dingledine et al., 1999). Die Freisetzung von Neurotransmittern wird durch ein elektrisches Signal (Aktionspotential) ausgelöst, das sich entlang der Nervenfaser, dem Axon, bis zur Nervenendigung, der Synapse, fortpflanzt. Nach der Freisetzung diffundieren die Neurotransmitter durch den synaptischen Spalt und binden an sogenannte Rezeptoren. Ionotrope Glutamatrezeptoren sind Ionenkanäle, die in die Membran der nachgeschalteten (postsynaptischen) Nervenzelle eingebaut sind. Sie zählen deshalb zu den Membranproteinen. Als ligandgesteuerte kationenselektive Ionenkanäle machen Glutamatrezeptoren (GluRs) die postsynaptische Membran nach Aktivierung durch Ligandbindung für bestimmte Kationen durchlässig. Der Einstrom von Ionen bewirkt eine Änderung des Membranpotentials. Die Stärke der synaptischen Übertragung ist lebenslang

---

<sup>1</sup> Neben den ionotropen GluRs (iGluRs) werden auch metabotrope Glutamatrezeptoren (mGluR) durch Glutamat aktiviert. Verglichen mit den ionotropen Glutamatrezeptoren begründen die metabotropen Rezeptoren eine separate Klasse von Glutamatrezeptoren, denn sie bilden keine intrinsischen Ionenkanäle. Ausser der extrazellulären Ligandbindungsdomäne gibt es keine Verwandheit in der Struktur von ionotropen und metabotropen Glutamatrezeptoren, die für die synaptische Modulation ebenfalls eine sehr wichtige Rolle spielen (Nakanishi, S. (1990), Molecular diversity of glutamate receptors and implication for brain function, *Science* 258, 597-630).

modulierbar; die sogenannte synaptische Plastizität wird als eine entscheidende Grundlage für die Erklärung von Lernen und Gedächtnis angesehen.

Drei synthetische Agonisten aktivieren die GluRs selektiv und wurden deshalb für die Klassifizierung der ionotropen Glutamatrezeptoren herangezogen. Bei den Agonisten handelt es sich um  $\alpha$ -Amino-3-hydroxy-5-methyl-4-isoxazol-4-propionat (AMPA), Kainat and N-Methyl-D-Aspartat (NMDA). Die ersten beiden Subtypen werden auch als non-NMDA-Rezeptoren zusammengefasst. Die Aktivierung und Desensitivierung der non-NMDA Rezeptoren ist schneller als die der NMDA-Rezeptoren. Aus molekularbiologischer Sicht (siehe Kapitel 1.3.2.) zeigen die drei Klassen der ionotropen Glutamatrezeptoren eine beträchtliche Diversität. So gibt es vier verschiedene Unterheiten vom AMPA-Subtyp, nämlich GluR-A, GluR-B, GluR-C und GluR-B. In dieser Arbeit steht die Strukturanalyse eines aus GluR-B Untereinheiten bestehenden AMPA-Rezeptors im Vordergrund. (Die weitere Unterteilung der NMDA- und Kainatrezeptoren kann dem Kapitel 1.3.2. auf Seite 6 entnommen werden.)

Bestimmte Abschnitte der Aminosäuresequenz von Glutamatrezeptoren sind durch hydrophobe Bereiche gekennzeichnet ((M1-M4) in Abbildung 6.1.A (A.)). Das durch verschiedene Untersuchungen etablierte Modell der Glutamatrezeptor-Topologie zeigt 3 Transmembrandomänen (M1, M3 und M4) und eine Membranschleife (M2) (Hollmann et al., 1994), (Kuner et al., 1996). Der Aminoterminus ist extrazellulär, der Carboxyterminus hingegen intrazellulär. Daraus ergibt sich die in Abbildung 6.1.A (B.) abgebildete Topologie (Paas, 1998). S1 und S2 kennzeichnen die Ligandbindungsdomäne.

Glutamatrezeptoren (GluR) sind Oligomere, die sich mit grosser Wahrscheinlichkeit aus vier Untereinheiten (Rosenmund et al., 1998), (Ayalon and Stern-Bach, 2001) zusammensetzen (siehe Kapitel 1.3.3.). Die Zusammenlagerung verschiedener Untereinheiten zu einem funktionellen Kanal setzt voraus, dass die Untereinheiten zum gleichen Subtyp gehören, d.h. AMPA Untereinheiten können nur mit anderen AMPA Untereinheiten einen Ionenkanal bilden. Das gleiche gilt für die Zusammensetzung von NMDA und Kainat-Rezeptoren. Das Modell eines tetrameren Glutamatrezeptors ist im Bild C. der Abbildung 6.1.A zu sehen.

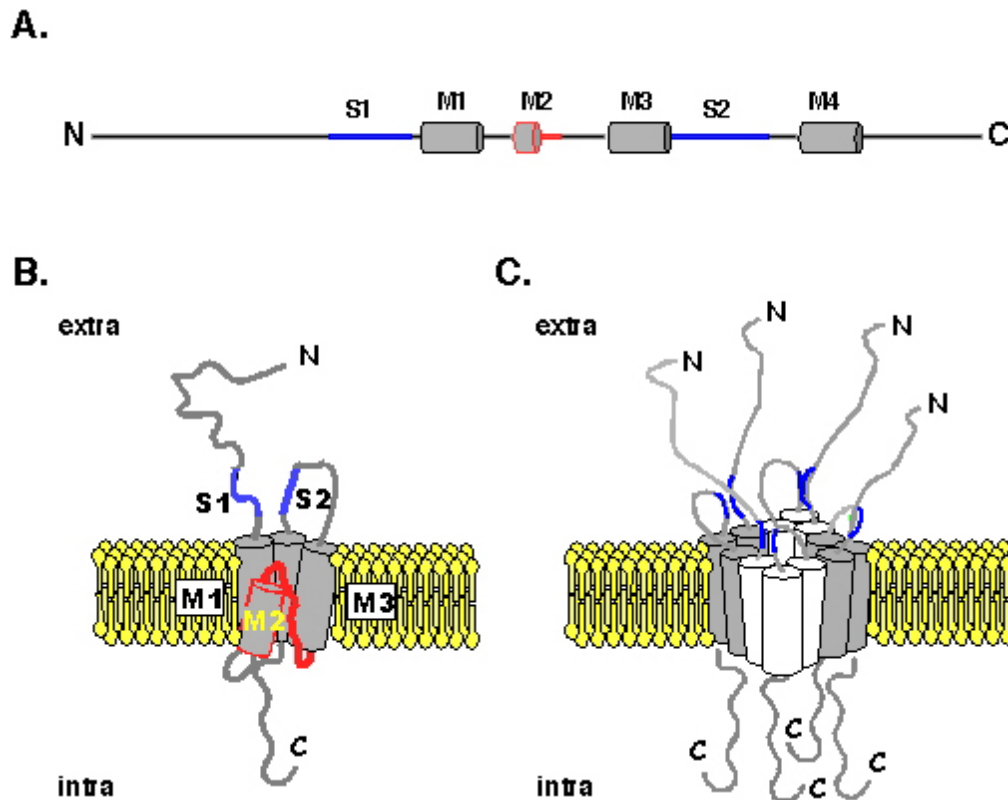
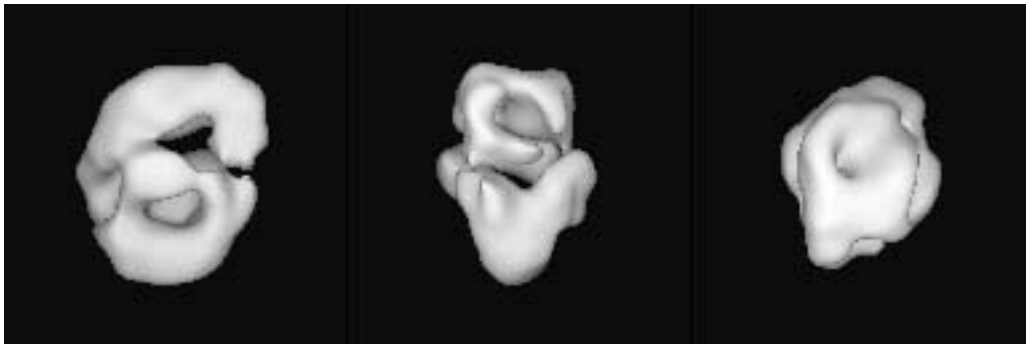


Abbildung 6.1.A: A) Die Strukturelemente einer GluR Untereinheit in einer schematischen Zeichnung vom Aminoterminus (N) zum Carboxyterminus (C). S1 und S2 kennzeichnen die Ligandbindungsdomänen, M1-M4 kennzeichnen die Transmembrandomänen. B) Die Transmembrantopologie einer einzelnen GluR Untereinheit nach (Paas, 1998). C) Modell eines kompletten Ionenkanals unter der Annahme einer tetrameren Stöchiometrie der Untereinheiten.

Die Bestimmung der Quartärstruktur eines vollständigen Glutamaterezeptors ist bislang nicht veröffentlicht<sup>2</sup>. Die strukturelle Analyse von Proteinen erfordert die Isolierung von reinem und funktionellem Protein. Im Vergleich zu den meisten löslichen Proteinen erfordert die Isolierung von Membranproteinen oft besonderer Optimierung. Falls das Vorkommen des Proteins in natürlichem Gewebe gering ist, so kann die strukturelle Analyse durch rekombinante Expression in einem geeigneten Wirtsorganismus zugänglich gemacht werden. Die Isolierung von Milligramm-Mengen eines rekombinanten homomeren GluR-B Rezeptors aus dem entsprechenden Baculovirusexpressionssystem (Keinänen et al., 1994) wurde in unserem Labor etabliert (Safferling et al., 2001) und wurde im ersten Jahr dieses Projektes fortgeführt. Durch zonale Ultrazentrifugation konnte gezeigt werden, dass die molekulare Masse des GluR-B Proteinkomplexes ca. 495 kD beträgt. Dieser Wert liegt in der Nähe des theoretischen Molekulargewichts eines tetrameren Ionenkanals, dessen Molmasse sich aus

<sup>2</sup> Für die Ligandbindungsdomänen (S1S2) der B Untereinheit des AMPA-Rezeptors gibt es eine Röntgenkristallstruktur (Armstrong, N., Sun, Y., Chen, G.-Q., and Gouaux, E. (1998), Structure of a glutamate-receptor ligand binding core in complex with kainate, *Nature* 395, 913-917). Verbunden durch einen Peptid-Linker lassen sich die beiden Domänen S1 und S2 rekombinant als lösliches Protein exprimieren.

vier GluR-B Untereinheiten (104 kD) und einer Detergenzmizelle von ca. 63-97 kD zusammensetzt (Safferling et al., 2001). Die elektronenmikroskopische Analyse des Proteinkomplexes von W. Tichelaar aus unserer Gruppe erfolgte 1999 durch Negativfärbung. Für die Strukturanalyse mit Hilfe der Software IMAGIC wurden 10 000 Proteinteilchen selektiert. Das Ergebnis der Bildrekonstruktion ist in der folgenden Abbildung 6.1.B gezeigt.



**Abbildung 6.1.B:** Erste 3D Rekonstruktion von 10000 Ansichten des GluR-B Proteinkomplexes. Die drei gezeigten Projektionen des Models haben die Dimensionen 17 nm × 14 nm × 11 nm. (Mit freundlicher Genehmigung von W. Tichelaar.)

Die projizierten Dimensionen des Models entsprechen einem Molekül mit den Dimensionen 17 nm × 11 nm × 14 nm. Das Model zeigt keine ausgezeichnete Symmetrie, die auf die Stöchiometrie des GluR hinweisen könnte. Das Molekül zeigt mit Färbemittel gefüllte Vertiefungen und innere Strukturen, die vielleicht an der Ionenleitung beteiligt sind.

## **6.2. Funktionelle und strukturelle Charakterisierung des GluR-B Ionenkanals**

In der Fortsetzung des oben beschriebenen Projektes wurden für die rekombinante Expression desselben Rezeptors (GluR-B homomer) stabil transformierte Insektenzellen eingesetzt. Dazu wurde die für die GluR-B Untereinheit kodierende und in Plasmiden enthaltene DNA in Insektenzellen transformiert (siehe APPENDIX A.2.2.). Im Vergleich zu dieser auf Dauerhaftigkeit angelegten Integration der Rezeptor DNA wird die Proteinexpression beim Baculovirusexpressionssystem durch Infektion mit rekombinanten Baculoviren initiiert. Der Vergleich zeigte, dass die mit Baculoviren erzielten Ausbeuten bei GluR-B etwa doppelt so hoch waren als bei stabil transformierten Zellen. Allerdings fallen bei stabil transformierten Zellen die eventuellen Nachteile der viralen Belastung auf die zellulären Sekretionsprozesse weg. Im Verlauf der elektronenmikroskopischen Analyse von baculoviral erzeugtem GluR-B Protein hat sich gezeigt, dass Proteine viralen Ursprungs unter Umständen selbst doppelt aufgereinigte GluR-B Proben verunreinigen können (siehe APPENDIX A.2.1.). Dieser Punkt ist

bei einer Einzelbildverarbeitung von grosser Relevanz, falls die virusspezifischen Proteinverunreinigungen eine ähnliche Grösse haben wie das eigentliche Zielprotein.

**Das Hauptziel dieser Arbeit war es, das Potenzial stabil transformierter Insektenzellen für die Expression von homomeren GluR-B Ionenkanälen zu bewerten und dabei die Stöchiometrie der Untereinheiten in diesem Ionenkanal aufzuklären. Zu diesem Zweck wurden biochemische und elektronenmikroskopische Techniken eingesetzt.**

Zur Isolierung des GluR-B Ionenkanals aus stabil transformierten Insektenzellen wurde das bestehende Aufreinigungsprotokoll für die Affinitätschromatographie an immobilisierten Metallionen (IMAC) (Safferling et al., 2001) optimiert, indem das Chargenverfahren durch das Durchflussverfahren ersetzt wurde (zur genaueren Erklärung der Optimierung siehe RESULTS 4.1.2.). Abbildung 6.C zeigt ein silbergefärbtes Gel mit den Eluaten der IMAC und Eluaten der abschliessenden Affinitätschromatographie mit immobilisiertem M1-Antikörper. Die auf den Bahnen 5-8 aufgetragenen GluR-B Proben wurden auch für die Einzelteilchenanalyse mittels Elektronenmikroskopie verwendet.

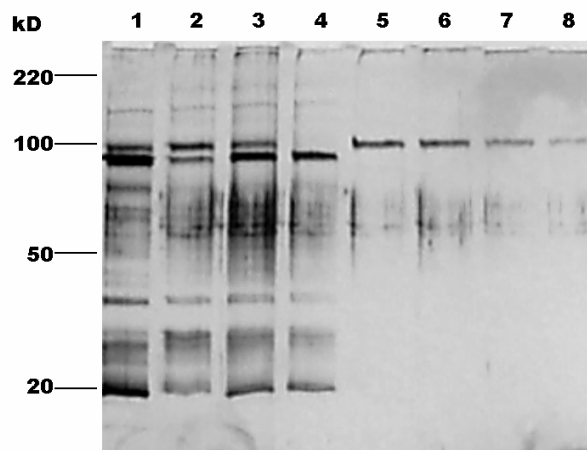


**Abbildung 6.2.A: Silbergefärbtes SDS-PAGE Gel. Das Gel wurde wie folgt beladen: Bahn 1 und 2, IMAC Eluate; Bahn 3, Auftrag Immunoaffinitäts-Chromatographie, Bahn 4, Durchfluss der Immunoaffinitäts-Chromatographie; Bahnen 5 bis 8, Eluate der Immunoaffinitäts-Chromatographie.**

Die Ligandbindungsaktivität von GluR-B wurde durch Filterbindungsexperimente mit dem Radioliganden [<sup>3</sup>H]-AMPA vor und nach der Isolierung aus den Membranfragmenten bestimmt. Die  $K_D$ -Werte sind für beide Proben ähnlich gross. Der  $B_{max}$ -Werte ist für die aufgereinigte Probe wie erwartet sehr viel (mehr als 200×) höher. Die Ergebnisse der Ligandbindungsexperimente sind im Kapitel 4.2.1 tabellarisch zusammengefasst.

Die oligomere Struktur des isolierten Ionenkanals wurde durch Quervernetzungsexperimente (Cross-linking) und Einzelteilchenanalyse von negativ gefärbten Proteinmolekülen bewertet. Die Quervernetzungsexperimente selbst erbrachten kein eindeutiges Ergebnis im Hinblick auf oligomere Struktur des komplett zusammengesetzten Rezeptors. Kontrollexperimente mit dem Lysat vom Rattenhippocampus zeigten, dass mit DTSSP ein geeigneter Cross-Linker verwendet wurde (siehe RESULTS 4.3.2.). Neben einem aus 4 Banden bestehenden Muster (siehe RESULTS 4.3.1.) lieferten die Quervernetzungsexperimente mit isoliertem GluR-B aber einen deutlichen Hinweis auf die Stabilität von dimeren GluR-B Strukturen, die im Einklang mit einer jüngst veröffentlichten Arbeit stehen (Ayalon and Stern-Bach, 2001). Diese Veröffentlichung liefert zusätzliche (Armstrong et al., 1998) Hinweise auf die Bedeutung von Dimeren in der Glutamaterezeptorstruktur und postuliert, dass sich ein kompletter Glutamaterezeptor aus einem Dimer-Paar zusammensetzt, wobei die Dimere zuerst gebildet werden. Die nachfolgende Abbildung 6.2.B zeigt negativ gefärbte GluR-B Ionenkanäle bei einer 46000× Vergrößerung. Die Aufnahme stammt von einem Philips EM 400 Elektronenmikroskop.

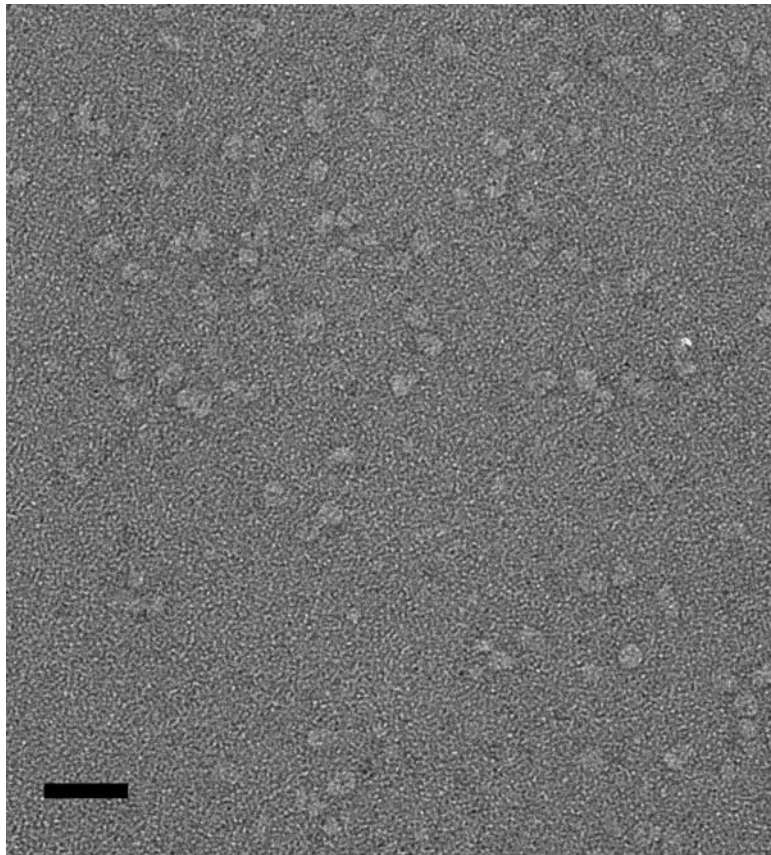


**Abbildung 6.2.B: GluR-B Moleküle negativ gefärbt in 2 % Uranylacetat. Der Balken entspricht 50 nm.**

Für die 3D Rekonstruktion wurden 500 der in Abbildung 6.2.B gezeigten Rezeptormoleküle ausgewählt. Dieser relativ kleine Datensatz besteht aus GluR-B Ionenkanälen deren Präservierung in Uranylacetat als besonderes vielversprechend eingeschätzt wurde. Dieser positive Effekt wurde auf die Verwendung frisch von einer Wasseroberfläche aufgefisher Kohlefilme zurückgeführt (siehe RESULTS 4.4.3.3.). Während der Klassifizierung dieses Datensatzes fiel auf, dass die beim Band-Pass-Filtern für die niedrigen Frequenzen gesetzten Cut-offs einen deutlichen Einfluss auf die erste Klassifizierung der unterschiedlichen zweidimensionalen Ansichten des Proteinkomplexes haben (siehe RESULTS 4.4.3.4.). Aus diesem Grund wurde der gleiche Datensatz mit 5 verschiedenen low-frequency cut-offs (LFCO) gefiltert (siehe Table 4.4.3.4.) und getrennt klassifiziert. Von den 5 resultierenden Klassifikationen wurden 3 (LFCO 0,005, 0,03 und 0,05) für die weiterführende 3D Rekonstruktion ausgewählt. Die Evaluierung der resultierenden 3D Modelle ergab, dass der mit einem LFCO von 0,03 gefilterte Datensatz eine Klassifikationen erlaubte, die zu einem 3D Modell (Modell GluR-BII/a siehe RESULTS Figure 4.4.3.4.H) führte, das im Vergleich zu den beiden anderen Rekonstruktionen konsistenter war. Am stärksten spricht für dieses Modell die Übereinstimmung der Input-Projektionen mit den Reprojektionen der 3D Rekonstruktion (siehe siehe RESULTS Figure 4.4.3.4.H).

Zur Verfeinerung des Modells GluR-BII/a wurden die beiden Projektionen mit der höchsten Standardabweichung vom Klassendurchschnitt (class average) eliminiert. Die verbleibenden 11 Projektionen bildeten die Input-Projektionen für die Berechnung eines verfeinerten Modells, GluR-BII/b, das auf einer neuen Zuordnung der Euler-Winkel beruht. Das Ergebnis dieser Berechnung ist in der nachfolgenden Abbildung gezeigt.

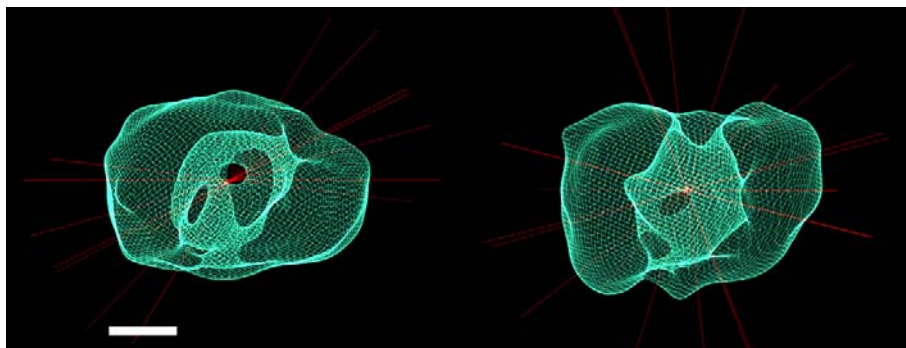


**Abbildung 6.2.C: Modell für GluR-B auf der Grundlage von 500 in 2% Uranylacetat gefärbten Ionenkanälen. Gezeigt ist eine Aufsicht und eine Seitenansicht, die beide einen zentralen Kanal erkennen lassen. Die roten Linien zeigen die Verteilung der Eulerwinkel (siehe auch Kapitel 5.2. DISCUSSION OF ELECTRON MICROSCOPY RESULTS). Der Balken entspricht 5 nm.**

Das Modell in Abbildung 6.2.C zeigt einen zentralen Kanal und hat die Dimensionen  $18 \text{ nm} \times 14 \text{ nm} \times 11 \text{ nm}$ . Die Stöchiometrie der Untereinheiten ist aus dem Modell, das mit grosser Wahrscheinlichkeit einen komplett zusammengesetzten GluR darstellt, nicht ablesbar. Ebenso wenig zeigt das Modell eine eindeutig vierzählige oder fünfzählige Symmetrie. Allerdings ist die erkennbare zweizählige Symmetrie im Einklang mit dem vorgeschlagenen Pair-of-Dimer Modell (Ayalon and Stern-Bach, 2001), das auf eine tetramere Struktur des oligomeren Ionenkanals schliessen lässt.

Die Ergebnisse dieser Arbeit zeigen, dass stabil transifizierte Insektenzellen eine durchaus geeignete Quelle für GluR-B Ionenkanäle sind. Nachteilig sind die geringen Ausbeuten. Allerdings kann durch weitere Selektion der Zellen die GluR Expression noch gesteigert werden (siehe APPENDIX A.2.2.). Bei höheren GluR-B Ausbeuten könnte zukünftig auch die Detektion des Rezeptors in vitrifizierten Proben in Verbindung mit Kryo-Elektronenmikroskopie und auch die 2D-Kristallisation gelingen. Die während dieses Projekts gemachten Kristallisationsexperimente (siehe APPENDIX A.3.) und Kryo-Experimente mit GluR-B Protein aus dem Baculovirusexpressionssystem (siehe RESULTS 4.4.1. und 4.4.2.) ergaben negative Ergebnisse. Das Potential der Kryo-Methode konnte allerdings in Kontrollexperimenten mit Tabak-Mosaik-Virus (TMV) gezeigt werden. Kryo-Daten von GluR-B würden die Berechnung eines genaueren Strukturmodells erlauben. Die Reprojektionen des hier besprochenen Strukturmodells GluR-BII/b aus der Abbildung 6.2.C könnten als Referenzen für das Alignment der vitrifizierten GluR Ionenkanäle dienen.

Für das langfristige Ziel der Rekonstitution des Rezeptors in Liposomen sollte die Delipidierung des Membranproteins während der Aufreinigung möglichst reduziert werden. Hier erscheinen zwei Ansätze sinnvoll. Die Aufreinigung des Proteins in einem Schritt durch die Erweiterung des tags am Carboxyterminus von nur 6 auf 10 Histidin-Reste. Ausserdem gibt es Hinweise, dass die Anwesenheit von Lipiden während der Aufreinigung für seine Rekonstituierbarkeit förderlich ist (Huganir and Racker, 1982).

## Referenzen von Kapitel 6

- Armstrong, N., Sun, Y., Chen, G.-Q., and Gouaux, E. (1998). Structure of a glutamate-receptor ligand binding core in complex with kainate. *Nature* 395, 913-917.
- Ayalon, G., and Stern-Bach, Y. (2001). Functional assembly of AMPA and kainate receptors is mediated by several discrete protein-protein interactions. *Neuron* 31, 103-113.
- Dingledine, R., Borges, K., Bowie, D., and Traynelis, S. F. (1999). The glutamate receptor ion channels. *Pharmacological Reviews* 51, 7-61.
- Hollmann, M., and Heinemann, S. (1994). Cloned glutamate receptors. *Annual Reviews in Neuroscience* 17, 31-108.
- Hollmann, M., Maron, C., and Heinemann, S. (1994). N-glycosylation site tagging suggests a three-transmembrane domain topology for the glutamate receptor GluR1. *Neuron* 13, 1331-1343.
- Huganir, R. L., and Racker, E. (1982). Properties of proteoliposomes reconstituted with acetylcholine receptor from *Torpedo californica*. *The Journal of Biological Chemistry* 257, 9372-9378.
- Keinänen, K., Köhr, G., Seeburg, P. H., Laukkanen, M. L., and Oker-Blom, C. (1994). High-level expression of functional glutamate receptor channels in insect cells. *Bio/Technology* 12, 802-806.
- Kuner, T., Wollmuth, L. P., Karlin, A., Seeburg, P. H., and Sakmann, B. (1996). Structure of the NMDA receptor channel M2 segment inferred from accessibility of substituted cysteines. *Neuron* 17, 343-352.
- Nakanishi, S. (1990). Molecular diversity of glutamate receptors and implication for brain function. *Science* 258, 597-630.
- Paas, Y. (1998). The macro- and microarchitectures of the ligand-binding domain of glutamate receptors. *Trends in Neurosciences* 21, 117-125.
- Rosenmund, C., Stern-Bach, Y., and Stevens, C. F. (1998). The tetrameric structure of a glutamate receptor channel. *Science* 280, 1596-1599.
- Safferling, M., Tichelaar, W., Kümmerle, G., Jouppila, A., Kuusinen, A., Kainänen, K., and Madden, D. R. (2001). First images of a glutamate receptor ion channel: oligomeric state and molecular dimensions of GluRB homomer. *Biochemistry* 40, 13948-13953.
- Seeburg, P. H. (1993). The molecular biology of mammalian glutamate receptor channels. *Trends in Pharmacological Sciences* 16, 359-365.

## APPENDIX

### A.1. RECOMBINANT EXPRESSION OF EUKARYOTIC MEMBRANE PROTEINS

By recombinant expression it is possible to isolate reasonable amounts of membrane proteins with low natural abundance for crystal structure analysis. While the expression of prokaryotic membrane proteins in *E. coli* proved to be quite successful, the recombinant expression of eukaryotic integral membrane proteins is still not a routine work. What makes the expression of membrane proteins so difficult? Compared to the expression of soluble proteins, which comprises transcription, translation and post-translational modifications, the biosynthesis of membrane proteins requires the additional step of membrane insertion.

Grisshammer and Tate reviewed the expression of integral membrane proteins for structural studies (Grisshammer and Tate, 1995). Their article was a guideline for this paragraph. It covers the most promising systems for the expression of membrane proteins like the glutamate receptors and has a focus on post-translational modifications. Beside glycosylation phosphorylation and disulfide bond formation are important post-translational protein modifications. Both eukaryotic and prokaryotic expression systems are capable of expressing disulphide-linked proteins. By phosphorylation many receptor proteins like the serine, threonine and glutamate receptor proteins are regulated. Phosphorylation of the C-terminal segment of the transmembrane domain M4 of the ionotropic glutamate receptor for example potentiates the response to agonist binding (Greengard et al., 1991). Glycosylation can be essential for folding, stability and activity of membrane proteins. Inhibition of glycosylation during protein expression can result in a complete loss of function. When glycosylation was blocked for example during expression of recombinant homo-oligomeric serotonin receptors by the addition of tunicamycin no ligand binding was observed in crude membrane preparations (Green et al., 1995). One possible interpretation of this is that glycosylation is required to reach the final structure and to preserve activity. Especially the findings about the importance of glycosylation suggest that over-expression trials with membrane proteins should start with host cells homologous to the source of the membrane protein, i.e. the biosynthesis of these cells should include the required post-translational modifications. Since they are of eukaryotic origin yeast and insect cells fulfill these requirements best.

Insect cells facilitate post-translational protein modifications and provide a eukaryotic environment for protein folding and protein assembly comparable to that in mammalian cells. In recent years insect cells have been used to express a remarkable number of different membrane proteins (Grisshammer and Tate, 1995). In the baculovirus expression system protein overexpression is induced by the infection of insect cells with a recombinant baculovirus. By genetic modification foreign genes can be incorporated into the DNA of the *Autographa californica* multiple nuclear polyhedrosis virus (AcMNPV). In nature this virus infects endothelium cells in the gut of insects like *Spodoptera frugiperda* (Sf) or *Trichoplusia ni*. The virus infection induces the expression of viral and foreign genes. Beside the virus-mediated protein expression in insect cells there are insect cells, which constitutively express a foreign gene called “stable insect cells”. The characteristics of both options and the GluR-B specific molecular biology in this respect are described in the following two paragraphs. In addition the baculovirus mediated expression is evaluated from the electron microscopist’s point of view.

## **A.2. RECOMBINANT EXPRESSION OF GLUR-B IN INSECT CELLS**

### **A.2.1. BACULOVIRUS MEDIATED EXPRESSION OF GLUR-B**

Our collaborators in Finland generated the recombinant GluR-B virus. Using PCR techniques and a pFastBac1 derivative containing a baculoviral signal peptide (ecdysteroid UDP-glucosyltransferase) a vector was made containing the cDNA of the full-length flop isoform of GluR-B from rat. The signal peptide was fused to a FLAG epitope (Hopp et al., 1988) and a cloning linker (RPHAMG). On the C-terminus the vector contained a hexahistidine tag (Schiöth et al., 1996) that is preceded by a four-residue linker (MNSR). Using the Bac-to-Bac protocol (Gibco) the recombinant baculovirus v506-2 was generated by co-transfection of the transfer vector containing the foreign gene with AcMNPV DNA that was followed by serial plaque purification (Keinänen et al., 1994).

When ligand gated ion channels are expressed by the baculovirus expression system it can be important to consider the baculovirus infection as a possible source of artifacts. What is the nature of these artifacts? Gene expression in baculoviruses is divided into four phases: immediate-early, delayed early, late, very late phase. For the overexpression of foreign genes the class of very late genes, which encode the polyhedrin protein and the p10 protein is most

important. Both proteins are essential proteins for the production of protective polyhedral virus capsids, which encapsulate virus particles in the nucleus of the host cell. Since occlusion bodies are not necessary to maintain an infection in cultured cells these proteins are dispensable *in vitro*. Therefore their genes can be deleted and replaced by foreign genes making them suitable for large-scale protein expression. Both polyhedrin genes and p10 genes are under the control of strong promoters. Thus the abundance of the corresponding proteins is high. Structural biologists have to keep in mind that such polyhedral virus capsids, which have a periodic structure can contaminate purified protein samples. Previously, AcMNPV capsids were found to contaminate the baculovirus-expressed NS1 protein that was isolated by pelleting through a gradient (Hewat et al., 1992), i.e. a rather crude purification step. However, in this project low concentrations of a helical tube-like structure were found in GluR-B samples that had been doubly purified by immobilized metal-affinity chromatography (IMAC) and immunoaffinity chromatography. The tubular structures in doubly purified GluR-B samples are most likely of baculoviral origin. Their diffraction pattern was compared with the diffraction pattern of tubular structures isolated from High5 cells after infection with wild-type AcMNPV baculoviruses. In this control experiment cells were harvested, solubilized and purified by immobilized metal-affinity chromatography (IMAC) as described in 3.3.2. The eluates contained high amounts of tubular structures, which were characterized by electron microscopy (Figure A.2.1.A shows such a tubular structure negatively stained in uranyl acetate).



**Figure A.2.1.A: Helical tube-like structure as found in purified GluR-B samples negatively stained in uranyl acetate. The bar corresponds to 100 nm.**

The diameter of stain-flattened tubules varies between 55 and 45 nm. This is consistent with a 50 nm diameter measured for another insect virus capsid, which looks very similar (Beaton and Filshie, 1976). According to the diffraction pattern the unit cell dimensions of the tubular structures found in purified GluR-B samples were measured to be ca. 54 Å × 85 Å, which is consistent with the literature (Beaton and Filshie, 1976). It was suspected that the p10 protein formed the capsids, which were never observed in the purified GluR-B samples from stable insect cells. However, Western-blotting and subsequent immunolabeling could not identify the contaminants as p10 protein. (Dr. L. King, Oxford Brookes University provided the p10 antiserum.)

### A.2.2. EXPRESSION OF GLUR-B IN STABLE INSECT CELLS

As an alternative to baculovirus-mediated expression our collaborators in Finland generated stable insect cells as a source for GluR-B and GluR-D protein. In February 2000 we started to use these cells instead of baculovirus infected insect cells for the isolation of GluR-B. To produce stable insect cell lines for the constitutive expression of GluR-B and GluR-D homomers the pActZ plasmid was used. The pActZ plasmid is a fusion of the actin promoter based on plasmid (pIE1/153A) (Farrell et al., 1998) and the IE2 promoter based plasmids (Invitrogen). By Fab7 live staining cell lines were selected. The Fab7 antibody fragment is specific for GluR-D and GluR-B and allows the location of the receptor protein in the insect cells. Results of Fab7 staining showed that the level membrane-inserted GluR protein is low compared to the amount of GluR protein retained in the endoplasmatic reticulum (see Figure A.2.2.A).

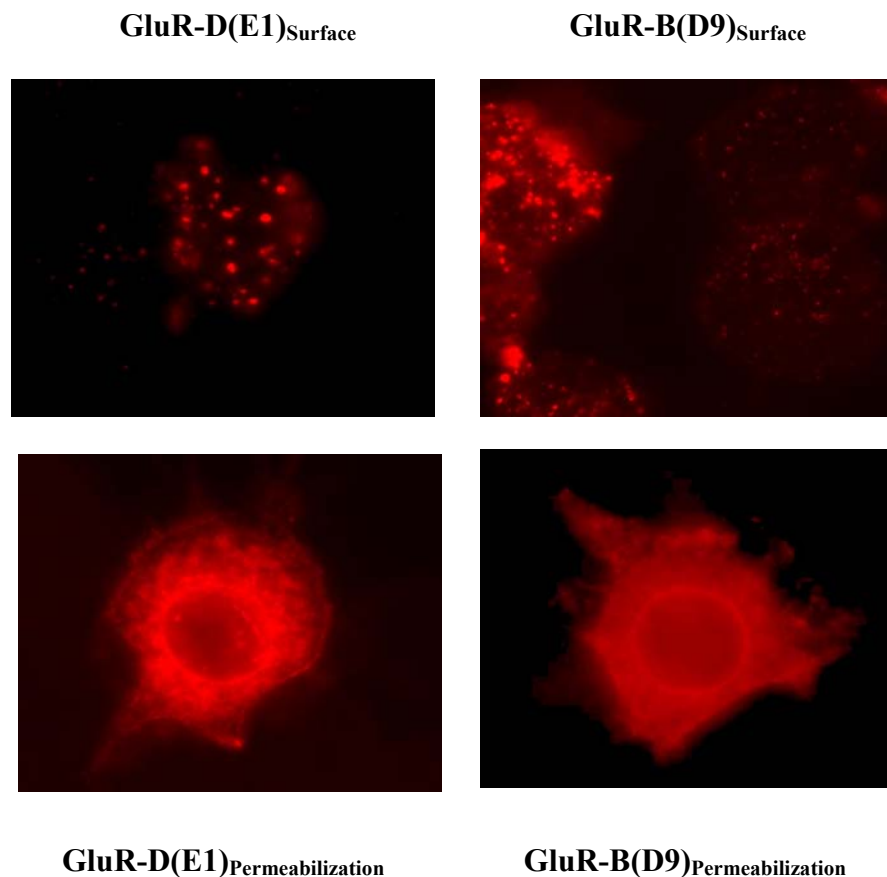


Figure A.2.2.A: Fab7 staining; permeabilized (top row) and non-permeabilized cells (bottom row) of stable insect cell lines expressing GluR-B and GluR-D were stained and are shown at a magnification of 100 $\times$ . (Courtesy of Dr. S. Coleman and Dr. D. Mottershead, Viikii Biocenter, University of Helsinki, Finland.)

### **A.3. TWO-DIMENSIONAL PROTEIN CRYSTALLIZATION**

#### **A.3.1. TWO-DIMENSIONAL CRYSTALS OF A H<sup>+</sup>-ATPase**

For the crystallization of integral membrane proteins a general approach has been proposed (Scarborough, 1994). This approach was very successful in the production of two-dimensional crystals of the *Neurospora crassa* plasma membrane H<sup>+</sup>-ATPase, solubilized in dodecyl- $\beta$ -D-maltoside (DDM) (Scarborough, 1994), (Cyrklaff et al., 1995), (Auer et al., 1999). In 1999 initial crystallization experiments with some other membrane proteins, applying the same conditions, were very promising (M. Auer, personal communication). However, so far none of these candidates has produced diffracting crystals. But recently the approach suggested by G. Scarborough was successful for another protein, which is the P-glycoprotein (P-gp). This ABC transporter hydrolyses ATP and extrudes cytotoxic drugs from mammalian cells. The two-dimensional crystals of this protein were used to determine projection structures of P-gp protein trapped at different steps of the transport cycle, which allowed correlation of protein structure and protein function (Rosenberg et al., 2001).

For the two-dimensional approach of G. Scarborough two forms of interaction are suggested to be important for the formation of protein crystals: first, interactions between the detergent micellar collars, which saturate the hydrophobic part of the membrane protein and second, interactions between protein surfaces. This order was chosen since protein-protein interactions cannot be characterized independently of the detergent, while those interactions, which involve only detergent molecules can. Therefore the micellar aggregation of the detergent in the presence of a precipitant was studied first. Before Dr. Scarborough searched for optimal conditions, under which the supersaturation ratios of the protein surfaces of the H<sup>+</sup>-ATPase and the detergent micellar collar were properly matched he analyzed the solubility properties of DDM. Seven polyethylene glycols (PEG) were found to induce DDM micellar aggregation at 5 mg/mL DDM over a range of PEG concentrations. After that the influence of the precipitants on the protein-detergent complex was investigated. For this purpose the approximate solubility of the DDM-ATPase complexes at concentrations of the effective DDM precipitants slightly (2%) below the concentration at which they induced visible micellar aggregation was determined. Since the DDM micellar collar should still be soluble under these conditions the occurrence of precipitation in these experiments reflected, the approximate solubility of the protein surfaces of the DDM-ATPase complex. With PEG 4000

conditions were found in which the potential crystallization zone of protein surfaces and the DDM micellar solubility possibly coincides (Scarborough, 1994). The resulting crystals consist of protein-detergent complexes in which the hydrophobic part of the protein is shielded by detergent molecules. In this project the *Neurospora crassa* plasma membrane H<sup>+</sup>-ATPase was used as a control system for two-dimensional crystallization experiments with baculovirus-mediated GluR-B protein (see Figure A.3.2.B).

### **A.3.2. TWO-DIMENSIONAL CRYSTALLIZATION OF BACULOVIRUS-MEDIATED GLUR-B PROTEIN**

The baculovirus-mediated expression of GluR-B yielded single-milligram quantities of protein, which were used for two-dimensional crystallization experiments. To apply the crystallization approach by G. Scarborough (see 4.4.4.1.) in GluR-B samples the detergent Triton X-100 was first exchanged for DDM (see 3.4.6.). After detergent exchange GluR-B was eluted with a protein concentration of ca. 20 µg/mL. Higher concentrations as required for crystallization setups were achieved by the use of centrifugal concentrators. The protein concentrations these stock solutions were at 300 µg/mL, 500 µg/mL and 666 µg/mL. (The values of protein concentrations given here are calculated according to the volume reduction and are therefore not exact.) Due to the dilution effect of the other additives the protein concentrations in the corresponding crystallization mixture were reduced to protein concentrations between 150 µg/mL and 460 µg/mL. Due to intensive concentration of GluR-B protein by centrifugal concentrators the concentrations of DDM in GluR-B stock solutions were as high as 10 mg/mL. As a consequence DDM concentrations in crystal mixtures were considerably higher than 1.28 mg/mL DDM, which was found to be ideal for the *Neurospora crassa* plasma membrane H<sup>+</sup>-ATPase. Concentration of PEG 4000 in these experiments was 10.5% (w/v).

The combined screening by phase-contrast microscopy at a magnification of 400 $\times$  and the analysis of negatively stained samples by electron microscopy at variable magnifications, which was effective for the H<sup>+</sup>-ATPase, did not reveal any periodically arranged protein molecules in any of the GluR-B crystallization mixtures. Mixtures were monitored for several days. A typical negatively stained sample taken from a crystallization mixture with GluR-B is displayed in Figure A.3.2.A. Specimen showed extended areas of aggregated protein and typically no single GluR-B protein molecules.



**Figure A.3.2.A:** Two-dimensional crystallization of GluR-B; the sample was negatively stained in 2% uranyl acetate at a magnification of 50 000 $\times$ . EM analysis of these specimens revealed extended areas of aggregated protein.

For the *Neurospora crassa* plasma membrane H<sup>+</sup>-ATPase it had been suggested to use a protein concentration in the final crystallization mixture (volume: 50  $\mu$ L) of ca. 1 mg/mL. However, the H<sup>+</sup>-ATPase was found to produce two-dimensional crystals even when the concentration in the crystallization mixture was only ca. 150  $\mu$ g/mL and the concentration of DDM was as high as 4.8 mg/mL (G. Scarborough and D. Madden, personal communication). The H<sup>+</sup>-ATPase was therefore used as for control experiments during this project. Figure

A.3.2.B shows two-dimensional crystal patches (see bottom left) of the  $H^+$ -ATPase obtained with PEG 4000.



**Figure A.3.2.B:** Two-dimensional crystallization of the *Neurospora crassa*  $H^+$ -ATPase; the sample was negatively stained in 2% uranyl acetate at a magnification of 30 000 $\times$ . On the left side at the bottom crystalline patches can be seen. It seems that the monomers have a preferred orientation (top views) relative to the carbon film.

Finally, with PEG 2000 and PEG 600 and two different the polyethylene glycols PEG 2000 and PEG 600 were tested. Both have shorter chain lengths than PEG 4000 and were found to induce aggregation of DDM micelles at concentrations lower than 15 % (w/v). When they were for two-dimensional crystallization according to the approach of G. Scarborough the crystallization mixture did not yield any crystals.

**REFERENCES OF THE APPENDIX**

- Auer, M., Scarborough, G. A., and Kühlbrandt, W. (1999). Surface crystallisation of the plasma membrane H<sup>+</sup>-ATPase on a carbon support film for electron crystallography. *Journal of Molecular Biology* 287, 961-968.
- Beaton, C. D., and Filshie, B. K. (1976). Comparative ultrastructural studies of insect granulosis and nuclear polyhedrosis viruses. *Journal of General Virology* 31, 151-161.
- Cyrklaff, M., Auer, M., Kühlbrandt, W., and Scarborough, G. A. (1995). 2-D structure of the *Neurospora crassa* plasma membrane ATPase as determined by electron cryomicroscopy. *The EMBO Journal* 14.
- Farrell, P. J., Lu, M., Prevost, J., Brown, C., Behie, L., and Iatrou, K. (1998). High-level expression of secreted glycoproteins in transformed lepidopteran insect cells using a novel expression vector. *Biotechnology & Bioengineering* 60 (6), 656-663.
- Green, T., Stauffer, K. A., and R., L. S. C. (1995). Expression of recombinant homooligomeric 5-HT<sub>3</sub> receptors provides new insights into their maturation and structure. *Journal of Biological Chemistry* 270, 6056-6061.
- Greengard, P., Nairn, A. C., and Stevens, C. F. (1991). Enhancement of the glutamate response by cAMP-dependent protein kinase in hippocampal neurons. *Science* 253, 1135-1138.
- Grisshammer, R., and Tate, C. G. (1995). Overexpression of integral membrane proteins for structural studies. *Quarterly Review of Biophysics* 28, 315-422.
- Hewat, E., Booth, T. F., Wade, R. H., and Roy, P. (1992). 3-D reconstruction of bluetongue virus tubules using cryoelectron microscopy. *Journal of Structural Biology* 108, 35-48.
- Hopp, T. P., Prickett, K. S., Price, V. L., Libby, R. T., March, C. J., Cerretti, D. P., Urdal, D. L., and Conlon, P. J. (1988). *Biotechnology* 6, 1204.
- Keinänen, K., Köhr, G., Seeburg, P. H., Laukkanen, M. L., and Oker-Blom, C. (1994). High-level expression of functional glutamate receptor channels in insect cells. *Bio/Technology* 12, 802-806.
- Rosenberg, M. F., Velarde, G., Ford, R. C., Martin, C., Berridge, G., Kerr, I. D., Callaghan, R., Schmidlin, A., Wooding, C., Linton, K. J., and Higgins, C. F. (2001). Repacking of the transmembrane domains of P-glycoprotein during the transport ATPase cycle. *The EMBO Journal* 20, 5615-5625.
- Scarborough, G. A. (1994). Large single crystals of the *Neurospora crassa* plasma membrane of H<sup>+</sup>-ATPase: an approach to the crystallisation of integral membrane proteins. *Acta Crystallographica Section D* 50, 643-649.
- Schiöth, H. B., Kuusinen, A., Muceniece, R., Szardenings, M., Keinänen, K., and Wikberg, J. E. (1996). Expression of functional melanocortin 1 receptors in insect cells. *Biochemical and Biophysical Research Communication*, 221, 807-814.

# First Images of a Glutamate Receptor Ion Channel: Oligomeric State and Molecular Dimensions of GluRB Homomers<sup>†</sup>

Markus Safferling,<sup>‡,§</sup> Willem Tichelaar,<sup>‡</sup> Günther Kümmerle,<sup>‡</sup> Annukka Jouppila,<sup>||</sup> Arja Kuusinen,<sup>||</sup> Kari Keinänen,<sup>||</sup> and Dean R. Madden<sup>\*,‡</sup>

*Ion Channel Structure Research Group, Max Planck Institute for Medical Research, Jahnstrasse 29, 69120 Heidelberg, Germany, and Viikki Biocenter, Department of Biosciences (Division of Biochemistry) and Institute of Biotechnology, Post Office Box 56, FIN-00014 University of Helsinki, Helsinki, Finland*

*Received June 4, 2001; Revised Manuscript Received September 5, 2001*

**ABSTRACT:** We have expressed, purified, and characterized glutamate receptor ion channels (GluR) assembled as homomers of the subunit GluRB. For the first time, single-milligram quantities of biochemically homogeneous GluR have been obtained. The protein exhibits the expected pharmacological profile and a high specific activity for ligand binding. Density-gradient centrifugation reveals a uniform oligomeric assembly and a molecular mass suggesting that the channel is a tetramer. On the basis of electron microscopic images, the receptor appears to form an elongated structure that is visualized in several orientations. The molecular dimensions of the molecule are approximately  $11 \times 14 \times 17$  nm, and solvent-accessible features can be seen; these may contribute to formation of the ion-conducting pathway of the channel. The channel dimensions are consistent with an overall 2-fold symmetric assembly, suggesting that the tetrameric receptor may be a dimer of dimers.

The ionotropic glutamate receptors (GluR)<sup>1</sup> are ligand-gated cation channels of the central nervous system, where they play an important role in both physiological and pathological processes (reviewed in ref 1). Pharmacologically distinct subfamilies of GluR have been identified. GluR with high affinity for AMPA ( $\alpha$ -amino-5-methyl-3-hydroxy-4-isoxazole propionate) are responsible for most fast excitatory synaptic signaling in the brain. Recent evidence also implicates the AMPA receptors in the activity-dependent modulation of synaptic strength (reviewed in ref 2).

AMPA receptors are formed by homo- or heterooligomers of the subunits GluRA–D (also known as GluR1–4) (3–5). The GluRB subunit is particularly important in determining the ion permeability characteristics of the channels: receptors containing GluRB have a very low calcium permeability compared to those not containing it (6). Interactions of the cytoplasmic C-terminus of GluRB with proteins of the postsynaptic density appear to play a key role in the targeting and localization of GluR ion channels (7) but not in the assembly of functional channels (8).

The direct structural information currently available for the AMPA receptors is a series of crystallographic structures

of the core of the ligand-binding domain of GluRB, representing ~25% of the molecular mass of the complete subunit (9). Little structural information is available on the interdomain and intersubunit interactions that are presumably important for GluR activation and desensitization. The oligomeric state of the glutamate receptors has also not been definitively established (reviewed in ref 1), although recent evidence suggests a dimer-of-dimers model (8).

While functional insect-cell expression of GluRD and GluRB/D ion channels and purification of GluRD AMPA receptor homomers have been previously reported, the purified protein exhibited levels of aggregation unacceptable for structural studies (10, 11; unpublished data). Here, we report the milligram-scale expression and purification of affinity-tagged GluRB AMPA receptors, optimized for ligand-binding activity, yield, and structural homogeneity. The resulting material permits assessment of the channel's stoichiometry and characterization of its gross structural features and molecular dimensions.

## EXPERIMENTAL PROCEDURES

**Plasmid and Baculovirus Generation.** Affinity-tagged cDNA containing the flop isoform of the rat GluRB subunit (SWISS-PROT accession number P19491, ref 4) was assembled by PCR techniques in a pFastBac1 derivative harboring a baculoviral signal peptide (ecdysteroid UDP-glucosyltransferase), fused to a FLAG epitope (12) and a cloning linker (RPHAMG). The vector also contained a C-terminal hexahistidine tag (13), preceded by a four-residue linker (MNSR). The C- and N-terminal tags are used for immobilized metal-affinity chromatography (IMAC) and immunoaffinity purifications, respectively, of the recombinant GluRB homomers. Correctness of all PCR-derived sequences was verified by DNA sequencing. The construct

<sup>†</sup> Financial support was provided in part by EU Grant BIO4-CT96-0589 of the Fourth Framework Program in Biotechnology (D.R.M. and K.K.), the Max Planck Society (D.R.M.), and the Academy of Finland (K.K.).

\* Corresponding author: Telephone +49-6221-486150; fax +49-6221-486437; e-mail madden@mpimf-heidelberg.mpg.de.

<sup>‡</sup> Max Planck Institute for Medical Research.

<sup>§</sup> Present address: Skirball Institute, New York University Medical Center, 540 First Ave., New York, NY 10016.

<sup>||</sup> University of Helsinki.

<sup>1</sup> Abbreviations: GluR, ionotropic glutamate receptor; AMPA,  $\alpha$ -amino-5-methyl-3-hydroxy-4-isoxazole propionate; MOI, multiplicity of infection; PMSF, phenylmethanesulfonyl fluoride; TX-100, Triton X-100; IMAC, immobilized metal-affinity chromatography.

omits the native C-terminal Ile residue of GluRB<sub>nop</sub> and thus corresponds to residues 1–861 of the mature sequence. Recombinant baculovirus v506-2 was generated using the Bac-to-Bac protocol (Gibco), and amplified in *Spodoptera frugiperda* Sf21 cells.

**Cell Culture and Protein Expression.** For initial characterization, Sf21 cells were infected and harvested as described for GluRD (11). Large-scale cell culture was performed in shaker flasks. Protein expression was performed in Sf21 or *Trichoplusia ni* High Five insect cells infected with multiplicity of infection (MOI)  $\geq 4$  in Ex-cell 400 medium (JRH Biosciences), and viral expansion was performed in Sf9 cells in TNM-FH medium supplemented as described (14). Cell viability was assayed 86 h after infection by staining with trypan blue (Gibco). If the viability was  $<95\%$  or cells had lost their round and uniformly clear appearance, they were harvested. Otherwise they were left shaking for another 4 h.

**Cell Harvest and Lysis.** All further steps were performed at 4 °C. Cells were harvested by use of a Contifuge 20 S, equipped with rotor type 8684 and a Pericor CD 240 peristaltic pump (Heraeus), at 2100g (4000 rpm) and a flow rate = 280 mL min<sup>-1</sup>. Alternatively, cells were centrifuged at 1500g for 10 min. The cell pellet was washed with 300 mL of TBS (150 mM NaCl and 50 mM Tris, pH 7.4) containing 0.1 mM phenylmethanesulfonyl fluoride (PMSF; Sigma) and then resuspended in 100 mL of lysis buffer (20 mM HEPES pH 7.4, and 5 mM EDTA), supplemented with 0.1 mM PMSF and Complete protease inhibitor tablets (one tablet dissolved in 500 mL of buffer; Roche Molecular Biochemicals). The suspension was divided into 16 aliquots, each of which was homogenized with a Polytron 1200 C (Kinematica) for 3  $\times$  10 s at 5000 rpm. Tubes were incubated on ice between pulses. Each tube was then filled with an additional 30 mL of lysis buffer and the membranes were pelleted at 31000g for 30 min. The pellet was resuspended and centrifuged twice more, the first time in lysis buffer and then in 20 mM HEPES, pH 7.4, 200 mM NaCl, and 0.5 mM EDTA, each supplemented with PMSF and Complete protease inhibitors as above. This treatment lysed  $\geq 99\%$  of all cells, as determined by visual inspection.

**Receptor Solubilization.** Pellets were pooled and suspended in 250 mL of solubilization buffer [20 mM HEPES, pH 7.4, 200 mM NaCl, and 10% (v/v) glycerol], supplemented with PMSF and Complete protease inhibitors as above. The protein concentration was determined by bicinchoninic acid assay (Pierce). The solubilize was diluted to  $\leq 4$  mg/mL protein with solubilization buffer, typically to a final volume of 2 L for a large-scale prep. Triton X-100 (TX-100; Roche Molecular Biochemicals; purified for membrane protein research) was added to 1.5% (v/v). The suspension was mixed for 90 min with a Reax-20 overhead mixer (Heidolph) at 4 rpm, and clarified by centrifugation, either at 75600g for 30 min or at 185000g for 15 min.

**Immobilized Metal-Affinity Chromatography.** Chelating Sepharose fast flow (Pharmacia, 10 mL) was charged essentially as described (11) with Zn<sup>2+</sup>, Ni<sup>2+</sup>, or Co<sup>2+</sup>. Before loading, the clarified solubilize was adjusted to 1 M NaCl and 5 mM imidazole. The suspension was gently mixed for 12 h at 4 rpm. Subsequently, the resin was recovered by filtration through a 500 mL glass frit (medium porosity; Schott). The Sepharose was washed with 5 column volumes (CV) of 20 mM HEPES, pH 7.4, 10% glycerol, and 0.1%

TX-100 (buffer A) containing 1 M NaCl and 10 mM imidazole, followed by wash steps with buffer A containing first 200 mM NaCl and 10 mM imidazole (3 CV), then 100 mM NaCl and 10 mM imidazole (3 CV), and finally 100 mM NaCl and 50 mM imidazole (5 CV). GluRB was eluted in buffer A containing 100 mM NaCl and steps of 100 (5 CV), 200 (5 CV), and 500 (10 CV) mM imidazole. These eluates were analyzed by SDS-PAGE, and GluRB-containing fractions were pooled to give a typical final volume of 200 mL for a large-scale prep. Protein bands in silver-stained gels were quantitated with 1D Image Analysis software (Kodak Digital Science).

**Immunoaffinity Chromatography.** M1  $\alpha$ -FLAG affinity gel (IBI Kodak/Sigma, 3 mL) was equilibrated in M1 buffer (TBS supplemented with 3 mM CaCl<sub>2</sub> and 0.1% TX-100). Pooled GluRB-containing fractions from the IMAC column were adjusted to 3 mM CaCl<sub>2</sub> and applied to the gel at 0.5–1 mL min<sup>-1</sup>. After the column was washed with 20 CV of M1 buffer, GluRB was eluted in 20 CV of TBS containing 500 mM NaCl, 10% glycerol, 0.1% TX-100, and 10 mM EDTA. The protein concentration was determined by Amido Black assay (Bio-Rad). Pooled M1 eluates (typically 60 mL) were concentrated by use of Centriplus-100 concentrators (Millipore) or Nanosep-100 concentrators (Pall-Filtron).

**Ligand-Binding Assay.** Binding assays were performed as described (11), with 25–50  $\mu$ g of protein per reaction. Protein activity was quantified as described (11), except that 15 nM [<sup>3</sup>H]AMPA (Dupont-NEN) was used. In competition binding assays, the concentration of radioligand was 5 nM, IC<sub>50</sub> values were determined by nonlinear curve fitting to a model for one-site binding (GraFit, Erithacus Software; Prism, GraphPad Software), and apparent affinities ( $K_i$ ) were determined by use of the Cheng-Prusoff equation (15).

**Glycerol Density-Gradient Centrifugation.** Analysis was performed in a linear, 20–80% (v/v) glycerol density gradient in TBS and 0.1% TX-100 (total volume 9.5 mL). GluRB (50  $\mu$ g in 0.5 mL) as well as the reference proteins thyroglobulin, apoferritin, and alcohol dehydrogenase (500  $\mu$ g in 0.5 mL) were centrifuged in an Optima LE-80K centrifuge using a Ti67 rotor (Beckman) for 16 h at 180000g (37000 rpm) at 4 °C. Fractions of 0.5 mL were collected. GluRB was quantitated by [<sup>3</sup>H]AMPA binding assay. Protein standards were quantitated by the method of Bradford (16).

**Electron Microscopy.** Purified GluRB (3  $\mu$ L) was applied to hydrophilic carbon films at a concentration of 20  $\mu$ g mL<sup>-1</sup>. The grid was washed with two droplets of 25 mM Tris, 20 mM NaCl, and 2 mM EDTA, pH 7.4, stained with 2% uranyl acetate and 0.1% glucose, and air-dried. The preparation was performed at 4 °C. Images were recorded at a nominal magnification of 50000 $\times$  with a Zeiss CEM 902 operating at 80 kV, with an electron dose of  $\sim 10$  e<sup>-</sup>/Å<sup>2</sup> and discarding electrons scattered inelastically with an energy loss greater than about 15 eV. The objective lens defocus was chosen such that the first reversal of the phase contrast transfer function was at  $\sim 0.05$  Å<sup>-1</sup>. The negatives were digitized with a Zeiss SCAI scanner at a resolution of 21  $\mu$ m.

The single particle image analysis was carried out essentially according to Schatz et al. (17) and Serysheva et al. (18) in the context of the IMAGIC-5 software system (19). More than 10 000 single-molecular images were selected. They were aligned with the “alignment by classification” approach (20), by which bias toward any specific reference

Table 1: Ligand-Binding Pharmacology of Recombinant GluRB Expressed in Sf21 Cells

ligand	$K_d$ (nM)	$IC_{50}^a$ ( $\mu$ M)	$K_I^b$ ( $\mu$ M)
AMPA	$16.8 \pm 2.3$		
L-Glutamate		$0.50 \pm 0.01$	$0.39 \pm 0.01$
kainate		$4.7 \pm 0.5$	$3.6 \pm 0.4$
CNQX <sup>c</sup>		$0.28 \pm 0.04$	$0.21 \pm 0.03$

<sup>a</sup>  $IC_{50}$  is the concentration required to displace 50% of radioligand binding. <sup>b</sup>  $K_I$  is the apparent affinity (15). <sup>c</sup> CNQX is 6-cyano-7-nitroquinoxaline-2,3-dione.

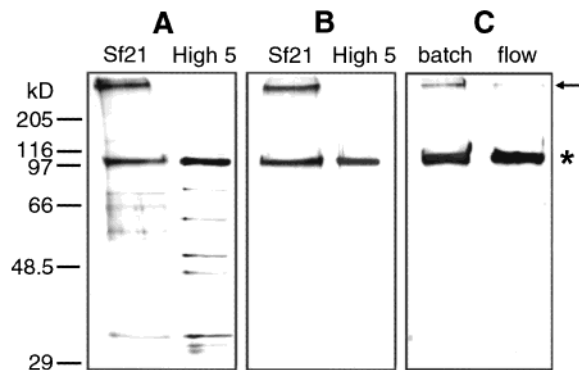


FIGURE 1: Comparison of GluRB expression conditions. (A, B) GluRB expressed in different insect cell lines, after purification by metal-chelate and immunoaffinity chromatography. (A) Silver stained SDS–polyacrylamide electrophoretic gel; (B) M1 $\alpha$ -FLAG Western blot of GluRB samples isolated from Sf21 and High Five cells. (C) M1 $\alpha$ -FLAG Western blot of GluRB from High Five cells harvested by conventional batch centrifugation (left lane) or continuous-flow centrifugation (right lane). In each comparison, equal fractions of the purified protein were loaded. The asterisk indicates the GluRB monomer band; the arrow marks the position of GluRB that did not enter the gel.

image is avoided. Class averages resulting from this procedure were used as the starting set of reference images for iterative cycles of multireference alignment (MRA), multivariate statistical analysis (MSA), and classification. One-fifth of the molecular images were discarded in the classification, and the average number of members per class was 25. The MRA–MSA–classification procedure was iterated until stable classes were obtained.

## RESULTS

**Protein Expression.** Sf21 cells infected with the GluRB-encoding baculovirus v506-2 produced a  $\sim$ 100-kDa band by SDS–PAGE that immunoreacted with a FLAG-specific antibody. This band was not observed in uninfected cells nor in cells infected with wild-type AcNPV baculovirus (data not shown). Cell membranes prepared from v506-2-infected Sf21 cells showed specific and high-affinity binding of [<sup>3</sup>H]-AMPA and a ligand-binding pharmacology typical of GluRB (Table 1) (21).

We next compared expression in Sf21 cells with that in High Five insect cells, which are suitable for the expression of a variety of membrane proteins (22) and for large-scale production (14). Equal volumes of Sf21 and High Five cells were infected with v506-2 at MOI = 5 and harvested 90 h later. Protein was purified by metal-chelate and  $\alpha$ -FLAG immunoaffinity chromatography and analyzed by SDS–PAGE and Western blotting (Figure 1A,B). The yield from High Five cells was 85  $\mu$ g/L, significantly higher than the

25  $\mu$ g/L obtained with Sf21 cells. Moreover, protein obtained with Sf21 cells showed an obvious high molecular mass band in both the silver-stained gel and the Western blot, reflecting partial aggregation (Figure 1A,B, arrow). Protein obtained from High Five cells exhibited much less aggregation, although some was occasionally detectable in highly developed Western blots (e.g., Figure 1C). Overall, the data suggest that High Five cells produce larger amounts of GluRB and provide an environment in which the ion channel is less prone to aggregation than Sf21 cells.

GluRB expression levels were then monitored as a function of the conditions of infection in High Five cells. The time course of radioligand binding was monitored during the course of infection and reached a maximum 86 h postinfection. The falloff in AMPA binding was rather sharp on either side of the optimal time point  $t_{max}$ . Twenty-four hours before and after  $t_{max}$ , AMPA binding was 30% and 50% less than the maximum, respectively. The ligand-binding activity of cells infected at different MOI showed maximal expression for MOI  $\geq$  3. In practice, the MOI was chosen between 4 and 5.

We also compared batch and continuous-flow centrifugation methods for cell harvest, since experience with seven-transmembrane helical proteins had indicated that continuous-flow centrifugation was advantageous in avoiding premature cell lysis (G. Schertler, personal communication). The yield of GluRB from cells harvested by continuous-flow centrifugation was 134  $\mu$ g/L, somewhat higher than the value obtained from the same batch of infected cells harvested with conventional batch centrifugation (104  $\mu$ g/L). In addition, the continuous-flow approach further reduced the slight GluRB aggregation detected with the batch method (Figure 1C).

**Purification of the Receptor.** Having optimized conditions for the overexpression and harvest of GluRB, we next attempted to improve the purification scheme. The construct contains a C-terminal hexahistidine tag and an N-terminal FLAG epitope, so initial purifications used a Ni<sup>2+</sup> column followed by  $\alpha$ -FLAG immunoaffinity chromatography. However, the immunoaffinity eluates exhibited several contaminants (Figure 1A). The purity of the IMAC eluates was very poor when Ni<sup>2+</sup> was used as the cation (Figure 2A, right-hand panel), and some of these contaminants evidently coeluted with GluRB during immunoaffinity chromatography (Figure 2B, right-hand panel, lanes e1 and e2). To improve the initial IMAC purification, Zn<sup>2+</sup> and Co<sup>2+</sup> were investigated as alternative cations. The use of Zn<sup>2+</sup> instead of Ni<sup>2+</sup> dramatically reduced contamination in the IMAC eluates and permitted the isolation of essentially pure material following immunoaffinity purification (Figure 2A,B, left-hand panels). It also resulted in elution of GluRB at somewhat lower imidazole concentrations than observed with Ni<sup>2+</sup>. The yield at this step was typically  $\sim$ 80%. The use of Co<sup>2+</sup> had an intermediate effect.

The optimized protocol has been reproducibly used in preparations at the 16 L scale. SDS–PAGE analysis of each step of a large-scale purification is shown in Figure 2C. In the final sample, GluRB is detected as a single band with an apparent molecular mass of 104 kDa, without indication of aggregation. This corresponds to the predicted amino acid sequence (99.1 kDa) together with  $\sim$ 4.9 kDa of glycosylation (at up to four potential N-linked glycosylation sites). Yields

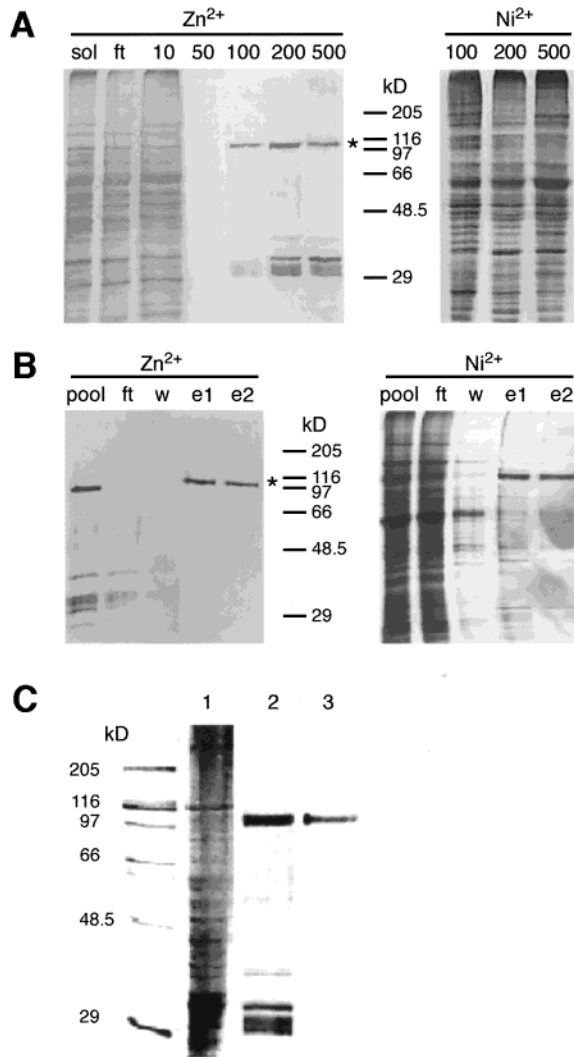


**FIGURE 2:** Purification of GluRB. (A, B) Role of metal-affinity cations. Silver-stained SDS-polyacrylamide electrophoretic gels are shown for the IMAC (A) and immunoaffinity (B) purification steps, with either Zn<sup>2+</sup> or Ni<sup>2+</sup> as cations. (A) IMAC. For Zn<sup>2+</sup>, solubilized membrane proteins (sol) are shown, together with column flowthrough (ft) and wash/elution steps at various imidazole concentrations (millimolar). For Ni<sup>2+</sup> only eluate fractions are shown. The asterisk marks the expected GluRB molecular mass. (B) Immunoaffinity purifications. For each cation, the pooled IMAC eluates (pool), the column flowthrough (ft), column wash (w), and two 10 mM EDTA eluates (e1 and e2) are shown. (C) Overview of final GluRB purification on a silver-stained SDS-polyacrylamide electrophoretic gel. Lane 1, Triton X-100 solubilized insect-cell membranes; lane 2, pooled IMAC eluates (Zn<sup>2+</sup>); lane 3, pooled immunoaffinity eluates. Lanes in panel C are from separate gels.

at this scale were consistently in the range of 80–130  $\mu$ g of highly purified GluRB/L of cells.

**Biochemical Characterization.** The purified, solubilized receptor had a  $K_D$  of  $18.2 \pm 0.9$  nM for [<sup>3</sup>H]AMPA and a  $B_{max}$  of 2140 pmol/mg of GluRB, as assayed by filter binding. Since filter binding is a nonequilibrium technique, the reported capacity does not necessarily reflect the specific activity of the protein. To establish approximately what fraction of GluRB is active, we performed filter-binding experiments with soluble GluRD ligand-binding domains known to exhibit ~100% specific activity by equilibrium dialysis measurements (23). Using the soluble construct, we

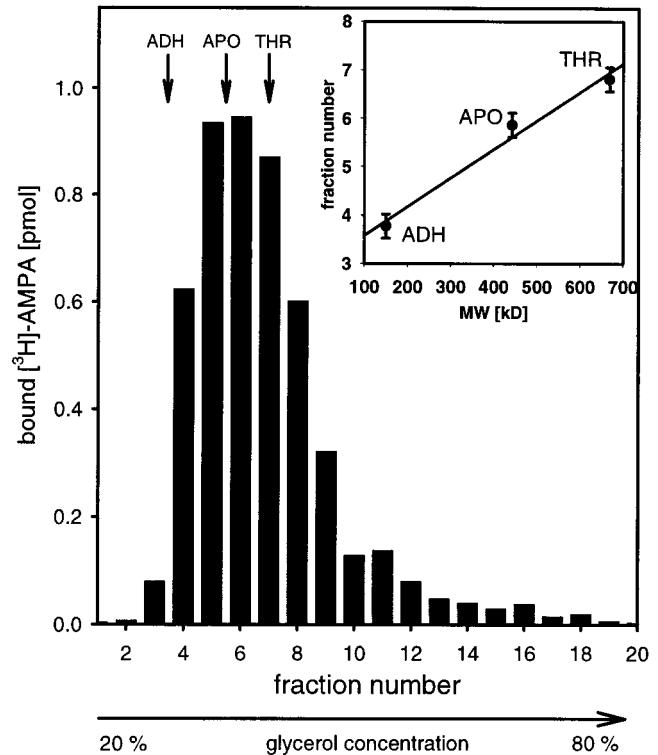


**FIGURE 3:** Density gradient centrifugation of Triton X-100-solubilized GluRB. The protein was quantitated by radioligand binding (bar graph). Standard proteins used for the calibration of the gradient (arrows above graph and inset) were thyroglobulin (THR, 669 kDa), apoferritin (APO, 443 kDa), and alcohol dehydrogenase (ADH, 150 kDa).

obtained a filter-binding signal that was consistently  $\leq 20\%$  of the theoretical maximum. Assuming that filter-binding studies detect a similar fraction of GluRB binding sites, the true number of AMPA binding sites would be close to the theoretical maximum of  $\sim 10\,000$  pmol/mg, for one agonist molecule per monomer.

Purified GluRB is assembled in a uniform oligomeric state as determined by density gradient centrifugation in glycerol (Figure 3) and sucrose (not shown). Its distribution in the gradient can be described as a single peak with a possible, small higher molecular-mass shoulder (fraction 11, Figure 3). The molecular mass of the GluRB complex was calibrated relative to soluble proteins (Figure 3, inset), yielding a value of 495 kDa. The GluRB peak is only slightly broader than those of the standard proteins, with a half-width of  $\sim 5$  fractions, vs  $\sim 4$  fractions for apoferritin.

**Electron Microscopy.** Purified GluRB homomers were negatively stained with uranyl acetate and visualized by electron microscopy (Figure 4A). Individual particles of uniform size are observed in several different orientations. More than 10 000 single molecular images were selected, aligned, classified, and averaged to improve the signal-to-noise ratio. Five out of a total of 155 class averages are shown in Figure 4C, together with corresponding single molecular images (Figure 4B). Since the molecule is elongated, the projections vary in appearance from approximately round to extended. The projected dimensions correspond to a molecule with a long dimension of 17 nm and a perpendicular cross section of  $11 \times 14$  nm. The particle also is indented or hollow, i.e., it contains internal solvent-

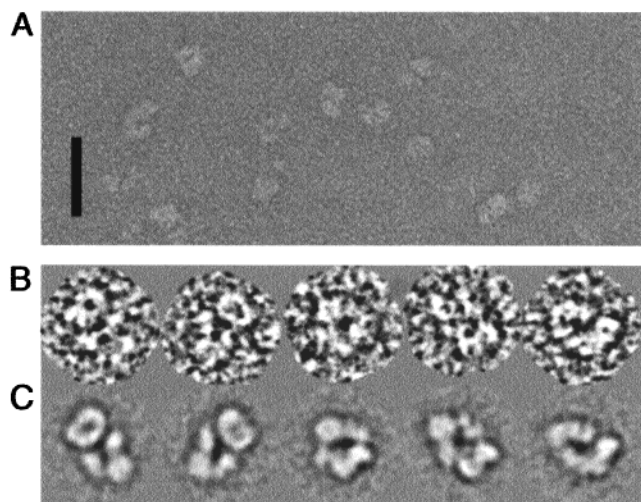


FIGURE 4: Electron microscopic images of negatively stained GluRB. (A) Representative field from an electron micrograph of negatively stained single particles. Scale bar, 50 nm. (B, C) Classification and averaging of single particles of GluRB. (B) Single particle images that were assigned to five different classes (of a total of 155), together with corresponding class averages (C). In panels B and C, the edge of one frame corresponds to 27 nm.

accessible volumes seen as stain-filled structures within the molecular outlines of the class averages. Equivalent features are seen in the unaveraged images, albeit with the expected lower signal-to-noise ratio.

## DISCUSSION

A major barrier to structural and functional studies of membrane proteins that are not naturally abundant is the difficulty of expressing the required milligram quantities with the required homogeneity and functionality (reviewed in ref 22). Here we report a system for the expression and purification of a homomeric GluRB ion channel that addresses several of these issues. This has permitted us to characterize the channel's hydrodynamic properties and to determine its overall structure and molecular dimensions by electron microscopy.

Several factors were essential in obtaining receptor preparations of the high biochemical quality required. The purity of the GluRB preparation was decisively influenced by the use of  $Zn^{2+}$  rather than  $Ni^{2+}$  or  $Co^{2+}$  cations during metal-chelate chromatography. This contrasts with observations made with GluRD, for which  $Ni^{2+}$  proved the most suitable cation (11). In our case, the improvement in purity appears to reflect a reduction of nonspecific binding of contaminants to the  $Zn^{2+}$  column. Although the binding of the hexahistidine tag was also weakened, consistent with peptide-binding experiments (24), the specificity of the interaction increased, permitting recovery of protein at much higher purity. Expression in High Five rather than Sf21 cells and harvest by continuous-flow centrifugation were important in minimizing protein aggregation, which had limited the usefulness of earlier glutamate receptor preparations from insect cells (11). Continuous-flow centrifugation is commonly used to harvest bacterial cells expressing recombinant proteins. However, our results suggest that it also may be an attractive alternative to batch centrifugation for pilot-scale expression of membrane proteins in the baculovirus system, where it has not yet found wide application.

GluRB yields a single peak in density-gradient centrifugation (Figure 3), confirming the uniformity of the oligomeric assembly. Although the peak is slightly broader than those of the standard proteins, this additional broadening may reflect heterogeneity in the TX-100 micelles, which typically range in size from 63 to 97 kDa (25). Assuming that one  $\sim 80$  kDa micelle is bound per complex, the observed 495 kDa molecular mass of the complex corresponds well to that expected for a tetrameric molecule ( $4 \times 104$  kDa + 80 kDa = 496 kDa). In contrast, a pentameric glutamate receptor should have a molecular mass of at least 580 kDa (520 kDa protein +  $\geq 60$  kDa detergent). Hence we conclude that the recombinant GluRB most likely forms a tetramer.

This finding is consistent with a growing body of electrophysiological and biochemical evidence that supports a tetrameric assembly for GluR (26–29). Such an assembly would be expected on the basis of the homology of the GluR transmembrane domains to tetrameric potassium channels (30–32). Our measurement is, however, inconsistent with experiments that suggest a pentameric stoichiometry, particularly for *N*-methyl-D-aspartate-selective GluR (33–35).

Single-particle images of the GluRB homomers in negative stain suggest that the ion channel is an elongated structure with solvent-accessible internal features (Figure 4), some of which may correspond to ion-conducting pathways in the channel. The distribution of perspectives and observed anisotropy of the particle are reminiscent of the voltage-gated sodium channel (36). The dimensions of the particle are consistent with its molecular weight and could accommodate a tetrameric assembly of  $\sim 100$  kDa protomers. The unequal particle dimensions are not consistent with a 4-fold symmetrical molecular assembly but would be consistent with internal 2-fold symmetry. To reconcile this observation with the presence of four subunits in the channel, one can speculate that the receptor may be assembled as a dimer of dimers, consistent with recent biochemical studies on the assembly of chimeric AMPA/kainate receptor subunits (8) and with the observation that the ligand-binding domain typically crystallizes in a dimeric form (9). The proposed 2-fold symmetry cannot be seen in the input projections (Figure 4C); however, symmetry can be masked by the orientations adopted by the particles on the film, as it was for most single-particle images of the 4-fold symmetric sodium channel (36). In our case, the putative internal symmetry axis may be preferentially oriented parallel to the plane of the carbon film and therefore inaccessible to direct visualization by electron microscopy.

A three-dimensional reconstruction of the molecular envelope of the GluRB homomer by angular reconstitution has been performed (data not shown). However, due to an unfavorable spatial distribution of perspectives and the lack of clear molecular symmetry that could be imposed during angular reconstitution, we cannot reliably interpret features beyond those that are visible in the input projections (Figure 4C). Nevertheless, good agreement between the model and the input projections confirms that the single GluRB channels were correctly preserved and imaged in negative stain and that the different class sums represent distinct perspectives of a single molecular structure. Thus, potential artifacts of the negative stain technique (e.g., partial staining and flattening; see ref 37) appear to have been minimized. This being the case, other experimental approaches are available

to deal with limited perspectives. In the random conical tilt reconstruction technique, collection of pairs of electron micrographs of tilted and untilted particles provides a set of perspectives for each class of particles sufficient to determine independent 3D reconstructions for each class (38). Similar reconstructions can be merged, providing a relatively complete set of perspectives on the particle. Imaging particles in vitrified buffer or stain may yield additional, complementary perspectives and provide an independent check on the absence of staining artifacts in the reconstruction. Alternatively, if we can independently identify the molecular symmetry (e.g., from a random conical tilt reconstruction), then that symmetry can also be used to improve the reconstruction of untilted images by angular reconstitution.

We have purified functional, recombinant GluRB homomers that reveal a probable tetrameric stoichiometry and an elongated structure that would be consistent with a dimer-of-dimers assembly for these ion channels. The protein is well-suited to further biochemical and structural analysis. In particular, antibody labeling of known sequence epitopes should permit assignment of domains within an improved molecular envelope. Furthermore, the ability to express milligram quantities of high-quality material should support two-dimensional crystallization and functional reconstitution experiments designed to provide higher resolution structural and functional data, respectively.

#### ACKNOWLEDGMENT

We thank V. Bader and H. Clasen for skillful technical assistance, Drs. K. C. Holmes and R. R. Schröder (Department of Biophysics, MPI, Heidelberg) for making available the EM facilities, Dr. M. Schatz (Image Science Software GmbH, Berlin) for helpful discussions, and Dr. G. A. Scarborough (UNC, Chapel Hill) for helpful suggestions on the manuscript. We gratefully acknowledge the initial and continuing support of this project by Dr. B. Sakmann (Department of Cell Physiology, MPI, Heidelberg).

#### REFERENCES

- Dingledine, R., Borges, K., Bowie, D., and Traynelis, S. F. (1999) *Pharm. Rev.* 51, 7–61.
- Rose, C. R., and Konnerth, A. (2000) *Nature* 405, 413–415.
- Hollmann, M., O'Shea-Greenfield, A., Rodgers, S. W., and Heinemann, S. (1989) *Nature* 342, 643–648.
- Keinänen, K., Wisden, W., Sommer, B., Werner, P., Herb, A., Verdoorn, T. A., Sakmann, B., and Seeburg, P. H. (1990) *Science* 249, 556–560.
- Boulter, J., Hollmann, M., Shea-Greenfield, O. A., Hartley, M., Deneris, E., Maron, C., and Heinemann, S. (1990) *Science* 249, 1033–1037.
- Hollmann, M., Hartley, M., and Heinemann, S. (1991) *Science* 252, 851–853.
- Osten, P., Khatri, L., Perez, J. L., Kohr, G., Giese, G., Daly, C., Schulz, T. W., Wensky, A., Lee, L. M., and Ziff, E. B. (2000) *Neuron* 27, 313–325.
- Ayalon, G., and Stern-Bach, Y. (2001) *Neuron* 13, 103–113.
- Armstrong, N. A., and Gouaux, E. (2000) *Neuron* 28, 165–181.
- Keinänen, K., Kohr, G., Seeburg, P. H., Laukkanen, M. L., and Oker-Blom, C. (1994) *Bio/Technology* 12, 802–806.
- Kuusinen, A., Arvola, M., Oker-Blom, C., and Keinänen, K. (1995) *Eur. J. Biochem.* 233, 720–726.
- Hopp, T. P., Prickett, K. S., Price, V. L., Libby, R. T., March, C. J., Cerretti, D. P., Urdal, D. L., and Conlon, P. J. (1988) *Bio/Technology* 6, 1204.
- Schiöth, H. B., Kuusinen, A., Muceniece, R., Szardenings, M., Keinänen, K., and Wikberg, J. E. (1996) *Biochem. Biophys. Res. Commun.* 221, 807–814.
- Madden, D. R., Abele, R., Andersson, A., and Keinänen, K. (2000) *Eur. J. Biochem.* 267, 4281–4289.
- Cheng, Y., and Prusoff, W. H. (1973) *Biochem. Pharmacol.* 22, 3099–3108.
- Bradford, M. M. (1976) *Anal. Biochem.* 72, 248–254.
- Schatz, M., Orlova, E. V., Dube, P., Jäger, J., and van Heel, M. (1995) *J. Struct. Biol.* 114, 28–40.
- Serysheva, I. I., Orlova, E. V., Chiu, W., Sherman, M. B., Hamilton, S. L., and van Heel, M. (1995) *Nat. Struct. Biol.* 2, 18–24.
- van Heel, M., Harauz, G., and Orlova, E. V. (1996) *J. Struct. Biol.* 116, 17–24.
- Dube, P., Tavares, P., Lurz, R., and Van Heel, M. (1993) *EMBO J.* 12, 1303–1309.
- Hollmann, M., and Heinemann, S. (1994) *Annu. Rev. Neurosci.* 17, 31–108.
- Grisshammer, R., and Tate, C. G. (1995) *Q. Rev. Biophys.* 28, 315–422.
- Abele, R., Lampinen, M., Keinänen, K., and Madden, D. R. (1998) *J. Biol. Chem.* 273, 25132–25138.
- Yip, T. T., Nakagawa, Y., and Porath, J. (1989) *Anal. Biochem.* 183, 159–171.
- Robson, R. J., and Dennis, E. A. (1977) *J. Phys. Chem.* 81, 1075–1078.
- Laube, B., Kuhse, J., and Betz, H. (1998) *J. Neurosci.* 18, 2954–2961.
- Mano, I., and Teichberg, V. I. (1998) *Neuroreport* 9, 327–331.
- Rosenmund, C., Stern-Bach, Y., and Stevens, C. F. (1998) *Science* 280, 1596–1599.
- Kuusinen, A., Abele, R., Madden, D. R., and Keinänen, K. (1999) *J. Biol. Chem.* 274, 28937–28943.
- Chen, G.-Q., Cui, C., Mayer, M. L., and Gouaux, E. (1999) *Nature* 402, 817–821.
- Wo, Z. G., and Oswald, R. E. (1995) *Trends Neurosci.* 18, 161–168.
- Doyle, D. A., Cabral, J. M., Pfuetzner, R. A., Kuo, A., Gulbis, J. M., Cohen, S. L., Chait, B. T., and MacKinnon, R. (1998) *Science* 280, 69–77.
- Ferrer-Montiel, A. V., and Montal, M. (1996) *Proc. Natl. Acad. Sci. U.S.A.* 93, 2741–2744.
- Premkumar, L. S., and Auerbach, A. (1997) *J. Gen. Physiol.* 110, 485–502.
- Hawkins, L. M., Chazot, P. L., and Stephenson, F. A. (1999) *J. Biol. Chem.* 274, 27211–27218.
- Sato, C., Sato, M., Iwasaki, A., Doi, T., and Engel, A. (1998) *J. Struct. Biol.* 121, 314–325.
- Cejka, Z., Kleinz, J., Santini, C., Hegerl, R., and Magaldi, A. G. (1992) *J. Struct. Biol.* 109, 52–60.
- Radermacher, M. (1988) *J. Electron Microsc. Technol.* 9, 359–394.

BI011143G

## **Eidesstattliche Versicherung**

Ich, Günther Kümmerle, erkläre an Eides Statt, dass ich die vorgelegte Dissertation selbständig angefertigt und mich anderer Hilfsmittel als der in ihr angegebenen nicht bedient habe, insbesondere, dass aus Schriften Entlehnungen, soweit sie in der Dissertation nicht ausdrücklich als solche mit Angabe der betreffenden Schrift bezeichnet sind, nicht stattgefunden haben.

Desweiteren erkläre ich hiermit, dass ich an keiner anderen Stelle eine Prüfungsverfahren beantragt, beziehungsweise die Dissertation in dieser oder anderer Form bereits anderweitig als Prüfungsarbeit verwendet oder einer anderen Fakultät als Dissertation vorgelegt habe.

G. Kümmerle

Heidelberg, den 18. Feb. 2002

**Personal data:**

Name: Günther Kümmerle  
Address: An den Röthen 82  
97080 Würzburg / Germany

Max Planck Institute for Medical Research  
Jahnstrasse 29  
D-69120 Heidelberg

Place of birth: Reutlingen / Germany

**Education:**

1998-2001	<b>Max-Planck-Institute for Medical Research</b> Ph.D. in biophysics in the Ion Channel Structure Research Group of Dr. D. R. Madden: "Structure and function of ionotropic Glutamate receptors". Supervisors Prof. D. Steinhilber (University of Frankfurt) and Prof. K. Holmes (MPI Heidelberg)	<b>Heidelberg, Germany</b>
1997-1998	<b>Institute for Theoretical und Physical Chemistry</b> Diploma thesis (6 months) in nuclear magnetic resonance (NMR) spectroscopy with Prof. J. Bargon Master Degree ("Diplomchemiker") Grade:1.0.	<b>Bonn, Germany</b>
1995-1998	<b>University of Bonn</b> Completed graduate studies in chemistry with a major in biochemistry.	<b>Bonn, Germany</b>
1991-1995	<b>University of Konstanz</b> Undergraduate- and graduate studies in chemistry.	<b>Konstanz, Germany</b>
1990-1991	<b>Medical Research Institute I of the Military Hospital</b> Compulsary military training. Worked as laboratory assistant in the medical laboratory of a military hospital.	<b>Hamburg, Germany</b>
1988-1990	<b>Wollert-Ellmendorff-Deutsche-Industrietreuhand (wedit) GmbH (CPA firm)</b> Apprenticeship. Trained as auditing assistant for medium-seized and large companies. Diploma: Auditing assistant ("Fachhilfe in steuer- und wirtschaftsberatenden Berufen"). Grade:1.0.	<b>Hannover, Germany</b>
1988	<b>Theodor-Heuss-High-School</b> High school diploma ("Abitur").	<b>Reutlingen, Germany</b>